R827028 Final Report

Development and Evaluation of Modeling Techniques for the Study of Interactions between Urban and Point Source Plumes and Regional Atmospheres in the Formation of Secondary Pollutants

Prepared for:

Dr. Paul Shapiro
National Center for Environmental Research and Quality Assurance (8723R)
U.S. Environmental Protection Agency
1300 Pennsylvania Avenue, N.W.
Room 51185
Washington, D.C. 20004

Prepared by:

M. Talat Odman
Department of Civil and Environmental Engineering
Georgia Institute of Technology
Atlanta, GA 30322-0512

and

D. Scott McRae
Department of Mechanical and Aerospace Engineering
North Carolina State University
Raleigh, North Carolina 27695-7910

April 14, 2003

TABLE OF CONTENTS

EXECUTIVE SUMMARY

Period Covered by the Report: January 15, 1999 to January 14, 2003
Date of Final Report: April 14, 2003
EPA Agreement Number: R827028
Title: Development and Evaluation of Modeling Techniques for the Study of Interactions between Urban and Point Source Plumes and Regional Atmospheres in the Formation of Secondary Pollutants
Investigators: M. Talat Odman and D. Scott McRae
Institution: Georgia Institute of Technology and North Carolina State University
Research Category: Air Pollution Chemistry and Physics
Project Period: January 15, 1999 - January 14, 2003

Objective(s) of the Research Project: The purpose of the study is to develop new modeling techniques and build on existing ones to improve the representation of emission sources in air quality models (AQMs). The interaction of point and urban source plumes with the surrounding atmosphere involves processes of critical importance to the formation, long-range transport and fate of secondary pollutants such as ozone. The relevant scale of these interactions are smaller than typical scales used in regional AQMs, therefore plumes are generally considered sub-grid scale. There are various uncertainties involved in the treatment of sub-grid scale processes. This research is focused on increasing the resolution of plume interactions thereby reducing the associated uncertainties.

Summary of Findings: This research contributed to regional-scale air quality modeling by introducing new methods and improving existing methods for the treatment of emission sources. The transport, transformation and fate of the plumes from emission sources were simulated with unprecedented accuracy and the model estimates of pollutant levels downwind were significantly improved. This should result in more accurate predictions of future air quality and lead to the design of more effective emission control strategies. The benefit of such strategies would be more economical solutions to air pollution problems and less risk to human health. The methods developed can individually be used in existing regulatory models but, more important, the framework developed here can also be adopted as the prototype for the next generation air quality models.

Research focused on three core areas: 1) the development of mass conservative techniques for coupling AQMs with meteorological models (MMs), 2) design of hand-over criteria for sub-grid scale reactive plume models, and 3) the development and application of an adaptive grid AQM. Inconsistent meteorological fields (when the density and the three components of the wind velocity do not satisfy the discrete continuity equation they are inconsistent) may lead to instabilities in AQMs. However, earlier solutions developed for some models sacrificed mass conservation. We investigated the gravity of the mass conservation violations and discovered that, depending on the amount of divergence along the trajectory of a plume, the mass of emissions can be significantly altered with flawed solutions. We found that the adjustment of the vertical wind component is an effective technique. Three methods for making the meteorological fields consistent with each other were implemented and incorporated into an AQM. Comparisons showed that the wind fields produced by the three methods were very similar to each other but they differed from those

supplied by the MM. The differences were not large enough to significantly affect any transport trajectories though, just sufficient to assure conservation of mass. All three methods strictly conserved the mass of emissions in point source plumes even under very complex meteorological conditions.

Sub-grid scale reactive plume models are used as a means of improving the accuracy with which point emission sources can be included in regional AQM simulations. They provide detailed initiation, reaction and propagation of the plume constituents from local sources at resolution scales not available in the regional AQM. However, in the past, these models have not improved the predictive skill of AQMs. We believe that this is primarily due to improper use of these so-called "plume-in-grid" models. When a predetermined hand over criterion is met, the plume is injected into the AQM grid, but the large numerical diffusion that it will experience can eliminate completely the high-resolution information coming from the sub-grid scale plume model. We developed a technique for determining when information from a plume-in-grid model can be accurately represented on a mesh with typical regional AQM scales. Plume distributions generated by the sub-grid models were analyzed using discrete Fourier transforms in order to obtain the frequency distribution and amplitude of the Fourier components. The transformed frequency distributions were then filtered to reflect the frequencies resolved by the coarser mesh of the regional scale model. An inverse transform of the filtered frequency distributions is then performed. The degree to which the resulting function agrees with the original function gives an indication of the effect of transferring the plume to the coarse grid. The idea that the computational mesh is a band-pass filter is used to develop automated hand over criteria. These criteria were implemented in an AQM and testing with various plumes showed that the plume-in-grid models would only be useful when AQMs have relatively fine grid resolution themselves. This conclusion provided justification for the next core research area, i.e., development of an adaptive grid AQM.

The development of the adaptive grid AQM started with an evaluation of the previously developed adaptor using complex terrain elevation fields, which, in terms of variability, are similar to secondary air pollutant fields. Starting with a uniform grid with less resolution than the original data, the grid was adapted with the objective of recovering the resolution of the original data as much as possible. The adaptor performed well but required several modifications to improve its convergence characteristics. This evaluation showed that the adaptive grid algorithm has the potential of significantly improving the accuracy of air quality predictions, especially when the regions of changing slope are far away from the boundaries. The next step was the development of two important components of the adaptive grid AQM, namely the processors for meteorological and emissions inputs. Since the processing must be performed after each grid adaptation during the simulation, it is critical to design efficient processors that consume very little computational time. We developed efficient intersection and search algorithms for input data processing. These algorithms take advantage of the fact that the topology of the grid is maintained during adaptation even though the location and shape of the grid cells change.

The concept of an adaptive grid AQM was implemented using the Multiscale Air Quality Simulation Platform (MAQSIP). A simulation with this model evolves as a sequence of adaptation and solution steps. During the adaptation step, the solution (i.e., concentration

fields) is frozen in time. A weight function that can detect the error in the solution is used to move the nodes of a structured grid. Iterative movement of the grid nodes continues until the solution error is reduced sufficiently. During the solution step, the grid is held fixed and the solution is advanced in time. However, before this can be done, the meteorological and emissions inputs must be mapped onto the adapted grid. This is done using the processors mentioned above. Using coordinate transformations, the non-uniform grid can be mapped into a space where it becomes uniform. The atmospheric diffusion equation in this new space is very similar in form to the equations solved by static, uniform grid AQMs, therefore the existing numerical algorithms are used to advance the solution.

Using the adaptive grid AQM that we developed, we simulated the July 7-17, 1995 ozone episode in the Tennessee Valley. The grid adapted to dynamic changes in the domain and the nodes clustered downwind of major emission sources with grid resolutions as small as 200 m. The NO_x fields showed gradients with a level of detail that is likely unprecedented for a regional simulation at this scale. Estimates of O_3 were compared to those from static grid models that require comparable computational resources. By placing higher resolution near point sources, the adaptive grid AQM estimated ozone concentrations more consistent with observations at downwind stations. Some of the long-range source-receptor relationships resolved by the adaptive grid AQM were completely missed by the static grid AQMs. Unfortunately, these relationships could not be established from the scarce observations. Nevertheless, a comparison to aircraft observations showed good agreement with plumes located along the flight paths. These comparisons also revealed a fundamental problem in how aloft initial and boundary conditions are assumed in AQM simulations. The O_3 performance of the model was evaluated using several different weight functions as criteria for adaptation. Surface NO_x, vertical column NO_x, and O_3 production rate were tried and they all produced very different grid adaptations. The use of column NO_x captured the plumes above the stable nighttime boundary layer that the surface NO_x weight function missed but also resulted in a more uniform grid during the day. A linear combination of the O_3 production rate and column NO_x seemed to produce the most desirable grid resolution characteristics but the differences in O_3 between the different simulations were too small to determine which weight function produces the best results.

Publications/Presentations: The results of this research were disseminated in various forms. *First, the following* refereed journal papers were published:

1. Srivastava, R. K., McRae, D. S. and Odman, M. T., "An adaptive grid algorithm for air quality modeling," Journal of Computational Physics, vol. 165, no. 2, pp. 437-472, December 2000.
2. Srivastava, R. K., McRae, D. S. and Odman, M. T., "Simulation of a reacting pollutant puff using an adaptive grid algorithm," Journal of Geophysical Research, vol. 106, no. D20, pp. 24245-24258, October 2001.
3. Srivastava, R. K., McRae, D. S. and Odman, M. T., "Simulation of dispersion of a power plant plume using an adaptive grid algorithm," Atmospheric Environment, vol. 35, no. 28, pp. 4801-4818, October 2001.

4. Khan, N. K., Odman, M. T. and Karimi, H., "Evaluation of algorithms developed for adaptive grid air quality modeling using surface elevation data," Computers, Environment and Urban Systems, in press.

Three more papers are in preparation and will be submitted soon:

1. Narayanaswamy, K., Al-Ashhab, S. McRae, D. S. and Odman, M. T., "Automated hand-over criteria for sub-grid plume models," in preparation.
2. Odman, M.T., Khan, M. N. and McRae, D. S., "Adaptive Grid Air Quality Model: Part I—Model Development," in preparation.
3. Khan, M. N. and Odman, M.T., "Adaptive Grid Air Quality Model: Part II—Application to Ozone and Model Evaluation," in preparation.

The following non-refereed papers appeared in conference proceedings:

1. Odman, M. T. and Russell, A. G., "Mass conservative coupling of non-hydrostatic meteorological models with air quality models," in Air Pollution Modeling and its Application XIII: Proceedings of the 23rd NATO/CCMS International Technical Meeting on Air Pollution Modelling and Its Application held in Varna, Bulgaria, September 28-October 2, 1998, pp. 651-660, (S.-E. Gryning and E. Batchvarova, Eds.), New York: Kluwer Academic/Plenum Publishers (2000).

2. Odman, M. T., Khan M. N., and McRae, D. S., "Adaptive grids in air pollution modeling: Towards an operational model," in Air Pollution Modeling and Its Application XIV, Proceedings of the 24th (Millennium) NATO/CCMS International Technical Meeting on Air Pollution Modeling and its Application held in Boulder, Colorado, May 15-19, 2000, pp. 541-549, (S.-E. Gryning and F. A. Schiermeier, Eds.), New York: Kluwer Academic/Plenum Publishers (2001).

3. Khan, M. N., Odman, M. T., Karimi, H. and Goodchild, M., "Developing and integrating advanced GIS techniques in an adaptive grid air quality model to reduce uncertainty," 4th International Conference on Integrating GIS and Environmental Modeling (GIS/EM4), Banff, Alberta, Canada, September 2-8, 2000.

4. Khan, M., Odman, T., Karimi, H. and Hanna, A., "Reducing uncertainty of air quality models through coupling adaptive grids with GIS techniques," 2nd International Conference on GIS for Earth Science Applications (ICGESA), Menemen, Turkey, September 11-14, 2000.

5. Odman, M. T. and Khan, M. N., "An adaptive grid model for urban to regional scale air quality problems," 2nd International Symposium on Air Quality Management at Urban, Regional and Global Scales, Istanbul, Turkey, September 25-28, 2001.

6. Odman, M. T., Khan, M. N., Srivastava, R. K. and McRae, D. S., "Initial application of the adaptive grid air pollution model," in Air Pollution Modeling and its Application XV: Proceedings of the 25th NATO/CCMS International Technical Meeting on Air Pollution Modelling and Its Application held in Louvain-la-Neuve,

Belgium, October 15-19, 2001, pp. 319-328 (C. Borrego and Guy Schayes, Eds.), New York: Kluwer Academic/Plenum Publishers (2002).

7. Odman, M. T., Khan, M. N., "Adaptive grid air quality model: Application to an ozone episode," American Meteorological Society 12th Joint Conference on the Applications of Air Pollution Meteorology with the Air and Waste Management Association, Norfolk, VA, May 20-24 2002.

8. Odman, M. T., Khan, M. N., Srivastava, R. K. and McRae, D. S. (2003) Evaluation of the adaptive grid air pollution model. *26th NATO/CCMS International Technical Meeting on Air Pollution Modelling and Its Application*, Istanbul, Turkey, May 26-30, 2003 (abstract accepted for poster presentation).

Finally, a Ph.D. dissertation and a final report described this research in detail. They are:

1. Khan, M. N., Development and Application of an Adaptive Grid Air Quality Model, Ph.D. Dissertation, Georgia Institute of Technology, Atlanta, GA, April 2003.

2. Odman, M. T. and McRae, D. S., "Development and Evaluation of Modeling Techniques for the Study of Interactions between Urban and Point Source Plumes and Regional Atmospheres in the Formation of Secondary Pollutants," Final report, 101 pp., U.S. Environmental Protection Agency, Washington, DC, 2003.

Supplemental Keywords: tropospheric, oxidants, nitrogen oxides, mathematics, analytical, Northeast

Relevant Web Sites: http://www.ce.gatech.edu/~todman/page2.html

LIST OF TABLES

LIST OF FIGURES

1 Introduction

1.1 Background and Objectives

Secondary air pollutants such as ozone and fine particulate matter continue to risk human health over the most populous areas of the U.S. There is significant transport of these pollutants between the states, especially in the northeastern part of the country. Given the regional nature of the problem, formulating regional emission control strategies would likely be more effective than a collection of strategies developed individually by each state. While there is debate over which strategies are more effective, there is little doubt that any strategy would be very costly. What is needed is a tool that can identify not only what control strategies will meet the air quality goals but do so at the lowest possible cost. Regional-scale Air Quality Models (AQMs) are scientifically the most defendable tools for such guidance. Regulatory agencies developing control strategies use AQMs to estimate exactly how much emission from which source must be reduced. AQMs are also very important research tools that help us understand physical and chemical phenomena leading to air pollution over regional scales. It is therefore critical to reduce the uncertainties associated with AQM use.

What motivated this project is our concern with the use of AQMs in studies that may have important policy implications without proper evaluation of their adequacy for intended applications. Uncertainties in the estimated amount of required controls can cause huge amounts of money to be misspent and still leave the public at risk. Current AQMs have various limitations and inadequacies; some will be discussed here. In particular, the treatment of point source and urban plumes is a known weakness of AQMs. This introduces large uncertainties in the long-range transport processes that are significant in regional ozone and fine particulate matter formation. The goal of this project is to improve existing models so that the interaction between the plumes and the surrounding atmosphere can be better resolved. Without such improvements, we cannot expect AQM estimates to discriminate between different types of controls, for example elevated point source versus surface area emissions.

A limited number of simulations where inert tracers where followed by AQMs showed that while the trajectories were generally satisfactory, the estimated amounts of tracers were orders of magnitudes off compared to observation (Brost et al, 1988). We believe that this problem is, in part, due to numerical inaccuracies in the models. For example, we have identified that some existing models do not even conserve mass. These errors are becoming more evident as inaccuracies related to other processes are being reduced. To increase confidence in the use of AQMs in the design of control strategies, for example for "source apportionment," especially for problems related to secondary pollutants, we must improve the characterization of transport in AQMs. Recently, better quality meteorological inputs became available due to the development of high-resolution non-hydrostatic models. We believe that this data is not being used to its full potential. Our first objective is to develop numerical algorithms that can accurately capture transport of pollutants in the PBL. Our goal is to elevate AQMs to a level where measured tracer concentrations in controlled experiments can be estimated much more accurately.

Another concern we have is related to the use of sub-grid scale reactive plume models. There are reports that these models do not improve the predictive skill of AQMs, at least on a regional scale (Kumar and Russell, 1996). We believe that this is primarily due to improper use of these so-called "plume-in-grid" models. We identified that without proper judgment of the numerical diffusion introduced by transport algorithms, the benefits from sub-grid scale models can easily be lost (Odman, 1997). Numerical diffusion can be relatively large at scales comparable to one or two grid lengths. This can wipe out the high-resolution information coming from the sub-grid plume model. The result may be identical to instantaneous mixing of the plume within the grid cell, which happens in the absence of plume-in-grid models. Our second objective is to develop proper "hand-over" criteria, such that the detailed information coming from the sub-grid plume model is blended effectively to the grid model.

A third issue is to increase the resolution of AQMs effectively and efficiently. Increasing the resolution uniformly everywhere can be computationally expensive. Methods have been proposed to increase the resolution locally where it is (believed to be) most needed. A common approach is nesting (or embedding) a fine resolution grid inside a coarse grid. Since observed concentration gradients are largest near emission sources the fine grid is usually placed over the source areas. At the interface of the two grids with different resolutions there are usually mass conservation problems. While mass of inert tracers can be easily conserved, the problem becomes more complex for reactive species. Another problem is reflection and refraction of waves traveling across the interface where grids of different resolution on each side act like different media. While grid nesting is simple and economical, it is not effective in capturing the complex interactions between plumes and the surrounding atmosphere. We believe that this is, in part, due to the problems cited above. For these reasons we prefer approaches other than grid nesting. There are two approaches of interest: finite element refinements (Odman and Russell, 1991a) and non-uniform structured grids (Mathur et al., 1992). In both of these approaches there is only one grid, so it is much easier to conserve mass. Also, the change in resolution is gradual with no apparent grid interfaces that may disturb the passage of waves such as plumes. Our third objective is to follow the most recent developments with the use of these two approaches as well as the plume-in-grid models in AQMs to determine the more viable approach for the study of the interactions between plumes and the surrounding atmospheres. One of the principal investigators, Dr. Odman, is using the finite-element refinement approach in the study of ozone and particulate matter formation in the southeastern United States (Odman et al, 2002).

The fourth and final objective is to develop an adaptive grid AQM. With the static grid techniques optimal use of computational resources or effectiveness of increased resolution is not guaranteed. For example, in grid nesting the finest grid and the extent of the area covered by this grid are determined intuitively. A static grid is also limited by the inability to adjust to dynamic changes in resolution requirements under different meteorological conditions. A desirable solution would be a dynamic grid algorithm that automatically adapts the grid to changing solution resolution requirements under the wide range of conditions of multi-day simulations. This way, computational resources can be used in the most effective way and the error minimized by placing finer resolution where it is most needed when it is needed. The dynamic adaptive grid algorithm we developed for transport of pollutants constitutes the basis for this effort (Srivastava et al., 1996). An important step in

developing the adaptive grid AQM is to accelerate the processing of emissions such that every time the grid is changed emission can be recalculated for the new grid. Current methods of emissions processing are very inefficient but this is not critical with static grid models since the processing is performed once before the simulation. An adaptive grid AQM also needs a component that can provide meteorological data on a constantly changing grid. Our goal is to develop the missing components and demonstrate the benefits of an adaptive grid AQM. Such a model can be used in studying the interaction of plumes with their surrounding with unprecedented detail and accuracy.

In summary, the goal of this research is to develop new modeling techniques to improve the representation of emission sources in air quality models (AQMs). The interaction of point and urban source plumes with the surrounding atmosphere involves processes of critical importance to the formation, long-range transport and fate of secondary pollutants such as ozone. The relevant scale of these interactions are smaller than typical scales used in regional AQMs, therefore plumes are generally considered *subgrid* scale. There are various uncertainties involved in the treatment of subgrid scale processes. This research is focused on increasing the resolution of plume interactions thereby reducing the associated uncertainties. Static multiscale and dynamic adaptive modeling techniques will be further developed and compared.

1.2 Overview

The rest of this report consists of six chapters describing the work performed to achieve the four objectives stated above during the January 1999-January 2003 period. Chapter 2 includes a discussion of the vertical wind adjustment methods that were developed for mass conservative transport of pollutants in the PBL. Chapter 3 describes the research conducted for the design of automatic hand-over criteria from sub-grid scale reactive plume models to regional scale AQMs. Chapter 4 includes performance evaluation of grid adaptation and point-source emission processing algorithms. Chapter 5 explains the concept of an adaptive grid AQM and describes its formulation, development and verification. The adaptive grid AQM that we developed is used to study plume interactions with the surrounding atmospheres in Chapter 6. Finally, conclusions are drawn in Chapter 7.

The results of this research were disseminated in various forms. First, the following refereed journal papers were published:

1. Srivastava, R. K., McRae, D. S. and Odman, M. T., "An adaptive grid algorithm for air quality modeling," Journal of Computational Physics, vol. 165, no. 2, pp. 437-472, December 2000.
2. Srivastava, R. K., McRae, D. S. and Odman, M. T., "Simulation of a reacting pollutant puff using an adaptive grid algorithm," Journal of Geophysical Research, vol. 106, no. D20, pp. 24245-24258, October 2001.
3. Srivastava, R. K., McRae, D. S. and Odman, M. T., "Simulation of dispersion of a power plant plume using an adaptive grid algorithm," Atmospheric Environment, vol. 35, no. 28, pp. 4801-4818, October 2001.

4. Khan, N. K., Odman, M. T. and Karimi, H., "Evaluation of algorithms developed for adaptive grid air quality modeling using surface elevation data," Computers, Environment and Urban Systems, in press (presented as Chapter 4).

Three more papers are in preparation and will be submitted soon:

1. Narayanaswamy, K., Al-Ashhab, S. McRae, D. S. and Odman, M. T., "Automated hand-over criteria for sub-grid plume models," in preparation (current form presented as Chapter 3).
2. Odman, M.T., Khan, M. N. and McRae, D. S., "Adaptive Grid Air Quality Model: Part I—Model Development," in preparation (current form presented as Chapter 5).
3. Khan, M. N. and Odman, M.T., "Adaptive Grid Air Quality Model: Part II—Application to Ozone and Model Evaluation," in preparation (current form presented as Chapter 6).

The following non-refereed papers appeared in conference proceedings:

1. Odman, M. T. and Russell, A. G., "Mass conservative coupling of non-hydrostatic meteorological models with air quality models," in Air Pollution Modeling and its Application XIII: Proceedings of the 23rd NATO/CCMS International Technical Meeting on Air Pollution Modelling and Its Application held in Varna, Bulgaria, September 28-October 2, 1998, pp. 651-660, (S.-E. Gryning and E. Batchvarova, Eds.), New York: Kluwer Academic/Plenum Publishers (2000) (presented as Chapter 2).

2. Odman, M. T., Khan M. N., and McRae, D. S., "Adaptive grids in air pollution modeling: Towards an operational model," in Air Pollution Modeling and Its Application XIV, Proceedings of the 24th (Millennium) NATO/CCMS International Technical Meeting on Air Pollution Modeling and its Application held in Boulder, Colorado, May 15-19, 2000, pp. 541-549, (S.-E. Gryning and F. A. Schiermeier, Eds.), New York: Kluwer Academic/Plenum Publishers (2001).

3. Khan, M. N., Odman, M. T., Karimi, H. and Goodchild, M., "Developing and integrating advanced GIS techniques in an adaptive grid air quality model to reduce uncertainty," 4th International Conference on Integrating GIS and Environmental Modeling (GIS/EM4), Banff, Alberta, Canada, September 2-8, 2000.

4. Khan, M., Odman, T., Karimi, H. and Hanna, A., "Reducing uncertainty of air quality models through coupling adaptive grids with GIS techniques," 2nd International Conference on GIS for Earth Science Applications (ICGESA), Menemen, Turkey, September 11-14, 2000.

5. Odman, M. T. and Khan, M. N., "An adaptive grid model for urban to regional scale air quality problems," 2nd International Symposium on Air Quality Management at Urban, Regional and Global Scales, Istanbul, Turkey, September 25-28, 2001.

6. Odman, M. T., Khan, M. N., Srivastava, R. K. and McRae, D. S., "Initial application of the adaptive grid air pollution model," in Air Pollution Modeling and its

Application XV: Proceedings of the 25th NATO/CCMS International Technical Meeting on Air Pollution Modelling and Its Application held in Louvain-la-Neuve, Belgium, October 15-19, 2001, pp. 319-328 (C. Borrego and Guy Schayes, Eds.), New York: Kluwer Academic/Plenum Publishers (2002) (presented as Chapter 5).

7. Odman, M. T., Khan, M. N., "Adaptive grid air quality model: Application to an ozone episode," American Meteorological Society 12th Joint Conference on the Applications of Air Pollution Meteorology with the Air and Waste Management Association, Norfolk, VA, May 20-24 2002.

8. Odman, M. T., Khan, M. N., Srivastava, R. K. and McRae, D. S. (2003) Evaluation of the adaptive grid air pollution model. *26th NATO/CCMS International Technical Meeting on Air Pollution Modelling and Its Application*, Istanbul, Turkey, May 26-30, 2003 (abstract accepted for poster presentation).

Finally, one Ph.D. dissertation resulted from this project:

1. Khan, M. N., Development and Application of an Adaptive Grid Air Quality Model, Ph.D. Dissertation, Georgia Institute of Technology, Atlanta, GA, April 2003.

The reader should consult Dr. Odman's web site for the current status of these publications (http://www.ce.gatech.edu/~todman).

References

Brost, R. A., P. L. Haagenson and Y.-H. Kuo (1988) The effect of diffusion on tracer puffs simulated by a regional scale Eulerian model. *J. Geophys. Res.* **93**, 2389-2404.

Kumar N. and A. G. Russell (1996) Development of a computationally efficient, reactive subgrid-scale plume model and the impact in the northeastern United States using increasing levels of chemical detail. *J. Geophys. Res.* **101**, 16737-16744.

Mathur, R., L. K. Peters and R. D. Saylor (1992) Sub-grid representation of emission source clusters in regional air quality modeling. *Atmos. Environ.* **26A**, 3219-3238.

Odman, M. T. and A. G. Russell (1991a) A Multiscale Finite Element Pollutant Transport Scheme for Urban and Regional Modeling, *Atmos. Environ.* **25 A**, 2385-2394.

Odman, M. T. (1997) A quantitative analysis of numerical diffusion Introduced by advection algorithms in air quality models. *Atmos. Environ.* **31**, 1933-1940.

Odman, M. T., Boylan, J. W., Wilkinson, J. G., Russell, A. G., Muller, S. F., Imhoff, R. E., Doty, K. G., Norris, W. B., and McNider, R. T. (2002) SAMI Air Quality Modeling Final Report, Southern Appalachian Mountain Initiative, Ashville, NC.

Srivastava, R.K., D. S. McRae and M. T. Odman (1996) Application of solution adaptive grid techniques to air quality modeling. 5th International Conference on Numerical Grid Generation in Computational Field Simulations, Starkville, Mississippi, April 1-

5, 1996, Proceedings Volume II, p. 1241-1258, NSF Engineering Research Center, Mississippi State University.

2 Coupling Air Quality and Meteorological Models

Paper published in (pp. 651-660): Air Pollution Modeling and its Application XIII: S.-E. Gryning and E. Batchvarova, Eds., New York: Kluwer Academic/Plenum Publishers, 2000.

==========

MASS CONSERVATIVE COUPLING OF

NON-HYDROSTATIC METEOROLOGICAL MODELS

WITH AIR QUALITY MODELS

M. Talat Odman and Armistead G. Russell

School of Civil and Environmental Engineering

Georgia Institute of Technology

Atlanta, Georgia 30332-0512, USA

2.1 Introduction

The high-resolution data produced by recent non-hydrostatic meteorological models (MMs) are expected to significantly improve the characterization of transport in air quality models (AQMs). The study of the formation of secondary pollutants should greatly benefit from this improvement. However, the use of data from non-hydrostatic MMs presents new problems to the air quality modeler. First, there is the *consistency* issue. The wind components together with air density satisfy the continuity equation in MMs. On the other hand, AQMs rely on the species continuity equation to enforce the principle of mass conservation. Though the continuity equation does not appear explicitly in their formulation, AQMs are expected to maintain a uniform mass mixing ratio field for an inert tracer after transport with the winds produced by the MM. This expectation could only realize if the two

models used the same *discretization*, i.e., grid, time step, and finite difference forms. However, the models may not share the same grid structure and the forms used for advection in AQMs are usually very different from those in MMs. Also, since the outputs of the MM are stored less frequently than the AQM time step, the input variables cannot be reconstructed exactly at the desired instants. Consequently, the winds and the air density used in AQMs may not be consistent (i.e., they do not satisfy the continuity equation) and the uniform tracer field cannot be maintained. The perturbation of uniform fields is usually more pronounced with data from non-hydrostatic MMs than with data from hydrostatic MMs for the same domains. These perturbations grow in time and may generate instabilities in AQM solutions. A second issue, species or tracer *mass conservation*, presents itself because of the attempts to establish consistency and produce stable results. In some existing AQMs, the conservation of species mass was sacrificed in order to obtain stable results. However, large mass conservation errors are not tolerable in AQMs used to establish source-receptor relationships for the design of emission control strategies. Therefore, it is desirable to establish consistency in a mass-conservative manner.

2.1 Methodology

The use of data from non-hydrostatic models may lead to unstable solutions due to the consistency problem, as described above. Some widely used AQMs adopted an approach where a uniform tracer is transported along with other species and the concentrations are renormalized using the deviation of the tracer from uniformity as the norm. As a result the uniform mixing ratio field is maintained. However, the approach overlooks that non-linear advection schemes are used in AQMs for high accuracy. These schemes would affect fields of different distributions differently. Most species of interest, especially the emitted ones, have spatial distributions far from being uniform. Therefore, renormalizing the concentration of a species based on the perturbation of a uniform field can increase or decrease its mass artificially. We found that the mass conservation errors introduced by this approach are very large. Here, we will refer to this approach as "the flawed method."

Species mass conservation is not sacrificed if the consistency of meteorological fields is established through the continuity equation. To satisfy the discrete continuity equation in the AQMs, wind or density fields (or both) from MMs must be adjusted. Lu et al. (1997) prefer adjusting the density field. Here we will describe three methods: two adjust the vertical wind component and a third adjusts the vertical flux. The methods also differ in the type of vertical advection algorithm used and whether a direct or iterative technique is used to solve for vertical wind component.

2.1.1 Method 1: Inverse Donor Cell

This method requires advection of air in addition to all the species and the use of the donor cell scheme for vertical advection.

$$c_k^{n+1} = c_k^* - \frac{\Delta t}{\Delta z_k}\left(w_{k+1/2}c_k^* - w_{k-1/2}c_{k-1}^*\right) \quad (1)$$

First, we apply horizontal wind components to the air density field, ρ^n, to obtain an intermediate field ρ^*. Any scheme can be used for horizontal advection; we used Bott's scheme (Bott, 1989). Then, we require that the density after the vertical advection operator is applied to ρ^*, be equal to ρ^{n+1}. The latter is calculated from the MM data by using linear interpolation in time. Thus, we need to calculate a new value for vertical velocity that would yield the desired value of density. Substituting concentrations with air densities, Equation (1) is solved for $w_{k+1/2}$ as

$$w_{k+1/2} = \frac{1}{\rho_k^*}\left(\frac{\Delta z_k}{\Delta t}\left(\rho_k^* - \rho_k^{n+1}\right) + w_{k-1/2}\rho_{k-1}^*\right) \tag{2}$$

Since $w_{1/2} = 0$, Equation (2) can be used starting from the surface layer (k=1) and moving to the top, each time using the vertical velocity computed for the previous layer. The winds at the top of the model will usually have a vertical component. The vertical velocities computed from Equation (2) must be used in Equation (1) to advect all other pollutant species. Note that the horizontal advection operator must always be applied before the vertical. Also, since the donor cell scheme is subject to the Courant stability condition, the case when the Courant number exceeds unity requires special treatment. Finally, the linear donor cell scheme is only first-order accurate.

2.1.2 Method 2: Inverse Bott Scheme

This method is very similar to Method 1 except a higher-order vertical advection scheme is used. Higher-order schemes are nonlinear because of the filters or flux limiters they use to eliminate the oscillations in the solution. Their non-linearity makes it difficult to solve for the vertical velocity field that would yield the air density ρ^{n+1} when applied to the horizontally advected air density field ρ^*. While a direct solution is not possible, iterative techniques can be used as suggested by Flatoy (1993). Here we used Bott's scheme with variable grid spacing for vertical advection. This scheme uses second-order area-preserving polynomials to represent the sub-grid distribution of concentration. The vertical velocity field can be calculated using the secant iteration technique.

$$w_{k+1/2}^{i+1} = w_{k+1/2}^{i} - \frac{w_{k+1/2}^{i} - w_{k+1/2}^{i-1}}{\rho_k^i - \rho_k^{i-1}}\left(\rho_k^i - \rho_k^{n+1}\right) \tag{3}$$

where ρ_k^i denotes the density field that the Bott's scheme would produce under the wind field $w_{k+1/2}^i$. To start the iterations two initial guess are needed, $w_{k+1/2}^0$ and $w_{k+1/2}^1$. The wind calculated by inverting the donor-cell scheme serves as $w_{k+1/2}^1$. The other initial guess is taken to be 90% of $w_{k+1/2}^i$. We interpreted convergence as ρ_k^i approaching ρ_k^{n+1} by a certain tolerance. Note that a uniform mixing ratio field advected with this method would be subject to very small perturbations, which can be reduced by decreasing the tolerance. We found that

a value of 0.5% is quite effective as a tolerance; smaller values led to unreasonably large number of iterations without too much improvement in the result.

2.2 Method 3: Inverse Donor Cell in 3-D and Russell and Lerner Scheme

This method is based on the approach described by Russell and Lerner (1981) and later used by Easter (1993). First the continuity equation is discretized in the following flux form.

$$\rho_{i,j,k}^{n+1} = \rho_{i,j,k}^{n} - \frac{\Delta t}{\Delta x}\left(F_{i+1/2,j,k}^{n} - F_{i-1/2,j,k}^{n}\right) - \frac{\Delta t}{\Delta y}\left(G_{i,j+1/2,k}^{n} - G_{i,j-1/2,k}^{n}\right) - \frac{\Delta t}{\Delta z}\left(H_{i,j,k+1/2}^{n} - H_{i,j,k-1/2}^{n}\right) \quad (4)$$

F, G, H are advective fluxes of air along the *x, y, z* directions, respectively. Then the species continuity equation is also written in the flux form.

$$c_{i,j,k}^{n+1} = c_{i,j,k}^{n} - \frac{\Delta t}{\Delta x}\left(A_{i+1/2,j,k}^{n} - A_{i-1/2,j,k}^{n}\right) - \frac{\Delta t}{\Delta y}\left(B_{i,j+1/2,k}^{n} - B_{i,j-1/2,k}^{n}\right) - \frac{\Delta t}{\Delta z}\left(C_{i,j,k+1/2}^{n} - C_{i,j,k-1/2}^{n}\right) \quad (5)$$

For consistency, the fluxes *A, B, C* must be related to their counterparts in Equation (4) by

$$A = Fr_x; B = Gr_y; C = Hr_z \quad (6)$$

where r_x, r_y, r_z are the average mixing ratios (i.e., c/ρ) crossing the grid cell boundaries in the *x, y, z* directions, respectively. We defined *F* and *G* as donor cell fluxes and solved Equation (4) for the vertical flux $H_{i,j,k+1/2}^{n}$ much like the solution for $w_{k+1/2}^{i}$ in Method 1. For comparison to other methods, we derived the corresponding vertical velocity by interpreting *H* also as a donor cell flux. The use of first-order accurate donor cell scheme for horizontal advection of air should not introduce large errors since the air density fields do not have the large gradients found in pollutant fields. It is more important to use higher-order schemes for advection of pollutant species. We used Bott's fourth-order area-preserving polynomials in the horizontal and his scheme for variable grid spacing in the vertical to compute the mixing ratios r_x, r_y, r_z.

2.3 Results and Discussion

Using the methods described above in an AQM (Odman and Ingram, 1996), we simulated a tracer experiment conducted during the Central California Air Quality Study (SARMAP). In this experiment inert tracers were released from different locations in the San Francisco Bay area and the Central Valley. All releases started at 6:00 PDT (Pacific Daylight

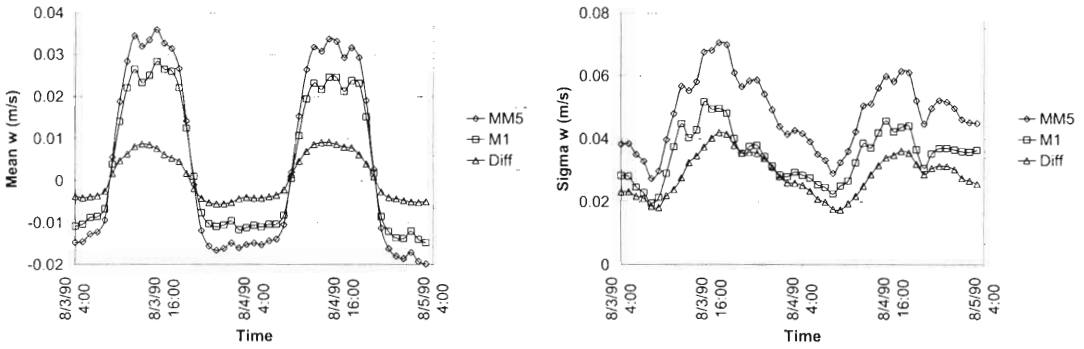

Figure 2-1 Time series of the mean (left) and standard deviation (right) of the first layer vertical velocity.

savings Time) on August 3, 1990 and lasted for 3-4 hours. The release rates were approximately uniform. Starting two hours before the releases and using fields generated by the NCAR Meteorological Model (MM5) we ran the model for 48 hours. The AQM grid covered the SARMAP domain with 32x39 cells of 12 km size. In the vertical, the grid extended to the stratosphere with 15 non-uniformly spaced layers starting with a thickness of 60 m at the surface and increasing upward. During the simulation, we did not only follow the tracer concentrations but the adjustments to the vertical wind components as well. When we analyzed these adjustments, we found a strong correlation with the terrain height. The adjustments were largest over the slopes of the coastal range and the Sierra Nevadas.

We found insignificantly small differences among the vertical velocities generated by the three methods. Therefore we will only use the velocity from Method 1 in our comparisons with the vertical wind components provided by MM5. The averages and the standard deviations of the MM5 and adjusted vertical wind components as well as their difference are illustrated in Figure 2-1 for the surface layer. The adjustment reduces the magnitude of the vertical wind by about 25% during the day when there is an upward component with an average of about 0.03 m/s and by 35% at night when the vertical velocity is downward. The standard deviations are also reduced. The standard deviations are smallest early in the morning and largest in the afternoon and remain so up to about level 11 where we reach the free troposphere.

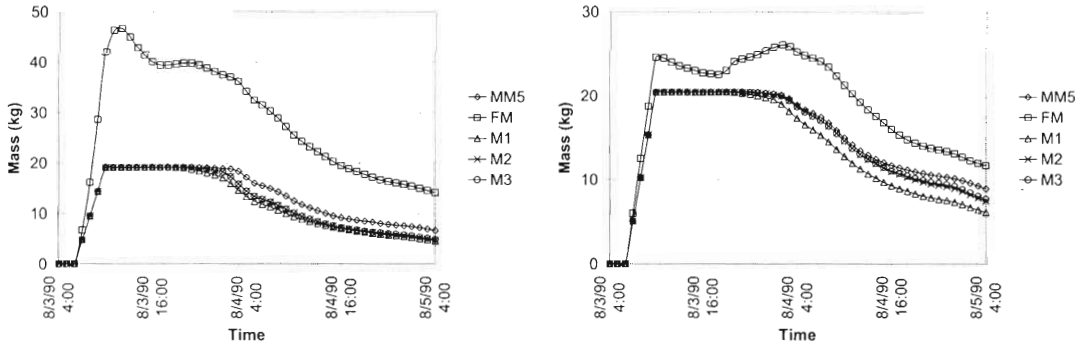

Figure 2-2 Time series of total mass of PMCH (left) and PMCP (right) as predicted by different methods: non-adjusted wind fields (MM5), flawed method (FM), and mass conservative Methods 1-3 (M1, M2, M3).

The averages and standard deviations are given in Table 2-1 for three different layers, the surface (0-60 m), the 5th (386-513 m) and the 11th layers (2155-3570 m). The values are reported at 700 PDT and 1500 PDT on August 3, 1990. In the PBL, relative to the magnitude of vertical velocity, the magnitude of the adjustment decreases with altitude. While the afternoon average adjustment is 21% at the surface it is only 8 % in the 5th layer. The relative difference starts increasing upon reaching the free troposphere. This may be related to the fact that the vertical velocity is small aloft and that the layer thicknesses are increasing with height. Also MM5 sets the vertical velocity to zero at the top of the troposphere while there is no such condition with the adjusted velocity. Data for the second day of the simulation had similar trends. The adjustment to the vertical velocity may be large in certain locations, especially over sloping terrain, but even then the absolute value of the vertical wind is small enough (few tenths of 1 m/s) that we do not expect to see a large impact on tracer or pollutant transport.

Table 2-1 Mean and standard deviation of vertical wind components in m/s.

		MM5		Adjusted[1]		Difference[2]	
Time	Layer	Mean	σ	Mean	σ	Mean	σ
700							
	1	-1.22E-02	3.29E-02	-8.55E-03	2.28E-02	-3.65E-03	2.10E-02
	5	1.25E-02	3.65E-02	9.06E-03	3.83E-02	3.42E-03	3.12E-02
	11	1.08E-02	1.01E-01	1.40E-02	1.23E-01	-3.19E-03	8.50E-02
1500							
	1	3.59E-02	6.75E-02	2.83E-02	5.17E-02	7.63E-03	3.74E-02
	5	3.26E-02	1.13E-01	3.00E-02	1.03E-01	2.60E-03	5.88E-02
	11	4.27E-03	1.69E-01	3.39E-02	2.26E-01	-2.96E-02	1.64E-01

[1]Method 1 is used to adjust the vertical velocity.
[2]The mean and standard deviation of the (MM5 - Adjusted) field.

The total mass of two tracers, PMCH and PMCP, as predicted by different methods is shown in Figure 2-2. The results of a simulation with unadjusted wind fields is also shown. The largest conservation error is associated with PMCH mass. This tracer was released from San Jose and has a trajectory over complex coastal terrain. While only 19 kg of tracer was released, the flawed method leads to an estimate of 46 kg of PMCH at 1100 PDT. Other methods are able to maintain total tracer mass at 19 kg as long as the tracer remains within the domain. The decrease in total mass after 2100 PDT is associated with tracer crossing the lateral or top domain boundaries. The mass conservation error of the flawed method is also significant (approximately 25 %) for the PMCP tracer released from Pittsburgh in the San Francisco Bay area. The error is not as significant for other releases from the Central Valley.

In Figure 2-3 the time series of observed and predicted PMCP concentrations are shown at two sites. The distance from the release point to these sites, Brentwood and Friant, are approximately 30 and 220 km, respectively. The observations are provided as 2-hour averaged concentrations. The predicted concentrations were also averaged to match observations. The peak concentration predicted by all methods are larger than the observed peak at Brentwood. Compared to the flawed method, all three mass conservative methods yield a peak value closer to the observation, but the overprediction is still of the order of 60-70%. The closest value to the observation is obtained when MM5 winds are used without any adjustment. The predictions of the flawed method are not too far off from those of mass conservative methods. This indicates that the mass conservation errors are small along the trajectory to this site. At Friant the predicted peaks are closer to the observations but they display a time lag. This is not surprising given the relatively larger distance of this site from the release point. In contrast to the former site, the use of unadjusted MM5 winds led to the largest overprediction. The peak predicted by Method 1 is the closest to the observation. At both sites the difference between observed and predicted concentrations are larger than the differences between different methods. Therefore, it is difficult to judge which method performs better in this tracer transport simulation.

Using the same model settings a five-day ozone episode (August 2-6, 1990) was simulated over the same domain. The ground level ozone concentrations at 1700 PDT on

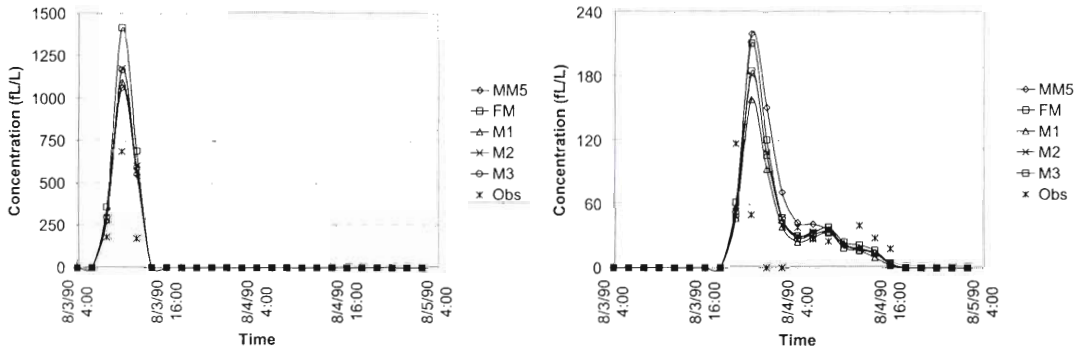

Figure 2-3 The time series of observed and predicted PMCP concentrations at Brentwood (left) and Friant (right).

August 5 are shown in Figure 2-4. The inconsistencies in MM5 wind fields led to instabilities during this simulation and yielded unreasonably high ozone. Methods 2 and 3 produced practically identical results therefore only Method 2 will be discussed. The differences between ozone levels predicted by the flawed method and Method 1 are of the order of 15 ppb near the coastal range. Method 1 predicts higher ozone concentrations in major source areas to the south of the San Francisco Bay, such as San Jose. On the other hand, further to the southeast (downwind), ozone concentrations predicted by Method 1 are lower. This may be due to an erroneous increase in the mass of nitrogen oxides in the flawed method. In comparison to Method 1, Method 2 predicted slightly higher (of the order of few ppb) ozone concentrations over the Central Valley and slightly lower concentrations over more complex terrain such as the coastal range and the foot-hills of the Sierra Nevadas. The maximum difference was observed at Fresno where Method 2 predicted 7 ppb higher ozone than Method 1. Recall that the differences between the vertical wind components of Method 1 and Method 2 were negligible. Therefore, the differences in ozone levels characterize the impact of using a more accurate vertical advection scheme in Method 2. Finally, the differences were more pronounced at night and early in the morning. For example at 900 PDT August 5, Method 1 predicted ozone levels 15 ppb lower than the flawed method at Sacramento and 25 ppb lower southwest of the Central Valley.

Figure 2-5 shows the maximum and the standard deviation of ground level ozone concentrations as predicted by different methods. On the first day, the flawed method predicts about 10 ppb lower peak ozone that the mass conservative methods. It also estimates a maximum concentration of 125 ppb at 900 PDT on August 5. This is about 45 ppb higher than the estimates of other methods. The peak ozone predictions of the flawed method are 10 to 20 ppb higher at night. Method 1 led to the lowest nighttime ozone estimates, with differences of up to 10 ppb from other methods early in the morning. The estimates of Methods 2 and 3 are almost identical. Method 1 resulted in the smallest standard deviation: as much as 1 ppb lower than other methods during the day and 1 to 2 ppb lower than Methods 2 and 3 at night. The nighttime standard deviation of the flawed method was the highest, about 2 to 4 ppb higher than Method 1.

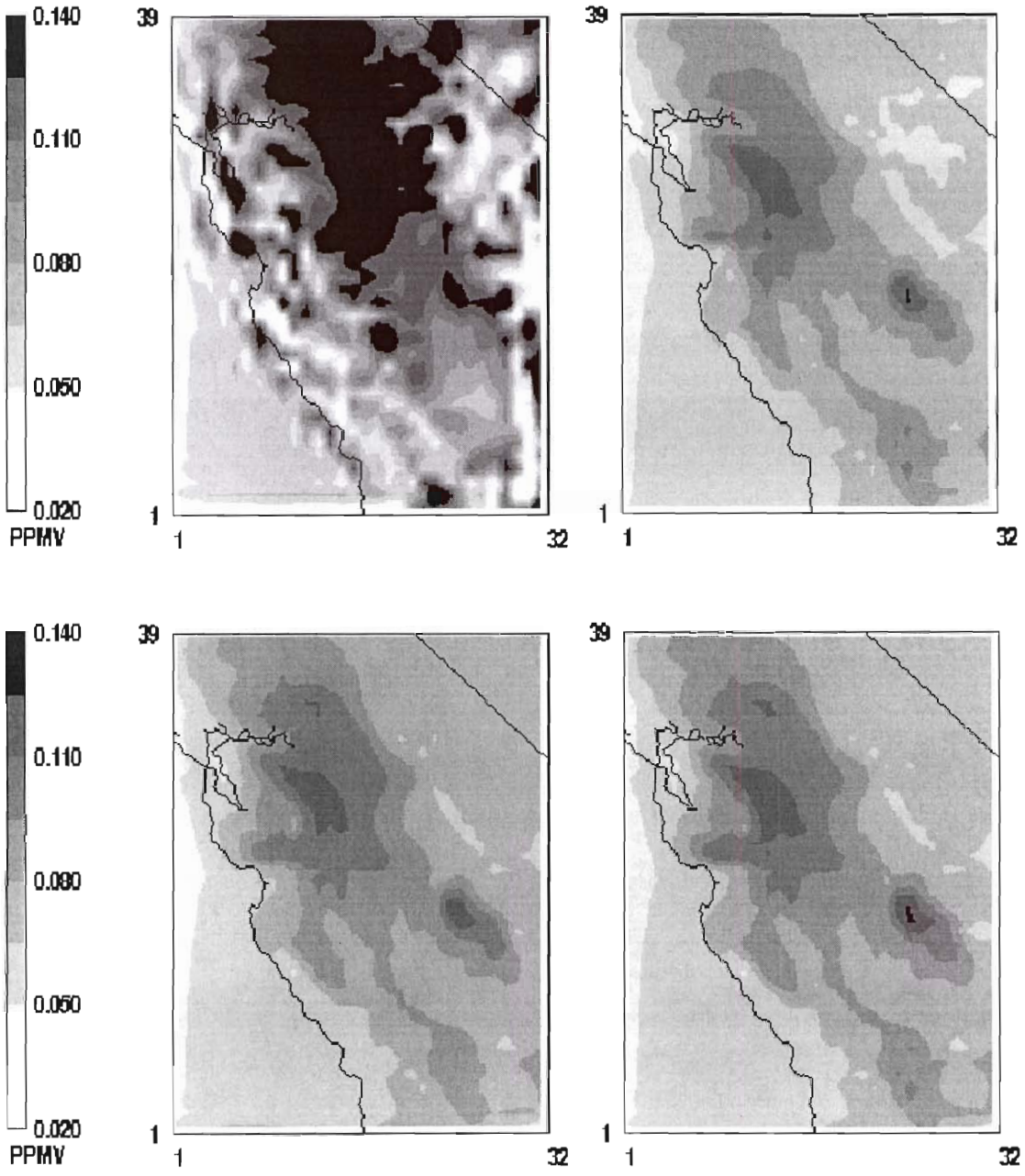

Figure 2-4 Spatial distribution of surface layer ozone at 1700 PDT August 5, 1990 as predicted by the non-adjusted wind fields (upper-left), flawed method (upper-right), and Methods 1 and 2 (lower left and right).

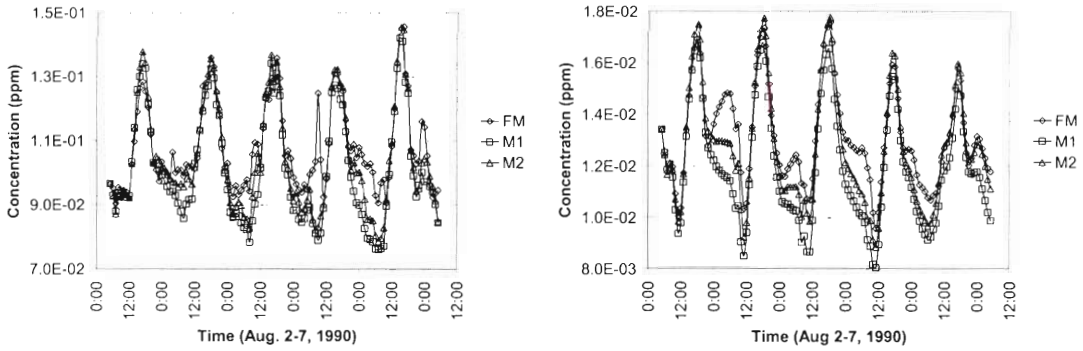

Figure 2-5 The time series of the maximum ozone concentration (left) and the standard deviation of surface layer ozone (right) as predicted by the flawed method (FM), and mass conservative Methods 1&2 (M1, M2).

2.4 Conclusions

The inconsistency of data from non-hydrostatic MMs may lead to instabilities in AQMs. Meteorological data can be made consistent without sacrificing the mass conservation characteristics of the AQM. Adjusting the vertical wind component proved to be an effective technique. We implemented and compared three methods for obtaining the vertical wind component from the discrete continuity equation. The methods differ in their vertical advection schemes. We found that the methods produced very similar vertical wind fields but these fields differed from those supplied by the MM. The adjustments reduced the vertical wind speed by an average of about 30% near the surface. The reduction was more pronounced at night when the winds have a weaker downward component. Also, the reduction decreased with altitude in the PBL but started increasing again in the free troposphere where the winds are practically horizontal. Thus, the adjustments may be large relative to the vertical winds but this is generally the case when the wind speeds are small. This implies that overall tracer transport would not be significantly affected by the adjustments. The tracer experiment simulation provided partial support for this hypothesis. Along a limited number of trajectories the original and adjusted wind fields yielded similar results. Unfortunately, the uncertainties in the tracer data and other parameters of the AQM are too large for more definite conclusions. We were unable to determine which one of the three methods best characterizes tracer transport. In an air quality simulation there were small differences in ozone levels predicted by the three methods. These are due to the use of vertical advection schemes of different accuracies. Methods with higher-order schemes seem to perform better but a more complete evaluation is needed at this point.

References

Bott, A., 1989, A positive definite advection scheme obtained by nonlinear renormalization of the advective fluxes, Mon. Wea. Rev. 117:1006.

Easter, R.C., 1993, Two modified versions of Bott's positive-definite numerical advection scheme, Mon. Wea. Rev. 121:297.

Flatoy, F., 1993, Balanced wind in advanced advection schemes when species with long lifetimes are transported, Atmos. Environ. 27A:1809.

Lu, R., Turco, R.P., and Jacobson, M.Z., 1997, An integrated air pollution modeling system for urban and regional scales: 1. Structure and performance, J. Geophys. Res. 102:6063.

Odman, M.T, Ingram, C., 1996, Multiscale Air Quality Simulation Platform (MAQSIP): Source Code Documentation and Validation, MCNC Technical Report ENV-96TR002, Research Triangle Park, North Carolina.

Russell, G.L., and Lerner, J.A., 1981, A new finite-differencing scheme for the tracer equation, J. Appl. Meteor. 20:1483.

3 Hand-over Criteria for Subgrid Scale Plume Models

3.1 Introduction

Sub-grid scale reactive plume models have received recent attention as a means of improving the accuracy with which point emission sources can be included in regional air quality model simulations. The goal of these sub-grid models is to provide detailed initiation, reaction and propagation of the plume constituents from local sources at resolution scales not available in the regional model. The standard implementation of a sub-grid model develops the plume in the fine-scale sub-grid and then, when a predetermined hand-over criterion is met, the plume is injected into the regional air quality model (RAQM) grid after which the plume becomes a component of the overall simulation.

In the past, these models have not improved the predictive skill of AQMs, at least on a regional scale (Kumar and Russell [1]). We believe that this is primarily due to improper use of these so-called "plume-in-grid" models. Odman [2] found that without proper judgment of the numerical diffusion introduced by transport algorithms, the benefits from sub-grid scale models can easily be lost. Numerical diffusion can be relatively large at scales comparable to one or two grid lengths. This can eliminate completely the high-resolution information coming from the sub-grid plume model. The result may be identical to instantaneous mixing of the plume within the grid cell, which happens in the absence of plume-in-grid models. Research has been performed to identify and begin to quantify the central issues in developing hand-over criteria so that plume in grid models can be employed in a manner that will preserve the potential accuracy improvement that this concept promises.

These hand-over criteria must have a foundation in the mathematical characteristics of the algorithm and include analysis of both mesh and modeled terms influence for both fine and coarse grids. Information coming from the sub-grid plume model must be blended effectively into the regional grid model. As an adjunct to the central issue of criteria, improved means for conservative transfer of sub-grid information to the regional grid is now possible, based on a conservative transfer algorithm developed under another grant.

An alternative to the use of plume in grid models is to adapt the regional grid to improve resolution and accuracy. The technology developed for the transfer criteria can also be used to assess the efficacy of the dynamic solution adaptive mesh algorithm (now included in a RAQM) when compared with sub grid propagation of plumes as an alternative.

The remainder of this report will present research findings and suggestions for future work. The theoretical basis for determining how computations are resolved by discrete meshes are examined followed by a procedure for determining frequency content in a given computational result. A procedure is demonstrated on model problems and 2-D plumes by which a sub-grid scale result is analyzed for frequency content and then filtered to approximate the effect of transfer to a coarser mesh. The procedure is extended to 2-D analysis of 3-D plumes and is also demonstrated on a full RAQM simulation obtained with a dynamic solution adaptive mesh. Finally techniques are developed that allow direct, continuous comparison of aircraft and simulation data regardless of aircraft track or altitude.

These techniques are then used as a basis for a suggestion for improving initialization of RAQM simulation. Finally, conclusions are drawn based on the research findings.

3.2 Theoretical Basis for Solution Propagation in Discrete Meshes

Fundamental work in error analysis points to Fourier analysis as a candidate tool for analyzing the propagation of a solution by a difference scheme in a discrete mesh [3]. This statement relies on the fact a single valued continuous function can be constructed by determining the appropriate coefficients for a sufficient number of terms in a Fourier series. When the function is defined on a discrete domain, the concept of allowable frequencies must be introduced [3]. For instance, the minimum frequency that can be "resolved" on a 1-D domain of extent 2L has a wave number of $2\pi / 2L = k = \pi / L$. This means that precisely one wavelength fits within the domain and that only one discrete node at the domain center is required to "resolve" the frequency. Conversely, if the domain is divided evenly into intervals of Δx, the maximum frequency that can be resolved is $k = 2\pi / 2\Delta x = \pi / \Delta x$. If the question of aliasing is ignored, then the discrete mesh can be said to be a band pass filter, admitting frequencies corresponding to $\pi / L \le k \le \pi / \Delta x$. In the context of constructing a function with a Fourier series, we see that instead of having an infinite number of frequencies to use, as is the case in a continuously defined domain, we only have a restricted set. Clearly, the fidelity of the constructed function must suffer because of the frequency deficit.

The basic justification for increasing the number of discrete nodes in a domain is to increase the set of available frequencies thereby increasing the fidelity of the function constructed by the numerical algorithm [4,5]. This also leads to the basic justification for a solution adaptive mesh; if the number of mesh nodes can be increased locally where the solution is varying rapidly rather than increased globally as required by constant mesh spacing, large savings in computational effort result for a specified level of solution resolution.

However, further elimination of frequencies from the solution results from the application of numerical integration schemes. Odman [2] analyzed four schemes applied to the advection equation and evaluated the amplification factor based on a modified equation analysis [3,4,5]. This work includes the diffusion based on the error terms due to the temporal and spatial derivatives of the advection equation but did not include the effects of the fluid turbulence model and the errors resulting from this term. The present analysis will investigate the diffusion due to the turbulence model and will compare the model equation analysis of these terms with the diffusion found by Odman.

In order to illustrate this concept, we apply a simple forward time centered space (FTCS) algorithm to the 1-D heat equation:

$$u_t + \alpha u_{xx} = 0$$

which becomes after differencing:

$$u_i^{n+1} = u_i^n + r(u_{i+1}^n - 2u_i^n + u_{i-1}^n)$$

where

$$r = \frac{\alpha \Delta t}{\Delta x^2}$$

If the FTCS algorithm were applied to a standard advection scheme, the resulting truncation error would be both dispersive and dissipative. However, since the major effect of atmospheric turbulence is strong dissipation, dispersion may be damped when a model for turbulence is included in the advection equation and will not be included in the present analysis. Therefore, the heat equation is an excellent model equation to study the combined effect of numerical schemes and mesh size on the solution.

The so-called "modified equation" [3] results from a Taylor's series expansion of the differencing scheme and is closely related to the actual differential equation solved by the specific scheme. For FTCS applied to the heat equation, the modified equation is:

$$u_t - \alpha u_{xx} = [-\frac{1}{2}\alpha^2 \Delta t + \frac{\alpha(\Delta x)^2}{12}]u_{xxxx} + [\frac{1}{3}\alpha^3 (\Delta t)^2 - \frac{1}{12}\alpha^2 \Delta t (\Delta x)^2 + \frac{\alpha(\Delta x)^4}{360}]u_{xxxxxx} + \cdots$$

Much information can be obtained about the comparative effect of integrating the original PDE and the modified PDE by performing a Fourier analysis of these equations.

Assuming a single 1-D Fourier component:

$$u(x,t) = e^{at} e^{ikx}$$

where k is a wave number corresponding to a given reduced frequency and e^{at} is a Fourier amplitude. Substitution of this single frequency solution into the heat equation gives:

$$a e^{at} e^{ikx} = -\alpha k^2 e^{at} e^{ikx}$$

or

$$a = -\alpha k^2$$

resulting in a Fourier amplitude of $e^{-\alpha k^2 t}$. This implies that the amplitude of a given frequency in the solution is reduced by $1/e^{\alpha k^2}$ for each unit of time advancement. The physical interpretation of this result is not surprising; high frequencies in the solution are damped dramatically during temporal integration of the heat equation.

A similar analysis of the modified equation for FTCS gives:

$$ae^{at}e^{ikx} = -\alpha k^2 e^{at}e^{ikx} + k^4[-\frac{1}{2}\alpha^2\Delta t + \frac{\alpha(\Delta x)^2}{12}]e^{at}e^{ikx} - k^6[\frac{1}{3}\alpha^3(\Delta t)^2 - \frac{1}{12}\alpha^2\Delta t(\Delta x)^2 + \frac{\alpha(\Delta x)^4}{360}]e^{at}e^{ikx}\cdots$$

which becomes

$$a = -\alpha k^2 - \frac{1}{2}\alpha^2\Delta t k^4 + \frac{\alpha(\Delta x)^2}{12}k^4 - \frac{1}{3}\alpha^3(\Delta t)^2 k^6 + \frac{1}{12}\alpha^2\Delta t(\Delta x)^2 k^6 - \frac{\alpha(\Delta x)^4}{360}k^6\cdots$$

Examination of this result reveals two interesting points:

1) The leading dissipative term in the truncation error of this first order method is due to the time derivative.

2) The leading error due to the diffusive term central difference approximation is anti-diffusive.

It is instructive to compare the relative magnitudes of the individual amplitude terms for the range of frequencies admissible by a typical mesh.

Let $r = \frac{\alpha\Delta t}{\Delta x^2} = \frac{1}{2}$, which is the stability bound for this method. For a domain of L=1, let $\Delta x = 0.1$ and $\alpha = 0.01$, which requires $\Delta t = \frac{1}{2}$. Note that since these equations are continuous rather than discrete, the actual range of frequencies corresponds to $0 \le k \le \infty$. However we are only interested in the frequencies that a given discrete mesh could resolve, i.e. $\frac{\pi}{L} \le k \le \frac{\pi}{\Delta x}$. For the present case, these are $\pi \le k \le 10\pi$. The end of range values for the unit time advancement Fourier amplitude for the terms appearing in the modified equation are given in Table 3-1.

Note that the lower frequencies are not damped very much during a unit time

Table 3-1 The range of Fourier amplitudes in modified heat equation.

a_j	$e^{a_j};k_{\min}$	$e^{a_j};k_{\max}$
$-\alpha k^2$	0.906	0.373
$-\frac{1}{2}\alpha^2\Delta t k^4$	0.998	~ 0.000
$\frac{\alpha(\Delta x)^2}{12}k^4$	1.001	3352
$-\frac{\alpha(\Delta x)^4}{360}k^6$	0.999	0.069

application of the numerical scheme, but that the highest frequencies resolved by the mesh are essentially eliminated from the solution after only a few applications of the integration scheme. This agrees with the conclusion of Odman [2] although the overall Fourier amplitudes that he found at k_{max} for four schemes ranged from ~ 0.35 to 0.6 at a Courant number of 0.75. Also, the reason that this explicit scheme becomes unstable for $r > \frac{1}{2}$ can be attributed to the anti-diffusive Fourier amplitudes, requiring that at least one or a product of the other amplitudes be at maximum 10^{-4} for stability at k_{max} for these conditions. Clearly the relative magnitudes of these Fourier amplitude terms would change for other conditions. However, the conclusion is inescapable that knowledge of the damping characteristics of both the sub-grid scheme and the coarse grid scheme must be included when devising plume handoff criteria.

In order to further illustrate this point, Figure 3-1 contains a not-to-scale sketch of the frequency domains for two mesh spacings superimposed on the same physical domain. The curves represent approximate amplitude versus wave number distribution in each case after some dissipation of the solution has taken place through successive application of an integration scheme. The wave number scales are the same in both cases, indicating that more frequencies are present for the fine mesh example. Here $\Delta x = 0.1$ and 0.01 respectively.

If the solution on the lower fine grid (sub-grid) is injected into the upper coarse grid, it is clear that much of the information present on the sub-grid will be lost, first through filtration by the mesh and second through subsequent dissipation by the coarse grid numerical scheme.

The analysis and discussion presented above indicates that it is unlikely that simple straightforward criteria will be found for the hand-over from the sub-grid. The next section will outline the development and testing of the candidate criteria.

3.3 Development and Investigation of Hand-over Criteria

Prior to discussion of the details of the criteria development, a brief review of the

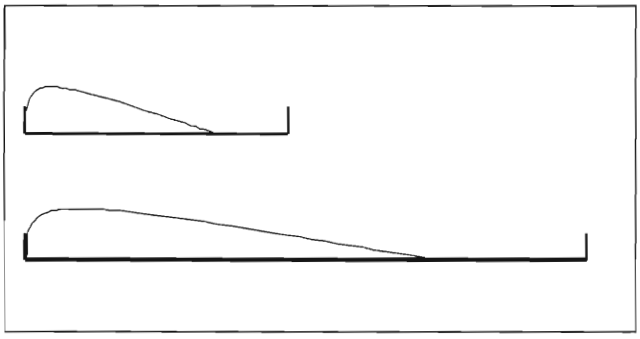

Figure 3-1 Illustration of comparative frequency spectrum for two mesh spacings.

reasons for sub-grid models should help focus the issues. The fundamental reason for use of a sub-grid plume model is that plume sources may be small physically compared to the normal grid spacing for a regional air quality model. Although the emission source output may be quite large in magnitude compared to local background levels, the immediate averaging of emission concentrations that takes place at full regional model grid spacing gives very poor resolution of the local chemistry. Since reaction rates vary with concentration, the reduction in concentration by orders of magnitude due to immediate averaging of the source output over a large cell will affect dramatically chemistry in the vitally important immediate vicinity of the source. A sub-grid model provides a reasonable means of addressing this problem in that it evolves the plume at much finer resolution than is available in the RAQM. However, inserting the results of sub-grid propagation of the plume into the regional model field has not been very successful. Therefore, a more detailed investigation of the factors affecting both the propagation of the solution and the success of inclusion of results from a sub-grid model was undertaken.

The space-time evolution of a pollutant plume is determined primarily by the following factors, whether the evolution takes place in a sub-grid or a regional model:

1) Accuracy and truncation error terms of the numerical integration scheme. The actual diffusion of the solution depends on these terms and on the diffusion due to the atmospheric turbulence model. Since there is no guarantee that both sub-grid and regional models will use the same scheme, this information must be obtained or derived in each case. For modern non-linear schemes, it may be difficult to derive the actual truncation error terms [2]. However, in most cases, generic terms based on order of accuracy are likely to be sufficient for determining handoff criteria.

2) Computational mesh cell volume magnitude and volume distribution. This is an absolute accuracy limiter for a given scheme.

3) Chemistry model. Since the reaction rates depend on local concentration of species, the preservation of local concentration peaks without excess diffusion is a key requirement for any model to give accurate plume propagation.

In order to provide a simple illustration of these issues, examples will be shown from the numerical work of Srivastava [6]. Figure 3-2, which illustrates a conical initial concentration distribution after a 360-degree rotation by a numerically integrated advection equation: a) on a fixed evenly spaced mesh and b) on a dynamic solution adaptive mesh. Note that the adapted mesh solution has preserved the "peak" of the distribution (the exact solution is advection of the initial distribution without change) whereas the evenly spaced mesh solution shows much greater diffusion. In the current context, this means that the numerical scheme had more frequencies available in the fine locally adaptive mesh with which to construct the solution thereby resulting in greater solution fidelity. Note that the integration scheme and the total number of nodes were the same in both cases.

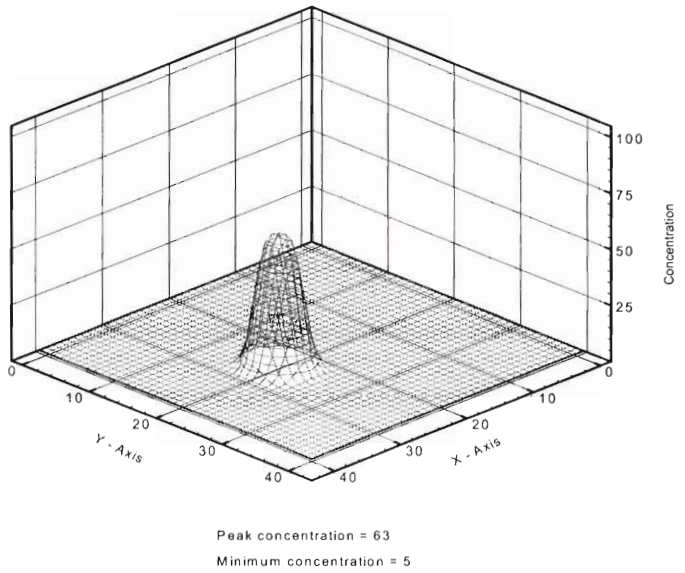

(a)

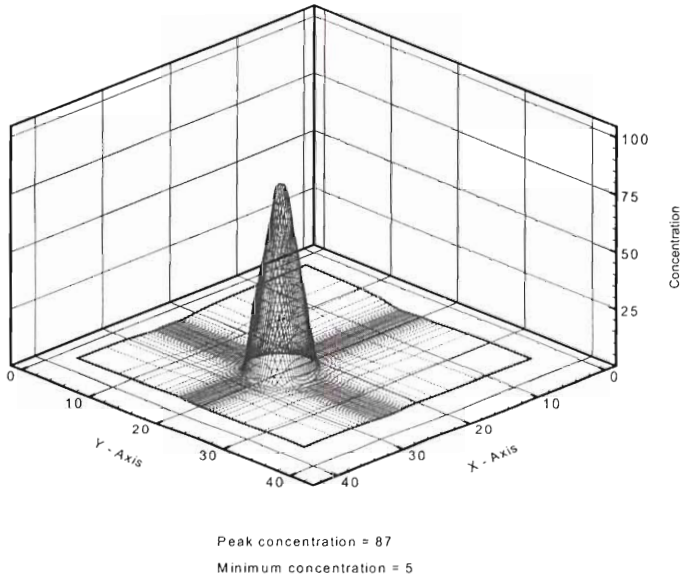

(b)

Figure 3-2 [6]. Rotating cone results obtained with (a) SGA-PPM (b) DSAGA- PPM

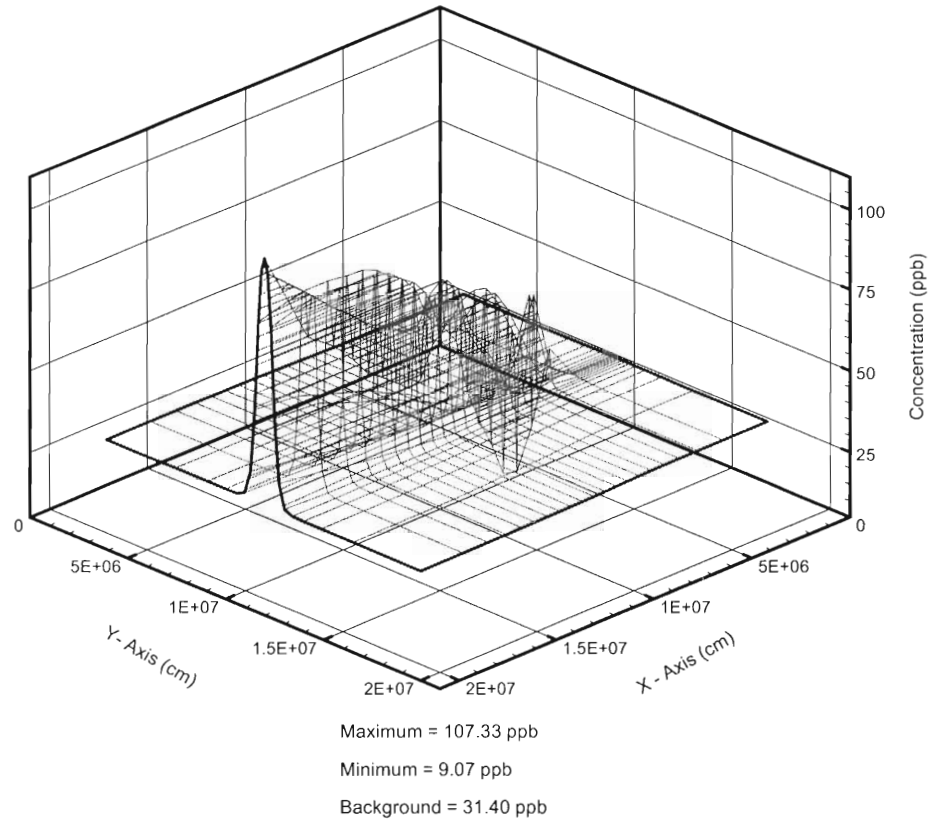

Figure 3-3 [6]. Three-dimensional depiction of DSAGA-PPM results for O_3 concentration at 40,000 seconds.

In order to illustrate the task of analyzing the frequency spectrum for a more realistic plume calculation, Figure 3-3 from [6] shows the ozone concentration of a sample highly resolved plume calculation after 40,000 seconds. The complex distribution of this single constituent supports the earlier statement that a simple hand-over criteria is unlikely to be successful.

3.4 Procedure

Based on the theory of the previous section, the following procedure has been developed:

1) The procedure begins with a sub-grid or other representative plume model, which is used to produce a well-resolved plume on a fine grid. Based on the diffusion of the plume and other (if warranted) development criteria, a downstream location is chosen to begin assessing the ability of the RAQM mesh to resolve the plume adequately. A line (for assessment of a plume defined in 2-D) or a surface (plume defined in 3-D) is then defined

perpendicular to the local advection direction for the plume. This choice is independent of the grids on which the plume or the RAQM is defined.

2) The chosen plume species distribution is then interpolated to nodes on the line or surface defined in 1. Sufficient nodes are used to preserve the species distribution that exists in the original plume. Higher order interpolation techniques are used to minimize loss of information.

3) A Discrete Fourier Transform (DFT) is performed on the interpolated distribution using Fast Fourier Transform (FFT) algorithms in order to obtain the frequency-amplitude spectra. The frequency-amplitude distribution is then shifted for convenient visualization to a frequency scale with zero frequency in the center and higher harmonics appearing on either side.

4) This centered frequency-amplitude distribution is then filtered to remove those frequencies that would not be resolved by the coarser RAQM mesh. The filtration is guided by the frequency resolution theory given in the mathematical background section.

5) An Inverse Fourier Transform (IFFT) is then performed to obtain the function in the physical space corresponding to the filtered distribution.

6) The last step is to examine the data as it approximately represents the solution as resolved by the coarse mesh and compare it with that of the original distribution in the refined grid plume. Two types of comparisons can be made. First, the original distribution as resolved by the refined grid and the distribution as the coarse mesh would approximately resolve it can be over-plotted. This will allow visual evaluation of the changes. Secondly, the comparison needs to be quantified in order to allow automation of the hand over criteria for injection of the plume into the regional grid. The Energy method, which is based on the square of the amplitudes in the Fourier transform, is examined as a criterion for comparison. Another alternative to the energy method is to pack the frequencies outside the cut off region after the filtration with zero amplitude and perform the inverse transform. This would result in a distribution in the physical space with the size of the domain being the same as the original distribution. Any of the standard norms could then be used for error analysis.

This procedure has been successfully employed to analyze plume cross-sections in one-dimension and two-dimensions. FFT algorithms are used for computing the DFT and its inverse for analysis of plume data, as they are computationally efficient. If the number of grid points in the domain is a power of two, a fast radix-2 FFT algorithm [2] is used. Otherwise a slower non-power-of -two algorithm is employed.

3.5 Illustrative Examples

3.5.1 Analysis in 1-D

The analysis technique is first demonstrated by analyzing a planar cross section of a typical plume from the work of Srivastava [3]. Figure 3-4 shows the ozone concentration in a

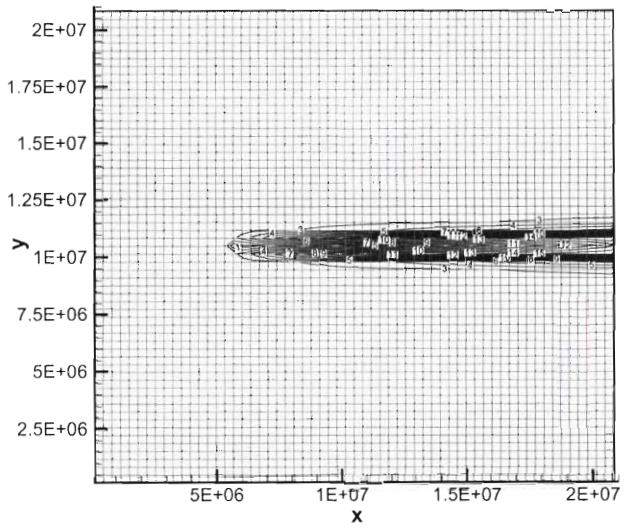

Figure 3-4 Typical 2-D plume.

plume resolved by a 61 x 61 uniform mesh. This plume is used to represent the solution obtained by a typical Plume-In-Grid model. A line (2-D) or a surface (3-D) is chosen perpendicular to the advection direction of the plume. A second order Bilinear-Interpolation technique is used to interpolate the plume distribution with sufficient points on the line or surface to ensure accuracy of the species distribution.

The analysis proceeds by selecting a location to begin testing the plume for maturity/diffusion at RAQM grid resolution scales. The ozone data of Figure 3-4 are interpolated to 200 grid points on a line perpendicular to the centerline 25 km from the source. Figure 3-5 shows the results of filtering frequencies corresponding to 151, 91 and 31 grid points respectively. The distribution in this case has most of the information in the lower frequencies. This means that the distribution will be relatively unchanged until projected to a mesh with significantly fewer nodes than the original. Filtration is shown with solid lines increasing in thickness as the mesh size is decreased. The effect of filtering the frequencies corresponding to the selected mesh sizes can be seen in Figure 3-6. For this species, the distribution reconstructed from the filtered frequency-amplitude data retains its initial character until filtered to 31 nodes (one half of the original mesh points). The energy function values are tabulated on Table 3-2.

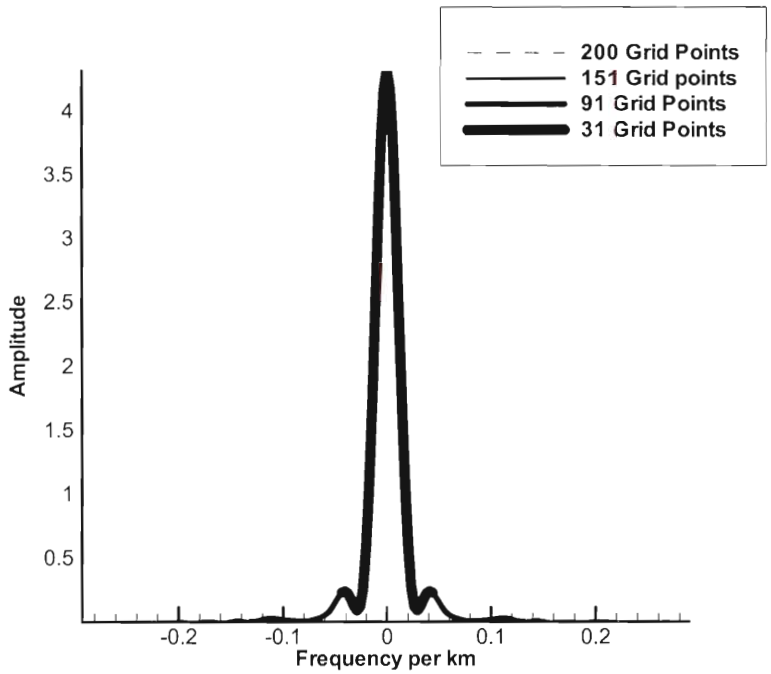

Figure 3-5 Frequency-amplitude spectrum for original and filtered data for O_3 species

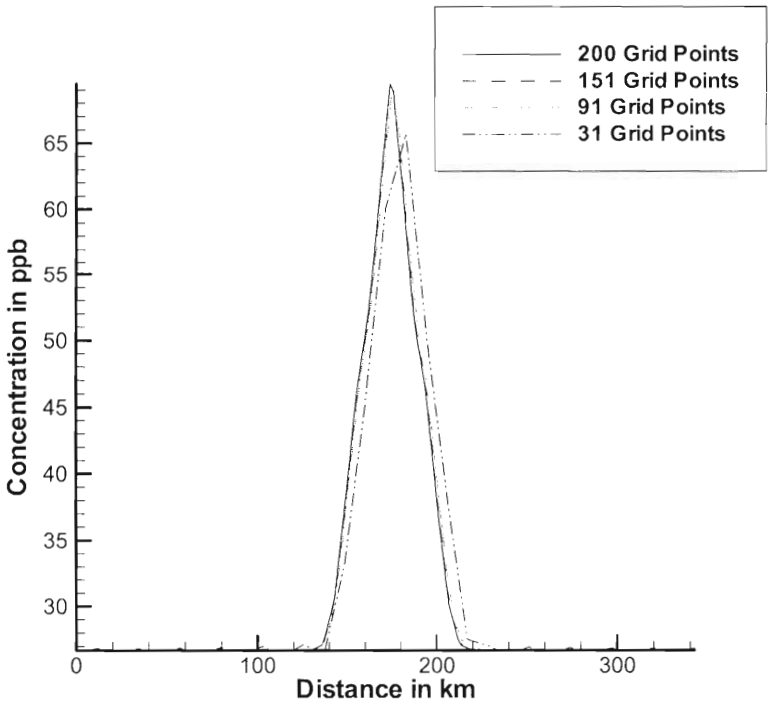

Figure 3-6 Original and filtered distribution of O_3 species in physical space

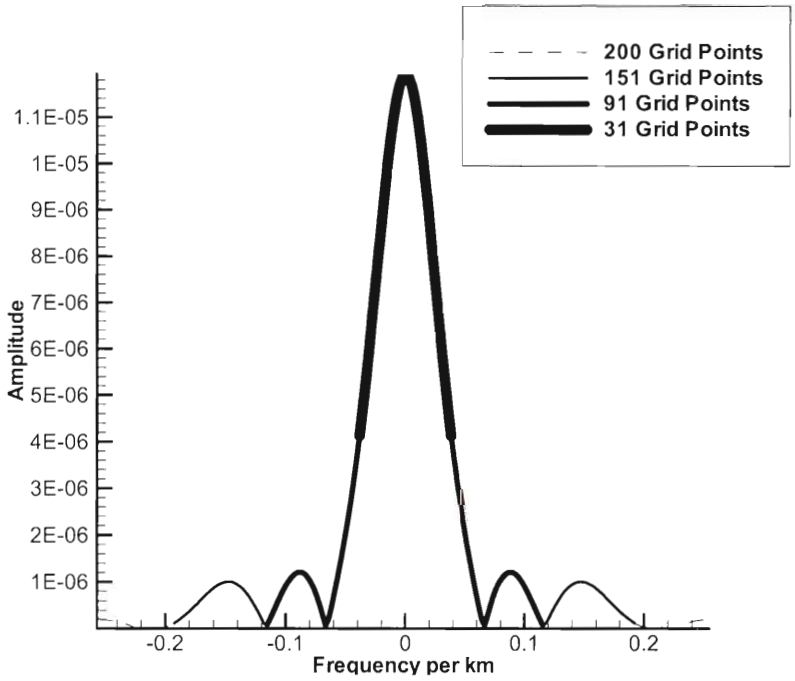

Figure 3-7 Frequency-amplitude spectrum for original and filtered data for OH species

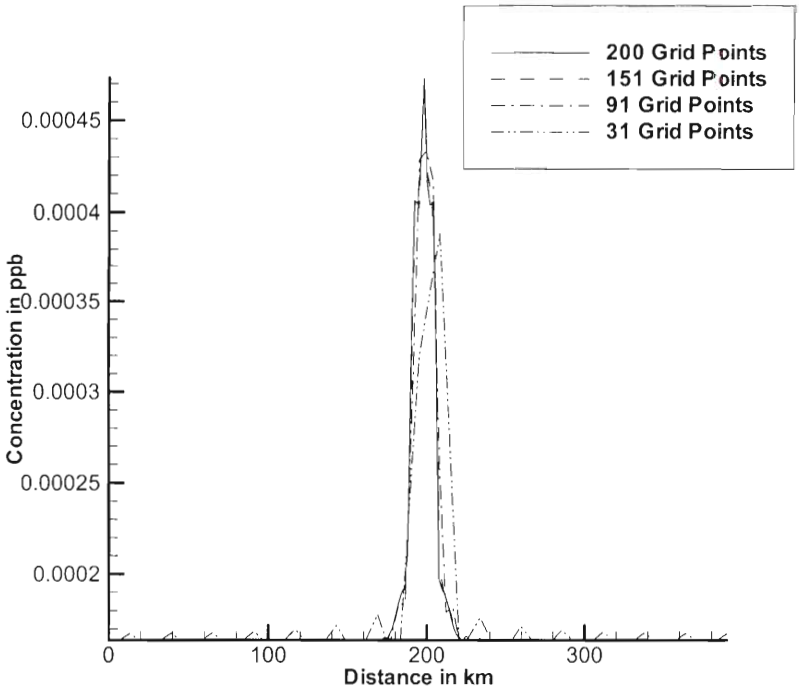

Figure 3-8 Original and filtered distribution of OH species in physical space

Table 3-2 Energy Function Values at Different Grid Sizes for the Two Species

Grid Size	Species 1	Species 2
200 Points	1.0000	1.0000
151 Points	0.9996	0.9977
91 Points	0.9995	0.9888
31 Points	0.9431	0.9320

Figure 3-7 and Figure 3-8 show the Amplitude–Frequency Spectrum and the original and filtered distribution for a different species (OH). It is observed that only the filtered distribution with 151 grid points closely reproduces the original distribution. This is also reflected in the values of Energy Function as shown on Table 3-2.

It is seen from the plots and the values of the Energy function, that a coarse grid would better resolve the first species (ozone) when compared to the second species (OH). This result can be inferred from the frequency-amplitude spectra. The filtering process involves the removal of higher frequencies, which in this case corresponds to smaller amplitudes in the spectra. The filtered distribution in physical space closely resembles the original distribution as long as the amplitudes that are filtered do not contribute significantly in the Inverse Fourier Transforms to physical space. However, if the frequencies corresponding to higher amplitudes contain significant information and are filtered, significant deviation from the original distribution in the physical space is observed. As seen in Figure 5, the amplitude is significant in the frequency range of -0.08 to +0.08 km^{-1}. If this range of frequencies is included in the inverse transform, the distribution resulting from the inverse transform should be similar to the original distribution in physical space. This is confirmed as the first species inverse resembles closely the original distribution for grid sizes with 151 and 91 grid points, and exhibits some variation when filtered to 31 grid points (Figure 3-6). In Figure 3-7, the distribution of the second species (OH) contains information in almost the entire frequency range from -0.2 to +0.2 km-1. Hence the distribution begins to depart from the original for less filtration than for ozone (Figure 3-8). This is also demonstrated by the values of the Energy function shown in Table 3-2. Thus at a particular location downstream from the source, it is essential that all of the important constituents in the pollution model be checked for resolution. The hand over criteria, based on the RAQM grid size, will provide an estimate of how much information will be lost if the plume is transferred at its current development.

3.5.2 Analysis in 2-D

The technique can be used to analyze 3-D sub-grid plumes to assess whether information will be lost in transferring to the full 3-D RAQM grid. In order that the results can be related to the 2-D to 1-D analysis above, one of the plumes described on a 2-D surface was rotated about its centerline axis and interpolated to a 3-D evenly spaced grid domain. This gives a 3-D distribution that, when sampled in 1-D as in the previous sub-section, will give essentially the same results. The 3-D to 2-D sampling results will then be conceptually easy to relate to the 1-D results.

The 3-D axis-symmetric distribution interpolated from a 61 x 61 x 61 mesh to a 200 x 200-mesh surface is shown in Figure 3-9. The resulting 2-D frequency-amplitude distribution obtained by FFT is shown in Figure 3-10. This distribution filtered to the equivalent of 77 x 77 points is shown in Figure 3-11. Figure 3-12 shows the filtered distribution after inverse transform to physical space. Comparison of Figure 3-12 with Figure 3-9 reveals that some detail has been lost but that the essential character of the distribution is preserved.

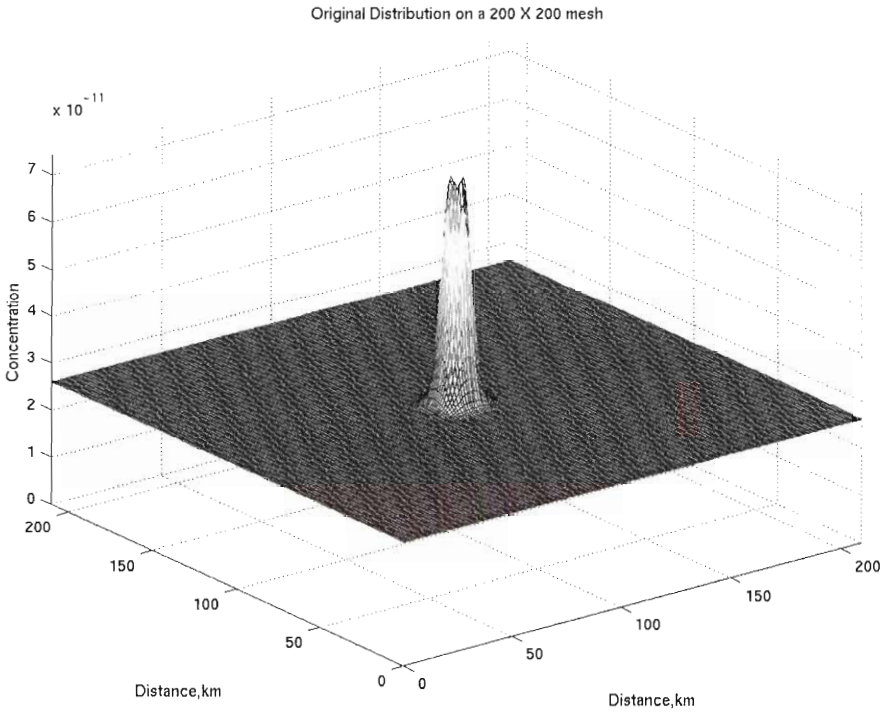

Figure 3-9 Original distribution on a 200 x 200 mesh surface

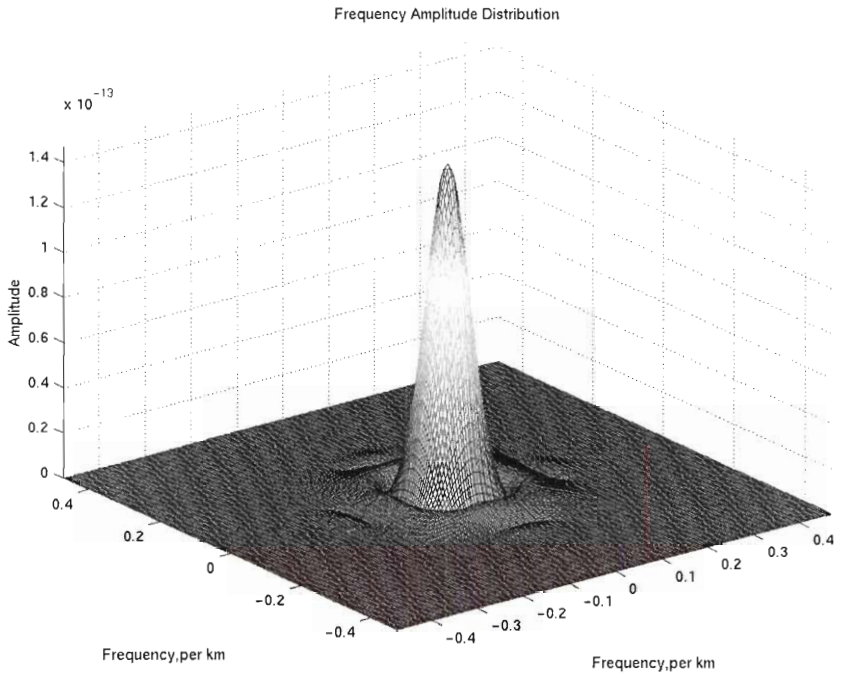

Figure 3-10 Frequency-amplitude spectrum corresponding to 200 x 200 mesh points

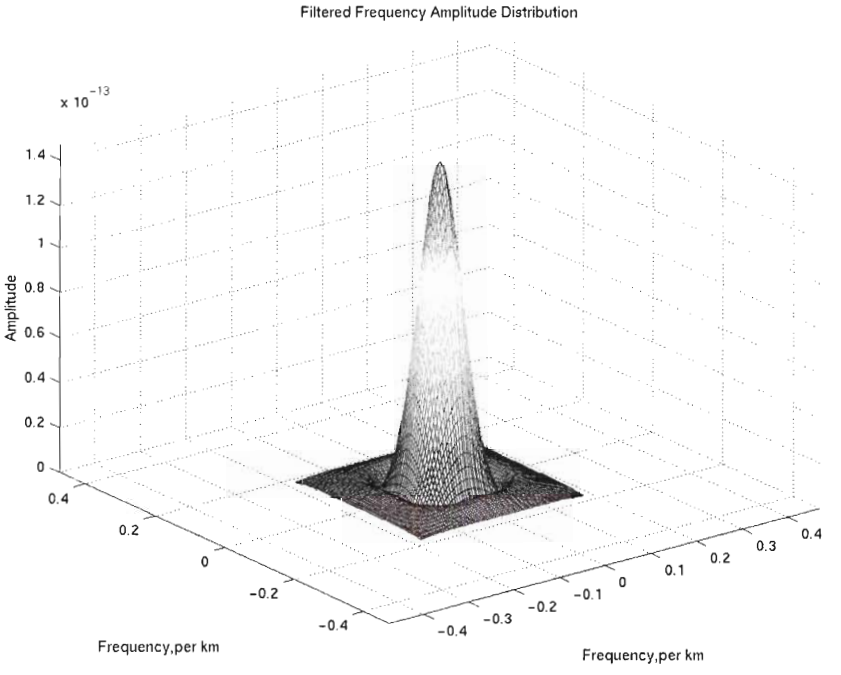

Figure 3-11 Frequency-amplitude spectrum corresponding to 77 x 77 mesh points

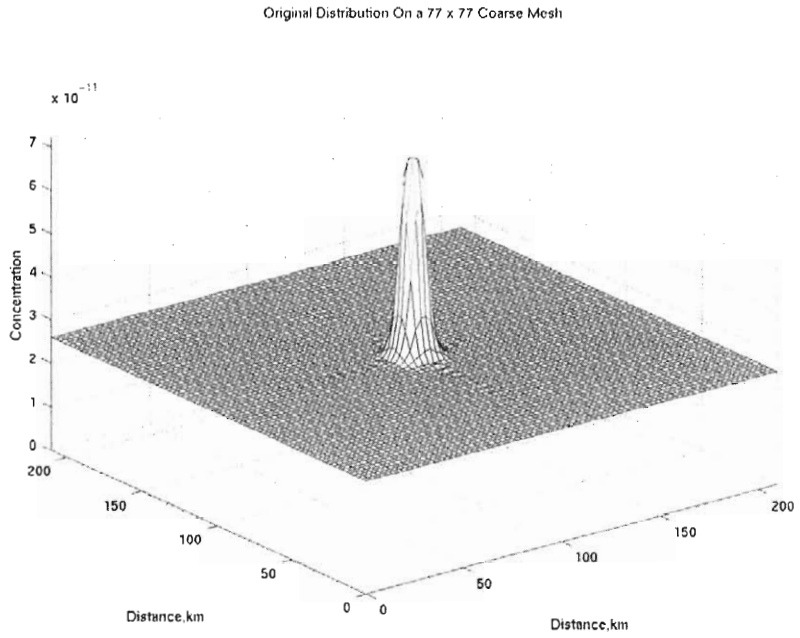

Figure 3-12 Filtered distribution in physical space on a 77 x 77 mesh surface

3.6 Analysis of Simulation Results- Adaptive mesh RAQM

Odman and Khan [2003] conducted a simulation of the TVA region during a period for which data are available, both from ground based and aircraft sampling flights. The model used contained a version of the NCSU adaptive mesh scheme, which was used to increase resolution where concentration gradients were high with the goal of a more accurate simulation. A simulation run conducted for the period 7-19 July 1995 for which emissions data were available through the SAMI air quality modeling study (Odman et al. 2002). The Emissions Modeling System (EMS-95) (Wilkinson, 1994) was used to access these data and prepare initial and boundary conditions for the simulation. An online video depicting the evolution of the adaptive mesh during this simulation is available at:

http://www.ce.gatech.edu/~todman/page2.html.

The analysis techniques developed and described in the previous section were used to demonstrate that the frequency content in an arbitrary section of the adaptive mesh simulation could be obtained and filtering followed by inverse transformation applied in order to ascertain the approximate effects of injecting the data into a coarser mesh.

As a demonstration, the analysis of a single data set output at a selected physical time in the simulation is shown. First the grid on which the data are defined is shown in Figure 3-13. The ozone concentrations corresponding to this grid are shown in Figure 3-14.

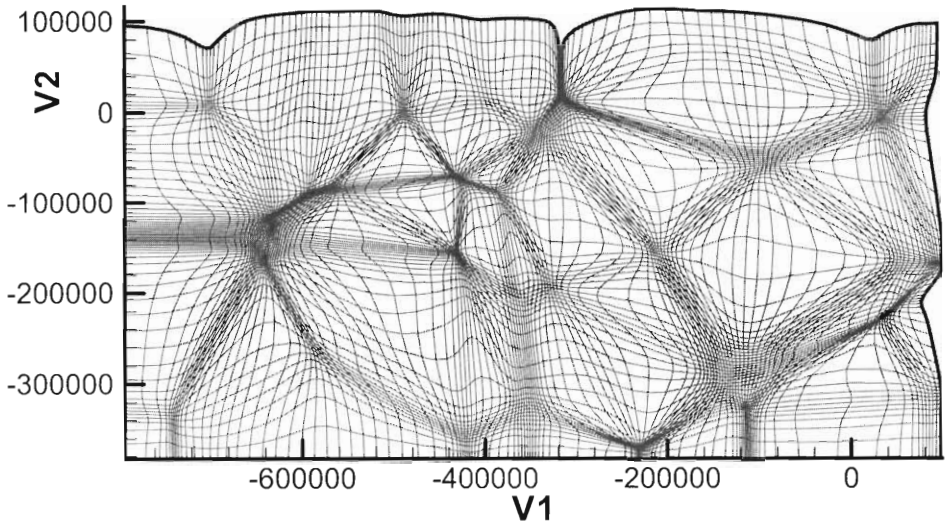

Figure 3-13 Adapted mesh for entire simulation region

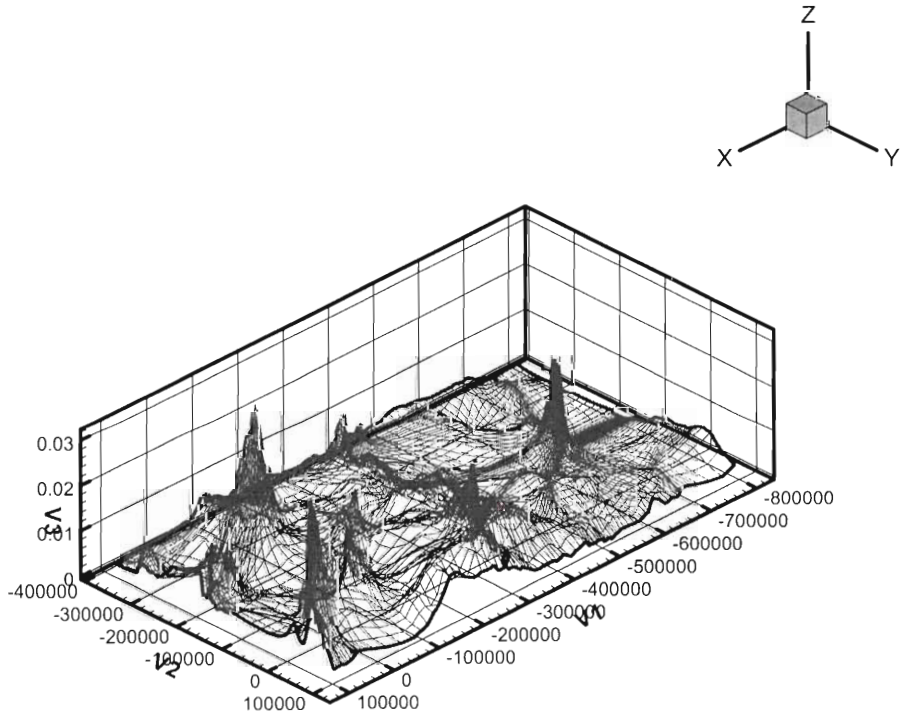

Figure 3-14 Ozone concentration distribution over the regional grid of Figure 3-13.

In order to demonstrate the use of the analysis technique on arbitrary grids, an x-y surface is selected from the computational simulation interpolated to a 50 x 50 evenly spaced mesh. Figure 3-15 is a plot of these interpolated data. In this instance, the entire region is chosen. Figure 3-16 depicts a plot of the frequencies present in this interpolated data. It is then filtered to remove frequencies that would not be resolved by a 41 x 41 mesh and then transformed back into physical space as shown in Figure 3-17. Comparison of Figure 3-15 and Figure 3-17 illustrates the change in the data that would be expected from a 20% increase in mesh spacing. It is also instructive to note the change that resulted from the original interpolation to the 50 x 50 mesh (compare Figure 3-15 with Figure 3-14).

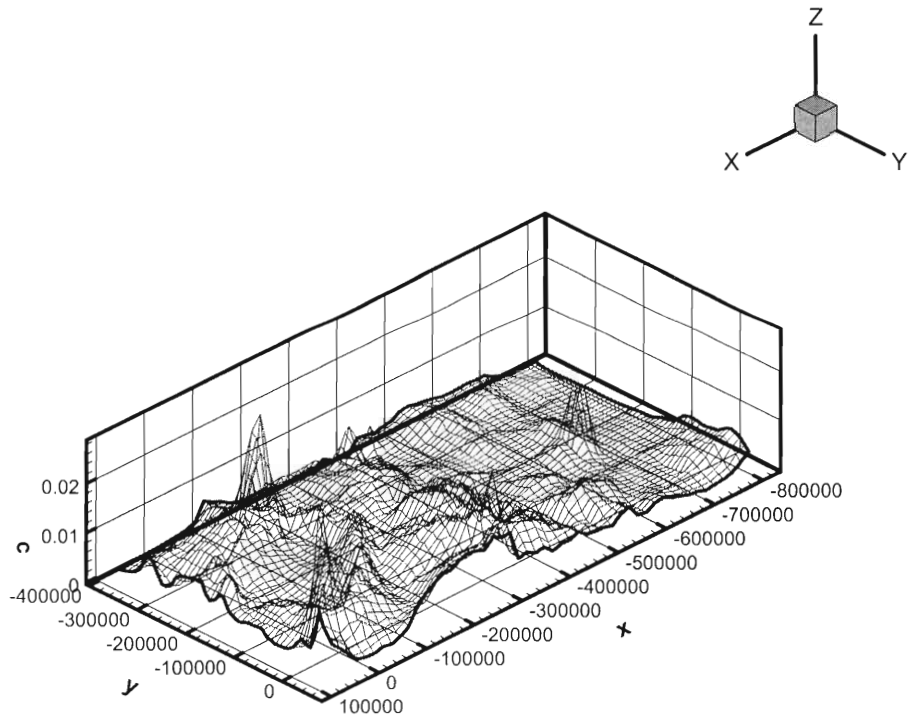

Figure 3-15 The original adapted mesh simulation (i.e., distribution in Figure 3-14) after interpolation to 50 x 50 mesh points.

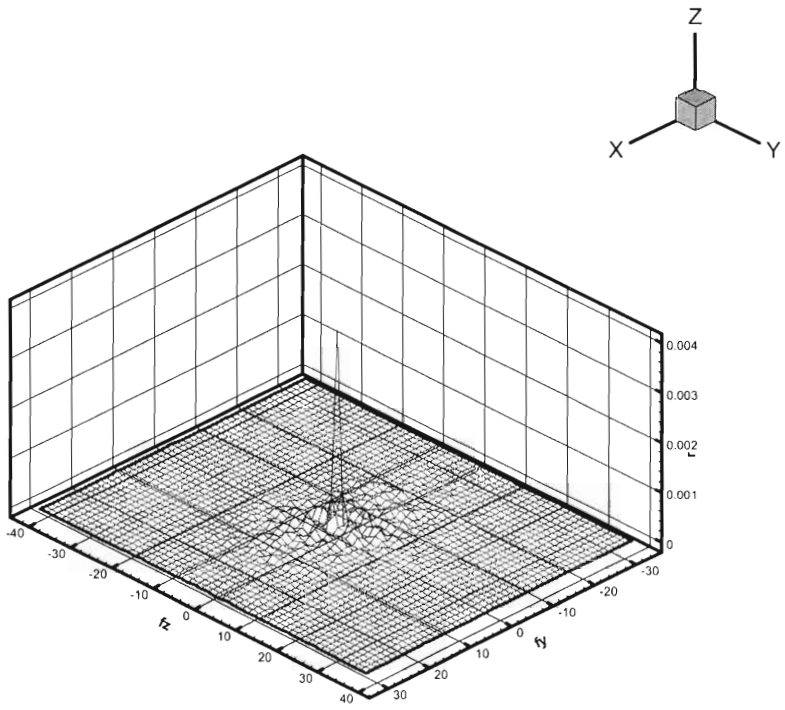

Figure 3-16 The frequency distribution present in the data interpolated to 50 x 50 mesh.

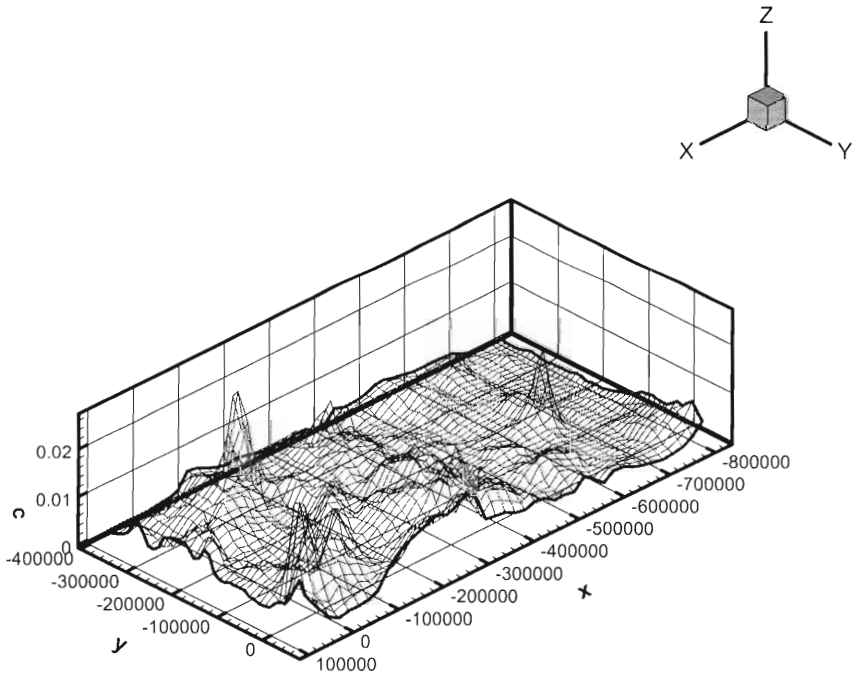

Figure 3-17 Concentration distribution after filtering and inverse FFT to physical space.

3.7 Analysis of Experimental Data

In the course of this research, it became apparent that issues exist with the analysis and use of experimental data that variations of the technology developed for plume analysis could greatly assist with analysis and display. Although many fixed and mobile stations exist, much of the approximately time-contiguous data is collected in-flight by aircraft equipped with sensors for specific species. These data are described along a curve in space that comprises the path of the aircraft in 3-D space plus time. When we compare this essentially 1-D description of the sample with the 1-D sample of the two- or three-dimensional sub grid plume simulations, the similarity of the data is obvious.

This similarity can be exploited as follows:

1) The Fourier analysis techniques used to evaluate the development of sub-grid plume models can also be used to evaluate the aircraft data to assess what simulation grid resolution would be needed to resolve the variations that exist in the experimental data.

2) With some modification, the techniques used to sample the simulation for Fourier analysis can also be used for direct comparison of an RAQM simulation with aircraft or other mobile platform data. This essentially involves, for each discrete sample point in the aircraft database, interpolating the simulation data to the same location in time and space. A line plot of these points would allow direct comparison of what the aircraft would measure if it "flew" through the simulation along the same path that it followed in reality.

The routines used to perform 1-D analysis of the 2-D plume simulations can be used to effect 1) above, with only modification of the input routine required.

The analysis noted in 2) uses the trilinear interpolation algorithms used to interpolate to an arbitrary surface in a 2-D analysis of a 3-D plume with interpolation between simulation time steps to maintain temporal accuracy of the comparison. To illustrate this routine Figure 3-18 shows a trace comparison of an entire DOE aircraft flight with the adapted mesh simulation.

Comments are offered concerning the use of the aircraft data. When several sampling aircraft are used that are sponsored by different organizations, the data are not always provided in a consistent format. This is further complicated by the practice of turning sensors/recording equipment off during periods when the aircraft is not in an identified plume/region of interest. Finally, data drop outs and seemingly random format shifts make reading the data files in for computational analysis labor intensive.

3.7.1 Suggestions for improving the utility of these data

1) If technically feasible, aircraft sensors should record continuously from wheels up to wheels down. Since simulation fields provide discrete data in both space and time for entire regions, continuous experimental data can provide valuable verification and

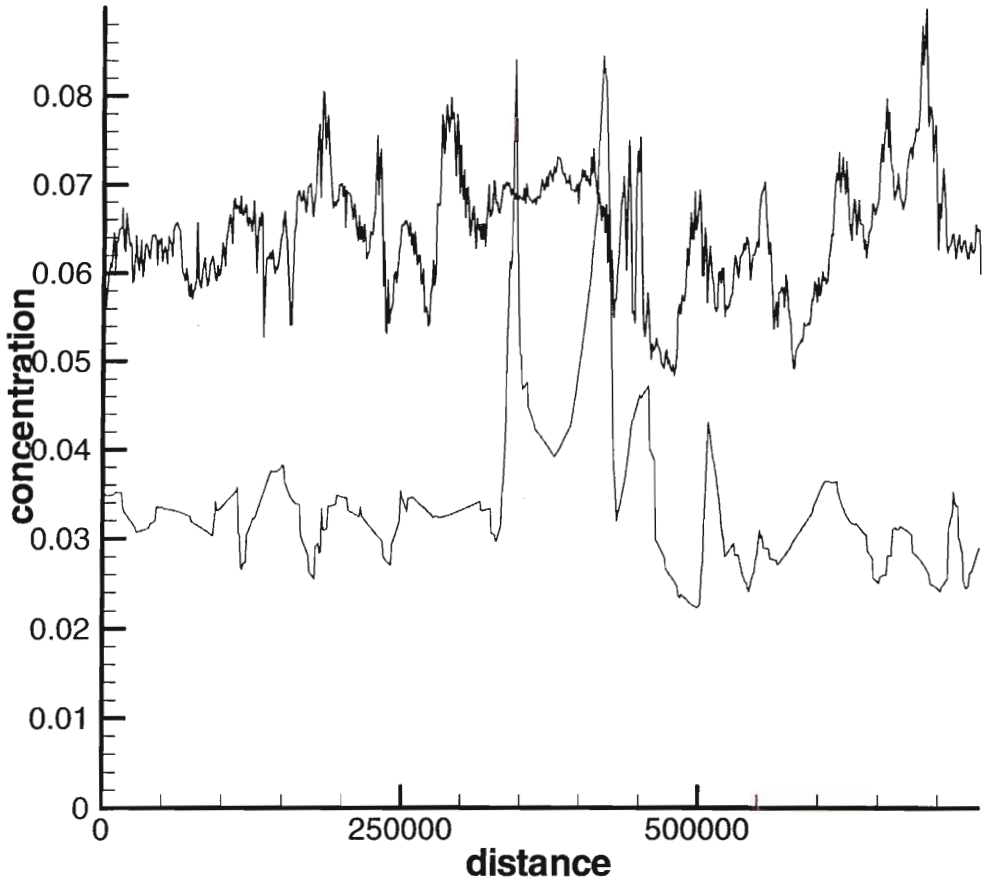

Figure 3-18 DOE aircraft flight data July 17, 1995, 1600 to 1800 GMT compared with adaptive mesh simulation.

assessment data at all times and locations rather than just when traversing identified plumes or regions of interest.

2) The monitoring agencies should agree on data presentation format.

3) A 0/1 switch should be provided to identify data dropouts or noted format variance. This would allow easy skip of suspect or code crashing data.

3.7.2 A proposed synergistic use of aircraft and Lidar data with techniques developed during this research.

It is clear in Figure 3-18 the average aircraft-sampled and simulated concentrations differ by approximately a factor of two during the period of this flight. Similar differences in average level were noted in the majority of samples checked in these data. This comparison illustrates dramatically the difficulty in specifying initial and boundary background concentration levels and wind field data for RAQM simulations based solely on fixed surface observations. Comparing the variations in the sampled and simulated data in Figure 3-18 reveals that the trends in the simulation are frequently similar to those in the observations and that if average concentrations were the same, agreement would be described as good over portions of the flight.

The capability developed during this project to interpolate simulation field data to an aircraft flight path for direct comparison could be used to improve simulation boundary and initial conditions dramatically over those obtained by the current practice of relying surface observation data. The procedure would use aircraft/Lidar to collect data along the boundaries of a region chosen for simulation. A routine would then be developed, based on the techniques developed to relate aircraft and simulation, to create initial and boundary information based on these extensive observations at altitude coupled with the known ground based observations. This would provide the correct background levels for the simulation region plus quantify plumes crossing the boundary. Additional flights on the interior could be made to refine the initial conditions at altitude in the vicinity of known sources. This would be particularly useful for creating data sets for use in verification of simulation codes.

3.8 Conclusions

Sub-grid scale reactive plume models have received recent attention as a means of improving the accuracy with which point emission sources can be included in regional air quality model simulations. However, in the past, these models have not improved the predictive skill of AQMs, at least on a regional scale. An analysis of mesh resolution and mesh related errors related to this issue was performed. Based on this analysis and the fundamental properties of numerical simulation, it was determined that the sub-grid models were being handed over to the regional model before the plume was developed sufficiently for resolution by the much coarser regional grid. The result was loss of information due to cell averaging of the detailed plume concentrations.

New hand-over criteria have been developed that will automatically assess the development and maturity of the plume relative to the resolution provided by the regional grid. Once these criteria are satisfied, then the plume can be injected into the regional grid with minimal loss of information. The procedure uses the fact that a curve or surface in space can be constructed by determining proper coefficients to a sufficient number of terms in a Fourier series. However, a computational grid will only resolve a range of frequencies determined by the grid spacing, essentially acting as a band pass filter. The smallest spacing in the computational grid will then absolutely determine the resolution available to represent any function on that grid.

The criteria are implemented by selecting the feature that is to be assessed against the resolution ability of the regional grid. A line or surface is defined that is perpendicular to the principle direction of advection, again assuming a plume feature. The concentration information is interpolated to an evenly spaced grid on the line or surface. A Fourier transform is performed to extract the frequencies present in the sub-grid solution, the range of which will be a function of the solution and the mesh. This transform is filtered to remove frequencies not resolved by the regional mesh and an inverse transform is performed to physical space. Comparison of the original and filtered distributions will then provide an indication of information loss due to the transfer without having to perform it. An energy method assessment of the two distributions has been shown to provide an initial criterion for automatically assessing the loss of information.

Testing of the procedure on model problems and simulated 2-D plumes demonstrated that this procedure provides a reliable indication of when a plume can be injected without significant degradation. The procedure can be included in sub-grid simulation codes as an automated check.

A study was also undertaken to assess the technique when applied to a simulation obtained with a new adaptive mesh RAQM developed by Odman and Khan [2003]. This work is not considered complete but confirmed the above results for the fundamental analysis. As part of this study, new techniques were developed for comparing aircraft data with simulation results.

Aircraft observations are made along a flight path with constantly varying altitude and surface position coordinates, so a routine was developed to interpolate the simulation data to the aircraft position so that a direct exact comparison can be made between them. A linear plot of these data can provide a comprehensive assessment of the simulation over large portions of the domain, as opposed to relying on point assessment. These results revealed a fundamental problem in how initial and boundary conditions are determined in AQM simulations and also revealed some issues in the collection and presentation of the aircraft data.

Although a widely accepted routine was used to initialize the simulation from surface observations, average concentration levels proved to be in error by as much as a factor of two when compared with aircraft observations. This problem can be mitigated if the ideas developed in this research are used to create a new paradigm for simulation initiation.

It was concluded that aircraft/Lidar should be used to make observations along the boundary of the simulation domain, which would then be used in a new routine based on the techniques developed herein to initialize the domain and boundaries. This would serve to provide much more accurate background data along the boundaries and should lead to much more useful verification data for simulation.

3.9 Future Work

The handover criteria must now be used in an actual plume study in order to determine the allowable values of the agreement parameters that give acceptable transfer error. Also, alternatives to the energy measure should be sought with controllable sensitivity to specific types of distributions.

The ideas proposed for improving the accuracy of simulation initiation should be exploited and a new initiation/forcing routine developed that will remove the obvious shortcomings of the present techniques and take advantage of new observation technologies.

References

Kumar N. and A. G. Russell, Development of a computationally efficient, reactive subgrid-scale plume model and the impact in the northeastern United States using increasing levels of chemical detail. *J. Geophys. Res.* **101**, 16737-16744, 1996.

Odman, M. T., A quantitative analysis of numerical diffusion Introduced by advection algorithms in air quality models. *Atmos. Environ.* **31**, 1933-1940, 1997.

Tannehill, J, C., Anderson, D. A., and Pletcher, R. H., *Computational Fluid Mechanics and Heat Transfer,* Taylor and Francis, 1997

Klopfer, G. H. and McRae, D. S., "Nonlinear Truncation Error Analysis of Finite Difference Schemes for the Euler Equations," *AIAA Journal* 21(4), 487-494 (April 1983).

Klopfer, G. H. and McRae, D.S. "The Nonlinear Modified Equation Approach to Analyzing Finite Difference Schemes," AIAA 81-1029, 5th AIAA Computational Fluid Dynamics Conference, Palo Alto, CA, 1981

Srivastava, R. K. A Dynamic Adaptive Grid Algorithm for Air Quality Modeling, Dissertation, North Carolina State University, August, 1998

4 Evaluation of Adaptive Grid Algorithms

Khan, N. K., Odman, M. T. and Karimi, H., Computers, Environment and Urban Systems, in press.

Abstract

An adaptive grid model is being developed to reduce the resolution-related uncertainty in air quality predictions. By clustering the grid nodes in regions where errors in pollutant concentrations would potentially be large, the model is expected to generate much more accurate results than its fixed, uniform grid counterparts. The repositioning of grid nodes is performed automatically using a weight function that assumes large values when the curvature (change of slope) of the pollutant fields is large. Despite the movement of the nodes, the structure of the grid does not change: each node retains its connectivity to the same neighboring nodes. Since there is no a priori knowledge of the grid movement, the input data must be re-gridded after each adaptation step, throughout the simulation. Emissions are one of the major inputs and mapping them to the adapted grid is a computationally intensive task. Efficient intersection algorithms are being developed that take advantage of the unchanging grid structure.

Here, the grid node repositioning and intersection algorithms are evaluated using surface elevation data. Two elevation data sets are reduced to one fourth of their sizes using uniform as well as adaptive grids. The first data set contains important terrain features near the boundaries while the second has all of its features far away from the boundaries. The compression of the first data set using grid node repositioning results in a maximum error that is 25% smaller compared to a uniform grid with the same number of nodes. The maximum error associated with the adaptive grid compression of the second data set is 60% smaller compared to the uniform grid compression. These results show that the adaptive grid algorithm has the potential of significantly improving the accuracy of air quality predictions, especially when the regions of changing slope are far away from the boundaries. The algorithms are computationally efficient, which implies that the overhead should not be limiting in air quality simulations.

4.1 Introduction

Emission control strategies that are being developed to improve air quality rely heavily on simulations with air quality models (AQMs). Control strategies can be very costly to implement and they have a direct bearing on public health and lifestyle. If the accuracy of AQM simulations can be improved, more effective strategies can be designed. One source of uncertainty in AQM simulations is attributed to the spatial resolution of the numerical grid, which is limited by the availability of computational resources. A large grid size is unable to resolve input data or capture the non-linear physical and chemical processes that occur over smaller spatial scales. To address this issue, nested grid or multi-scale modeling techniques have been developed that use finer grid resolution in regions of interest and coarser grids elsewhere (Odman et al. 1997). These techniques are limited by not knowing, a priori, where to place the finer resolution grids, loss in solution accuracy due to grid interface problems

(Alapaty et al. 1998), and the inability to adjust to dynamic changes in the solution. An alternative approach to achieving local resolution involves using dynamic adaptive grids, which are not subject to the aforementioned limitations. Using a weight function that represents the error in the solution (i.e., in pollutant fields), grid nodes are clustered in regions where they are needed the most.

Probably the most restrictive issue in the development of adaptive grid AQMs is the processing of emissions for a continuously moving grid. Emission inventories include hundreds of compounds emitted from a variety of sources ranging from large utility plants to motor vehicle tailpipes. Geographical information systems (GIS) are used to retrieve the raw emissions data from the inventories and generate gridded, time-varying emissions in terms of the chemical species represented in the models. In adaptive grid models, the shape and location of grid cells change after each adaptation. A source that lies in a grid cell might lie in another cell after adaptation. Therefore, the processing of emissions data must be performed in real time, after each adaptation of the grid. The task of locating a point (e.g., stacks), line (e.g., roads) or an area (e.g., farm) source within a grid is referred to as the *intersection* problem (Karimi et al. 1999). Efficient intersection algorithms are needed to reduce the overhead of re-gridding emission inputs in real time.

This paper describes the grid-node repositioning and point source intersection algorithms, and discusses their performance in a test problem consisting of adapting a grid to terrain elevation data. The reason for using elevation data in this exercise is the similarities between complex terrain and pollutant fields, in terms of changing slopes. The major difference between an elevation field and a pollutant field is that the former is static while the latter changes in time. However, in AQM simulations, the evolution of pollutant fields is captured in discrete time steps. Each time step is followed by a grid adaptation step such that the pollutant field can be better resolved. Hence, the test with terrain elevation data emulates a single adaptation step of an actual AQM simulation where time evolution is stopped and the grid is adapted to the pollutant field. As long as the terrain is complex enough to imitate typical pollutant fields, we may view this test as a robust evaluation case for the grid-node repositioning algorithm. The test case also evaluates the point-source intersection algorithm in an indirect way. While the elevation of repositioned nodes is calculated, there is a need to locate the cell of the elevation data grid that contains the node location. While there are more efficient ways of performing this task, we use the point-source intersection algorithm, which was designed for a similar purpose: to locate the fixed position of a point source over a moving grid. This way we are able to evaluate both the grid-node repositioning and point source intersection algorithms in the same test.

4.2 Methodology

The adaptive grid methodology used here is based on the Dynamic Solution Adaptive Grid Algorithm (Benson and McRae, 1991). Since it is described in detail in Srivastava et al (2000), it will only be highlighted here. The method employs a constant number of grid nodes that partition a rectangular domain into N by M quadrilateral grid cells. The nodes move throughout the simulation but the grid structure remains the same (i.e., topology does not change). In other words, each node is still connected to the same neighboring nodes but the length of the links and the area of the grid cells change. One of the advantages of using a

structured grid is that, through a coordinate transformation, the non-uniform grid in the physical space can be mapped onto a uniform grid in the computational space. The solution of partial differential equations that govern atmospheric diffusion is simpler on a uniform grid.

The movement of the nodes is controlled by a weight function whose value is proportional to the error in the solution. The nodes are clustered around regions where the weight function bears large values, thereby increasing the resolution where the error is large. Since the number of nodes is fixed, refinement of grid scales in regions of interest is accompanied by coarsening in other regions where the weight function has smaller values. This yields a continuous multiscale grid where the scales change gradually. Unlike nested grids, there are no grid interfaces, which may introduce numerous difficulties due to the discontinuity of grid scales. The availability of computational resources determines the number of grid nodes that can be afforded in any AQM. By clustering grid nodes automatically in regions of interest, computational resources are used in an optimal fashion throughout the simulation.

4.2.1 Weight Function and Grid Node Repositioning

The grid nodes are moved using a weight function along with a center-of-mass repositioning scheme. The weight function must be such that its value is large in regions where grid nodes need to be clustered. There are also some requirements for the resulting grid in order to assure an accurate numerical solution of governing partial differential equations. The grid must be free of highly skewed cells, and there must be a smooth transition from small to large cells with no voids in regions where the pollutant field is relatively uniform. Laflin and McRae (1996) developed a weight function that satisfies these requirements and is very easy to compute. The value of the weight function for grid cell (*i,j*) is calculated as:

$$w_{i,j} = \nabla^2(\phi)_{i,j} + w_{min} \tag{1}$$

where ∇^2 is a discrete approximation to the Laplacian operator of the form

$$\nabla^2(\phi)_{i,j} = \frac{1}{4}\left(\phi_{i-1,j} + \phi_{i+1,j} + \phi_{i,j-1} + \phi_{i,j+1} - 4\phi_{i,j}\right), \tag{2}$$

which also represents the error between the grid node value of field variable ϕ and the value obtained from the interpolation of ϕ values in the neighboring cells. A relatively small value of $\nabla^2\phi$ for any cell indicates that the grid can support relatively accurate interpolations of ϕ in the neighborhood of that cell. A minimum weight, $w_{\min}$, inhibits evacuation of grid nodes from regions of uniform ϕ.

The weight function above can result in the formation of concave or highly skewed grid cells. Since such grid cells are undesirable, a diffusive filter is applied to smooth this weight function (Srivastava et al., 2000). The final weight function is obtained by applying an area weighting to the smoothed weight function.

$$\widetilde{w}_{i,j} = A_{i,j}^{1+e}\left(w_{i,j}^{\text{filtered}}\right) \tag{3}$$

The parameter e controls weighting with respect to the cell area A: a positive value gives more weight to larger cells and promotes gradual transitions from larger to smaller cells.

Repositioning of the grid nodes is accomplished by a *center-of-mass* scheme proposed by Eiseman (1987), which defines the new position of the grid node, $\vec{P}^{new}$, as:

$$\vec{P}^{new} = \frac{\sum_{i=1}^{4} w_i \ \vec{P}_i}{\sum_{i=1}^{4} w_i} \tag{4}$$

where $\vec{P}_i$ are the position vectors of the centroids of four cell sharing the grid node and w_i are the values of the weight function at those locations.

If the maximum movement of all grid-nodes is below a preset tolerance, the grid is considered to have resolved the field sufficiently. Otherwise, the weight function is recomputed and the grid adaptation procedure is reiterated. The movement tolerance used here is, for any node, 5% of the distance to the closest node.

4.2.2 Point Source-Grid Cell Intersection Algorithm

Since the locations of the grid nodes have changed in the physical space, input data such as emissions must be re-gridded. As mentioned before, there are three major types of emissions being input into an AQM: emissions from point, line and area sources. Gridding of these emissions requires finding the intersections of each source type with the adapting grid cell. The structure of the grid at hand and the quadrilateral shape of the cells can be exploited to develop efficient intersection algorithms. This way the overhead involved in the re-gridding operations can be significantly reduced.

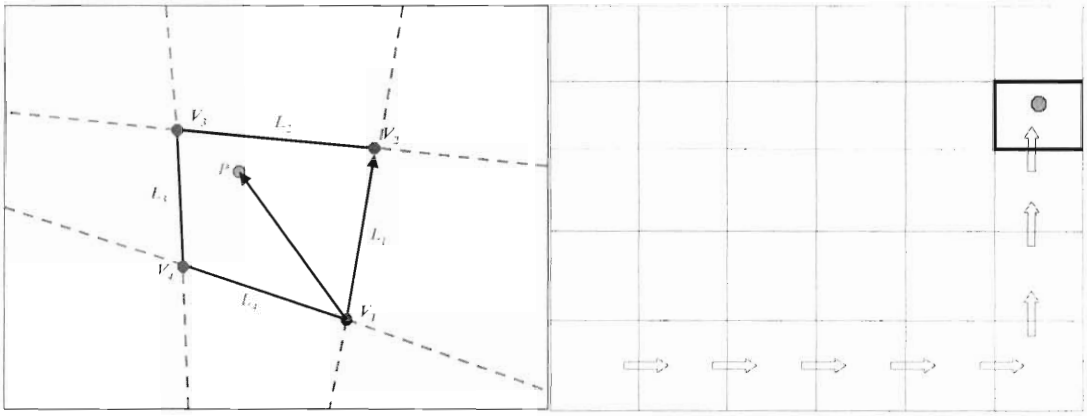

Figure 4-1 Locating a point P in a grid cell (left). Arrows indicating the search as it proceeds to locate point P in N by M grid cells (right).

Intersecting point sources with the grid is the easiest one. A search is conducted over all grid cells to find out which one encloses the point source. The following algorithm has been developed. As illustrated in Figure 4-1 starting from any vertex, two vectors are drawn: one to the next vertex in the counterclockwise direction and another to the point source location. If the cross product of the first vector with the second vector is negative (in a right-handed coordinate system), then the point source is outside this cell. In this case, checking the sign of the cross product is continued from the neighboring cell that shares with the original cell the side marked by the first vector above. In a structured grid where the cells are stored in an N by M array, finding this neighboring cell is trivial. If the cross product is positive, the process is continued from the next vertex of the cell. If the process yields positive cross products for all four vertices, then the point is inside that cell.

In general, the adaptive grid is initialized as a uniform grid. After the initial adaptation, the changes in pollutant fields during the air quality simulation are usually not dramatic enough to require a sudden adaptation from a uniform grid to a grid that can support a very complex field. In other words, the grid node movements would never be as large as they were in the initial adaptation step. In fact, it is very likely that the cell containing the point source prior to grid node repositioning would not move too far away from that source. Therefore, the point source can be located much faster by starting the search from the cell where it was found in the previous search. Efficient algorithms that take advantage of the topology of the grid, as well as the small change in pollutant field assumption, have also been developed for line and area sources (Odman, 2001). However, they are not discussed in this paper.

4.3 Applications to Surface Elevation Data

The adaptive grid algorithm was applied to problems with increasing complexity and relevance to air quality modeling. Starting with pure advection tests (Srivastava et al., 2000), it was applied to reactive flows (Srivastava et al., 2001a) and to the simulation of a power-plant plume (Srivastava et al., 2001b). In all these applications, the adaptive grid solution was more accurate than a static, uniform grid solution obtained by using the same number of grid

nodes. These applications, though being very relevant, had at best only a few flow features to be resolved. Here, the objective is to evaluate the potential performance of the algorithm in a regional-scale air quality simulation where hundreds of features such as puffs and plumes would have to be resolved simultaneously. To achieve this objective without performing an actual simulation, surface elevation data are used as a surrogate for pollutant concentration fields as described below.

The spatial distribution of surface elevation over complex terrain resembles pollutant concentration fields in many ways. Over large regions of flat surface such as oceans, lakes, valleys and plains, there are local features with large curvature in coastal areas, foothills, and mountain peaks. The only notable difference is that surface elevation is constant over time. However, recall that the grid adaptation procedure is applied by freezing the evolution of the pollutant field, thus, at any instant, the complexity of a pollutant field can be well represented by a surface elevation field. The application consists of reducing the number of data points by 75%. First, every other data point in x- and y-direction is eliminated. Then, the remaining points are relocated according to the curvature of the terrain. Finally, the ability of the grid-node relocation algorithm in retaining the accuracy of the original surface elevation data is evaluated.

Note that the purpose of this exercise is not to reproduce specific features of the terrain such as hill top lines. For surface elevation data, there are methods (e.g., the very important point or VIP method; Tsai, 1993) specifically designed for eliminating unimportant points from a uniform grid and retaining important ones. Note that such methods cannot be used in air quality modeling where the pollutant fields are changing in time.

4.3.1 Application to the United States-Mexico Border Area

The surface elevation data for the United States-Mexico border area (Joseph, 1997) were processed onto a uniform 136x80-cell fine grid with a 6.25-km resolution (Figure 4-2).

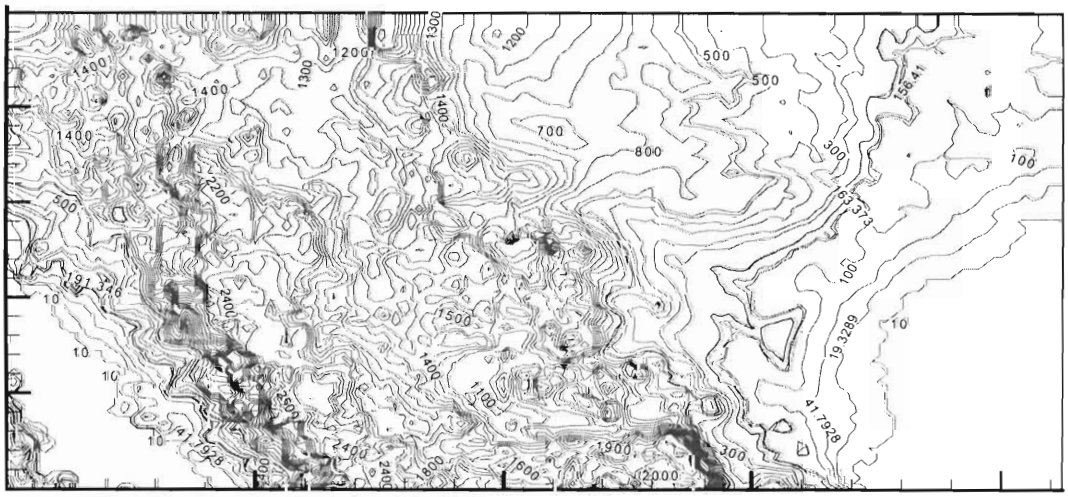

Figure 4-2 Surface elevation for the United States-Mexico border area.

The same data were also mapped on a coarse grid with 68x40-grid cells, and uniform 12.5-km resolution. This second grid serves as the static grid with which the adaptive grid is compared. It also constitutes the starting point for the adaptive grid. A weight function was computed based on the curvature of the terrain and the grid nodes were repositioned. After the coordinates of the adapted grid are computed in the physical space, the elevation of the grid nodes was obtained by bilinear interpolation from the fine grid. During this procedure, it is necessary to find the fine grid cell containing any given node of the adaptive grid. For this, we used the above described intersection algorithm developed to search for the grid cell that contains any given point source.

In order to assess if the adapted grid captures the surface elevation more accurately than the coarse grid, which is static and uniform, surface elevation from both grids is interpolated back onto the fine grid. Thus, there are three sets of surface elevation data on the fine grid: one from the DEM data set, another that is interpolated from the coarse grid, and a third one interpolated from the adaptive grid. These data sets are used in calculating and comparing the errors from the adaptive and coarse grids. The adaptation process is continued until all the node movements are below the preset relative tolerance of 5%.

The evolution of the grid during the adaptation process was visualized to see if the grid-repositioning algorithm created any highly skewed cells or voids in areas of flat terrain. The grid node movements were large in the beginning, but decreased as shown in Figure 4-3. However, there were short periods during which large grid node movements were observed. These movements were almost always associated with the movement of boundary nodes. The grid movement tolerance was achieved after 353 iterations.

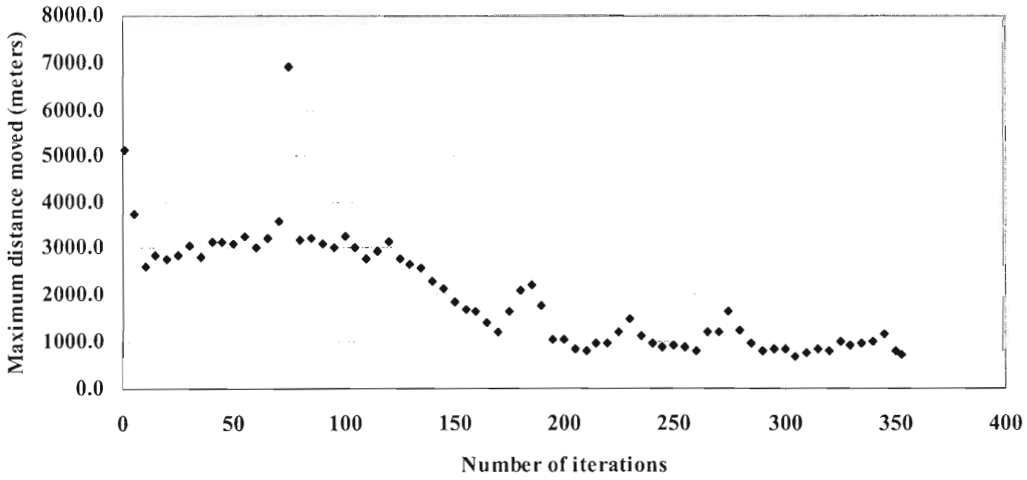

Figure 4-3 Maximum distance moved by any grid node as a function of grid repositioning iterations in the application to the United States-Mexico border area.

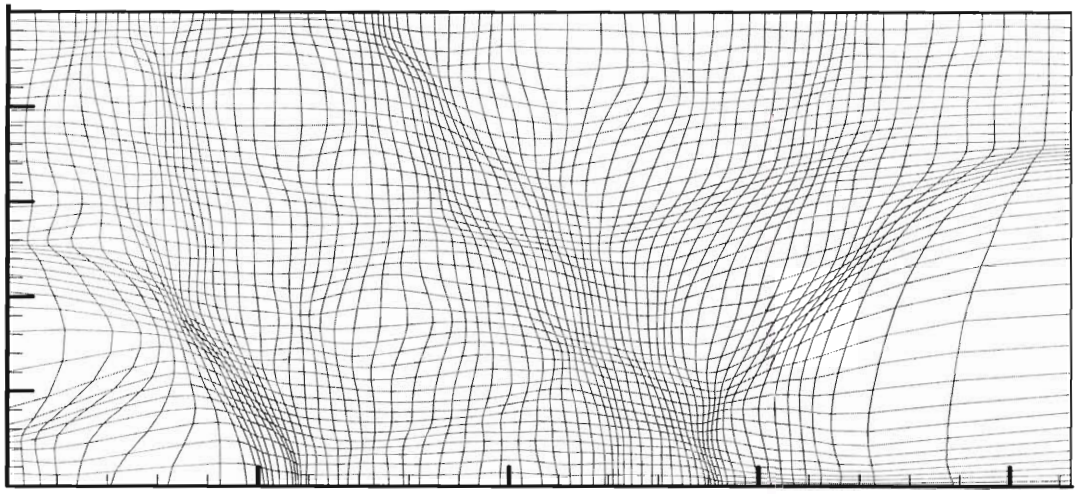

Figure 4-4 The grid adapted to the terrain features of the United States-Mexico border area.

The final configuration of the grid is shown in Figure 4-4. The transitions from coarse to fine resolution (or vice versa) are smooth and no highly skewed cells or voids are visible. In general, the grid nodes are clustered in regions with abrupt changes in surface elevation. Particularly noticeable is the clustering of grid nodes near the southern boundary where such changes are more prominent.

The difference between the interpolated surface elevation (either from the adaptive grid or from the coarse grid onto the fine grid) and the value from DEM data at any fine grid node is defined as the nodal error:

$$E_{i,j} = \left| \phi_{i,j}^{\mathrm{DEM}} - \phi_{i,j}^{INTERPOLATED} \right| \tag{5}$$

The domain wide maximum nodal error as a function of grid node repositioning iterations is shown in Figure 4-5. Also shown in Figure 4-5, is the maximum error for a sub-domain obtained by excluding all grid nodes that are located within 100 km of the domain boundary. The smaller maximum error for the sub-domain indicates that the error is larger at nodes closer to the boundaries of the domain. This is due to the fact that boundary nodes are allowed to move in one-dimension only.

The maximum nodal error decreases from the initial value of 671 m, which is also the maximum error for the coarse grid, to 490 m after 353 iterations (Figure 4-5). The increases in maximum error after periods of monotonic decrease correspond to shifts in maximum error from one area of the geographic domain to another. Recall that, since the number of nodes is fixed, the adaptive grid algorithm is clustering the nodes around one terrain feature at the expense of decreased resolution elsewhere. Therefore, while the local error around one terrain feature is decreased, it may start to increase around some other feature. The decreasing trend in the maximum error is promising and is much more pronounced in the

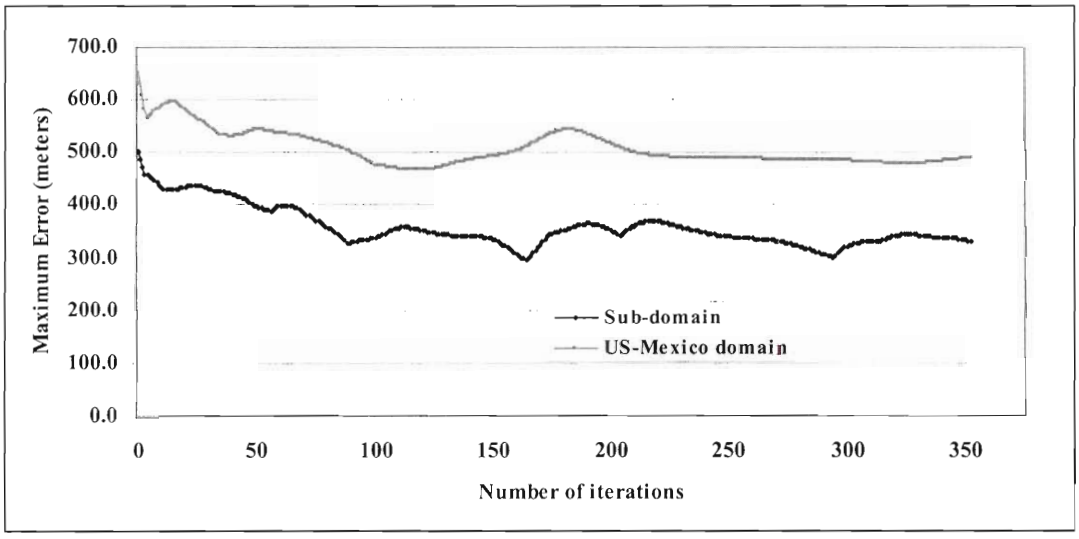

Figure 4-5 Maximum error as a function of grid repositioning iterations in the application to the United States-Mexico border area.

sub-domain. In fact, the maximum error decreases exponentially in the sub-domain, from 502 m to 329 m after 353 iterations. This suggests that the grid is converging towards a state where the domain-wide maximum error is minimized, although the final grid, which satisfied the node movement tolerance, does not correspond to the minimum local error.

In summary, the maximum error is 25% less on the adaptive grid than on a uniform coarse grid. The adaption and repositioning process is able to reduce the maximum error more efficiently at nodes that are located away from the boundaries of the domain. Maximum error in the sub-domain decreased by 35%. It was further observed, that the maximum error might shift from one location to another several times during the iterative grid-node repositioning process, and it is not necessarily minimized at the end, when the movement tolerance is met. The rate of convergence is not very fast, but since the grid-node repositioning algorithm is inexpensive (all 353 iterations were completed in 750 seconds on a 200 MHz processor) this does not pose a limitation. The resulting grid fulfills all of the requirements set forth for accurate numerical solution of partial differential equations.

4.3.2 Application to the Island of Hawaii

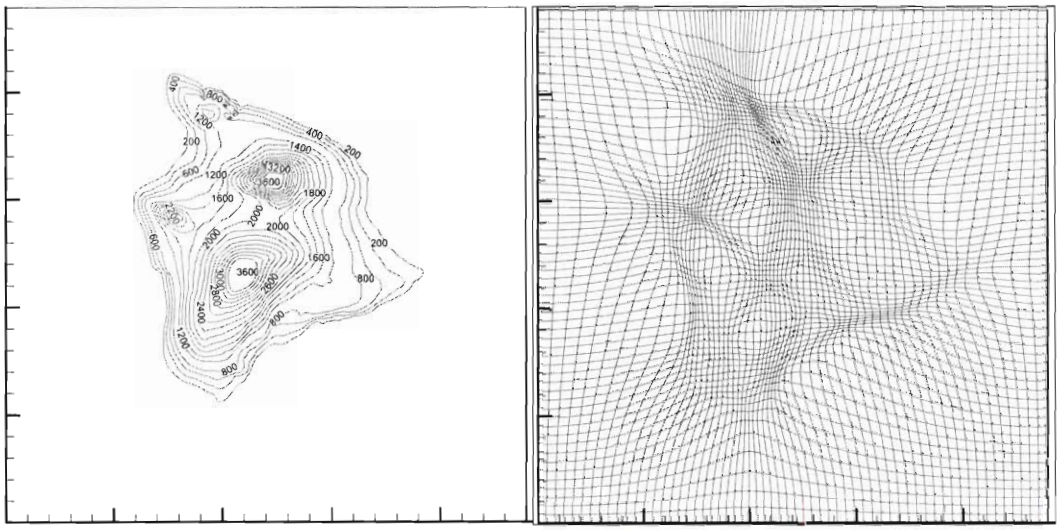

Figure 4-6 Surface elevation for the island of Hawaii (left) and the grid adapted to the terrain features (right).

In the application above, the presence of prominent terrain features near the boundary had a significant impact on the results. The region surrounding the Island of Hawaii was selected for a second application. Since all the boundaries of this domain are over the ocean (Figure 4-6, left), the performance of the adaptive grid algorithm can be better assessed in this application. The surface elevation data from the DEM (USGS, 1997) was mapped onto a uniform 120x120-cell fine grid with a 4-km resolution. The same data was also processed on a coarse grid with 60x60-grid cells and uniform 8-km resolution. The procedure used in this application is the same as the one in the previous application.

There are no highly skewed cells present in the final configuration of the grid shown in Figure 4-6 (right). This configuration was achieved in 375 iterations. As desired, the grid nodes are clustered around the areas with sudden changes in surface elevation. The movement of the grid nodes decreased exponentially (Figure 4-7) and in a more monotone fashion compared to the previous application (compare to Figure 4-3). However, the rate at which the movement tolerance was achieved was approximately the same in both applications.

As shown in Figure 4-8, the maximum nodal error, which had an initial value of 520 m, decreased by 60% to a value of 198 m after 375 iterations. During this exponential decrease, brief periods of increase are observed. These correspond to shifts in maximum error from one area of the geographic domain to another, as it was the case in the previous application. The decreasing trend in the global maximum error is more pronounced than in the previous application (compare to Figure 4-5). Clearly, the grid is converging towards a state where the domain-wide maximum error is minimized, although the final grid, which satisfied the node movement tolerance, does not correspond to the minimum local error. In

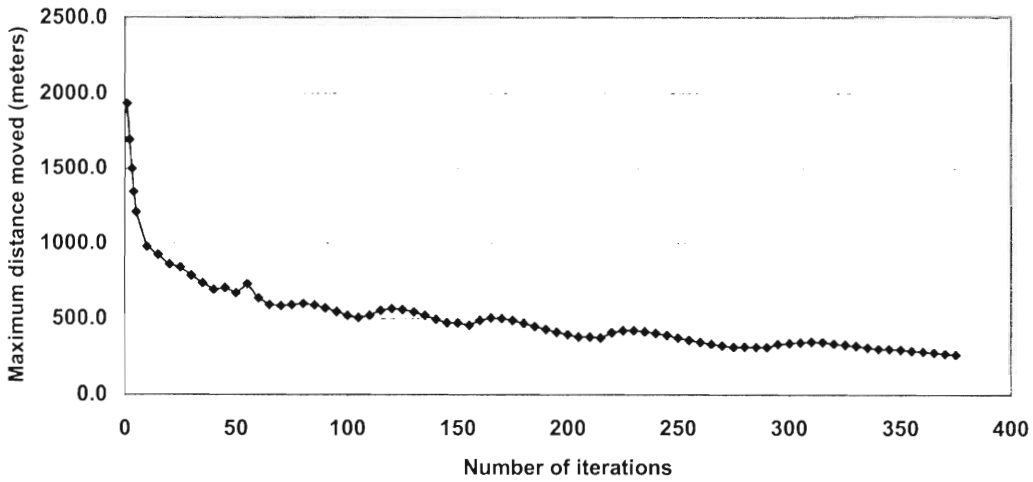

Figure 4-7 Maximum distance moved by any grid node as a function of grid repositioning iterations in the application to the island of Hawaii.

order to reduce the maximum error below 198 m, which is the minimum in Figure 4-8, the number of grid nodes would have to be increased.

Also analyzed was the cumulative error defined as:

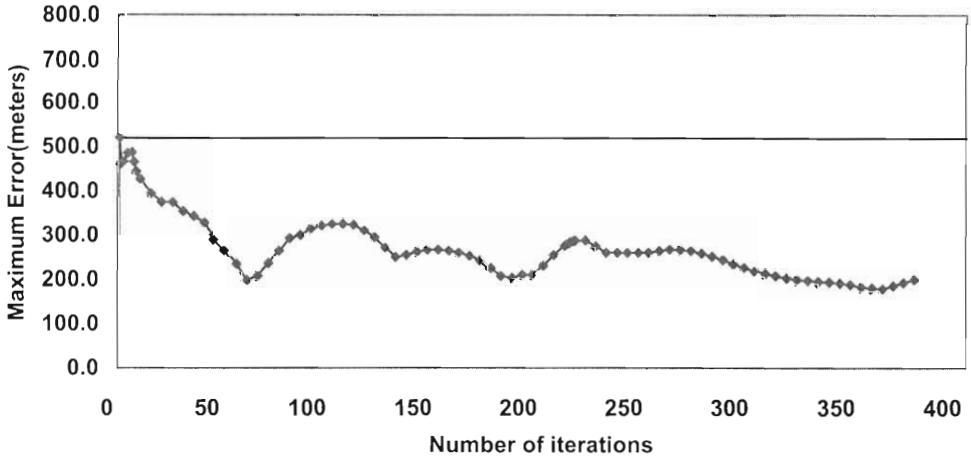

Figure 4-8 Maximum error as a function of grid repositioning iterations in the application to the island of Hawaii.

$$E^{cum} = \sum_{cg} \left| \phi^{DEM} - \phi^{INTERPOLATED} \right| + \sum_{fg} \left| \phi^{DEM} - \phi^{INTERPOLATED} \right| \quad (6)$$

As shown in Equation 6, the cumulative error has two components. The first component is the error on the fine grid nodes that also belong to the coarse grid (cg) and the second component is the error at the remaining nodes of the fine grid (fg). After an initial period of increase (up to about the 10th iteration), there is an exponential decrease in cumulative error (Figure 4-9). Clearly, the initial increase in the cumulative error is coming from the first component. Recall that the adaptive grid was initially the same as the coarse grid and that the surface elevation values for all the nodes were derived from the DEM data. Thus, the error at the nodes shared by the coarse and fine grids is zero. Once the node movement starts, the error at those nodes can only increase, but it reaches a plateau after about 15 iterations. Meanwhile, the cumulative error component for the nodes that are only on the fine grid decreases exponentially. At about the 10th iteration, the decrease in the second component offsets the increase in the first component, so the overall cumulative error starts decreasing. The monotonic decrease of the cumulative error afterwards shows that the grid adaptation is effectively increasing the accuracy of surface elevation, globally. Overall, the cumulative error decreased by more than 25% compared to the initial (coarse) grid.

In summary, the error in representing surface elevation data with four times fewer nodes than the original fine grid is smaller on the adaptive grid than the uniform coarse grid. Maximum error may shift from one location to another during the grid-node repositioning process. However, the cumulative error decreases almost monotonically indicating that the global error is effectively minimized.

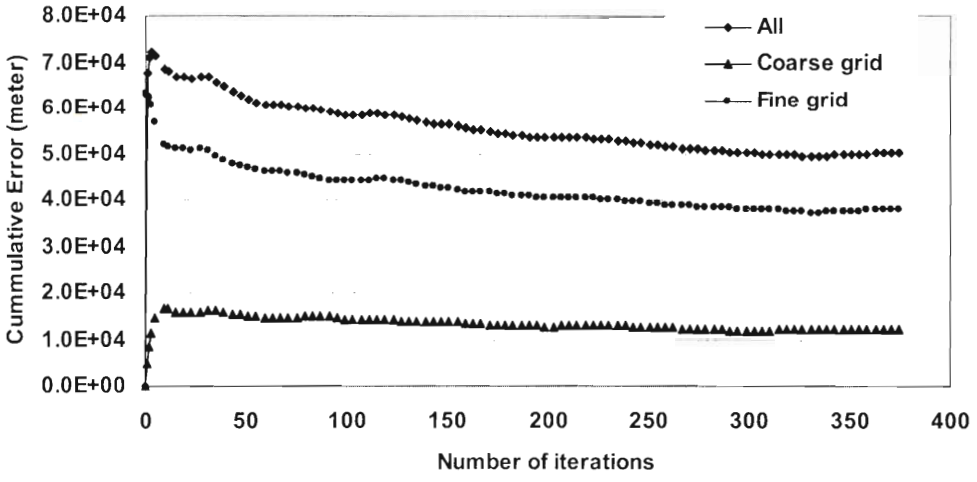

Figure 4-9 Cumulative error and its breakdown to the nodes that are also on the coarse grid and those that are only present on the fine grid.

4.4 Conclusion

An adaptive grid AQM is being developed (Odman et al., 2001). In this paper, the grid node repositioning and the point-source-grid-cell intersection algorithms were evaluated, for both efficiency and accuracy, using terrain elevation data. The algorithms were found efficient enough that the overhead of grid adaptations or re-gridding of emissions should not be restrictive in AQM simulations. The adaptive grid improves the accuracy considerably over a uniform grid with the same number of nodes. The maximum error decreased by 25% due to grid adaptations in an application to the terrain of the United States-Mexico border area. The adaptive grid algorithm performs better when regions with large curvature in surface elevation are located away from the boundaries of the domain. This is evident from the analysis of error at nodes that are located more than 100 km from the domain boundaries. The decrease in maximum error at such nodes is 35%. Finally, in a second application to a region surrounding the island of Hawaii where the changes in terrain slope are far away from the boundaries, the maximum error decreased by 60% and the cumulative error decreased by 25%. Similar improvement of accuracy can be expected in AQM results where pollutant fields resemble terrain fields in terms of complexity. The boundaries of the domain must be far away from emission sources that may create large changes in the gradients of pollutant concentrations.

Acknowledgements

This work was supported by the U.S. Environmental Protection Agency (Grant No. CR82505 and Assistance Agreement No. R 827028-01-0).

References

Alapaty, K., Mathur, R., and Odman, T., 1998. Intercomparison of spatial interpolation schemes for use in nested grid models. *Monthly Weather Review,* **126**, 243-249.

Benson, R. A., and McRae, D. S., 1991. A Solution adaptive mesh algorithm for dynamic/static refinement of two and three-dimensional grids. In *Proceedings of the Third International Conference on Numerical Grid Generation in Computational Field Simulations* (Barcelona, Spain).

Eiseman, P. R., 1987. Adaptive grid generation. *Computational Methods and Application in Mechanical Engineering*, **64,** 321.

Joseph, D., 1997. Defense Mapping Agency 30 Seconds Elevations. Prepared and maintained by data support section, Scientific Computing Division, National Center for Atmospheric Research.

Odman, M. T., 2001. Processing of Emissions Data for Adaptive Grid Air Quality Modeling. Final Report to MCNC (Contract # D96-7050-000). Georgia Institute of Technology, Atlanta, GA.

Karimi, H. A., Brandymeyer, J. E., Wong, D. C., and Bourgeois, A. J., 1999. A Parallel Polygon Intersection Algorithm for Adaptive Grid Models. *In Proceedings of*

International Conference on Parallel and Distributed Processing Techniques and Application, pp.553-559.

Laflin, K. R., and McRae, D. S., 1996. Three-dimensional viscous flow computations using near-optimal grid redistribution. In *Proceedings of First AFOSR Conference on Dynamic Motion CFD*, Rutgers University, New Jersey.

Odman, M. T., Mathur, R., Alapaty, K., Srivastava, R. K., McRae, D. S., and Yamartino, R. J., 1997. Nested and adaptive grids for multiscale air quality modeling. In *Next generation environmental models and computational methods,* edited by G. Delic, M. F. Wheeler (Philadelphia, PA: SIAM), pp. 59-68.

Odman, M. T., Khan M. N., and McRae, D. S., 2001. Adaptive grids in air pollution modeling: Towards an operational model. *Air Pollution Modelling and Its Application XIV*, S.-E. Gryning and F. A. Schiermeier, Kluwer Academic/Plenum Publishers, New York, 541-549.

Srivastava, R. K., McRae, D. S. and Odman, M. T., 2000. An adaptive grid algorithm for air quality modeling. *Journal of Computational Physics* **165**, 437-472.

Srivastava, R. K., McRae, D. S. and Odman, M. T., 2001a. Simulation of a reacting pollutant puff using an adaptive grid algorithm. *Journal of Geophysical Research*, **106**, 24,245-24,258.

Srivastava, R. K., McRae, D. S. and Odman, M. T., 2001b. Simulation of dispersion of a power plant plume using an adaptive grid algorithm. *Atmospheric Environment*, **35**, 4801-4818.

Tsai, V. J. D., 1993. Delaunay Triangulations in TIN Creation: An Overview and a Linear-Time Algorithm. *International Journal of Geographical Information Systems*, **7**, 501-524.

USGS, 1997. Digital Elevation Models for Hawaii. United States Geological Service. (http://edcwww.cr.usgs.gov/glis/hyper/guide/1_dgr_demfig/states/HI.html)

5 Development of Adaptive Grid Air Quality Model

Paper published in (pp. 651-660): Air Pollution Modeling and its Application XV: C. Borrego and Guy Schayes, Eds., New York: Kluwer Academic/Plenum Publishers, 2002.

==========

INITIAL APPLICATION OF THE ADAPTIVE GRID AIR QUALITY MODEL

M. Talat Odman, Maudood Khan, Ravi Srivastava, and D. Scott McRae*

5.1 Introduction

Grid size (or resolution), when inadequate, can be an important source of uncertainty for air quality model (AQM) simulations. Coarse grids used because of computational limitations may artificially diffuse the emissions, leading to significant errors in the concentrations of pollutant species, especially those that are formed via non-linear chemical reactions. Further, coarse grids may result in large numerical errors. To address this issue, multi-scale modeling and grid nesting techniques have been developed (Odman and Russell, 1991; Odman et al., 1997). These techniques use finer grids in areas that are presumed to be of interest (e.g., cities) and coarser grids elsewhere (e.g., rural locations). Limitations include loss in accuracy due to grid interface problems and inability to adjust to dynamic changes in resolution requirements. Adaptive grids are not subject to such limitations and do not require *a priori* knowledge of where to place finer grids. Using grid clustering or grid enrichment techniques, they automatically allocate fine resolution to areas of interest. They are thus able to capture the physical and chemical processes that occur in the atmosphere much more efficiently than their fixed grid counterparts.

The adaptive grid methodology used here is based on the Dynamic Solution Adaptive Grid Algorithm (DSAGA) of Benson and McRae (1991), which was later extended for use in air quality modeling by Srivastava et al. (2000). It employs a structured grid with a constant number of grid nodes. The modeling domain is partitioned into $N \times M$ quadrilateral grid cells. The grid nodes are re-positioned in a two-dimensional space throughout the simulation

* Talat Odman, Georgia Institute of Technology, Atlanta, Georgia, 30332-0512, talat.odman@ce.gatech.edu, Telephone: 770-754-4971, Fax: 770-754-8266. Maudood Khan, Georgia Institute of Technology, Atlanta, Georgia, 30332-0512. Ravi Srivastava, U.S. Environmental Protection Agency, Research Triangle Park, North Carolina, 27711. Scott McRae, North Carolina State University, Raleigh, North Carolina, 27695-7910.

according to a weight function which represents the resolution requirements. The areas of the grid cells change due to grid node movements but the connectivity of the grid nodes remains the same. Further, since the number of grid nodes is fixed, refinement of grid scales in some regions is accompanied by coarsening in other regions where the weight function has smaller values. This results in optimal use of computational resources and yields a continuous multiscale grid where the scales change gradually. Unlike nested grids there are no grid interfaces, therefore, numerical problems related to the discontinuity of grid scales are avoided.

The adaptive grid algorithm was applied to problems with increasing complexity and relevance to air quality modeling. Starting with pure advection tests (Srivastava et al., 2000), it was applied to reactive flows (Srivastava et al., 2001a) and to the simulation of a power-plant plume (Srivastava et al., 2001b). In all these applications, the adaptive grid solution was more accurate than a fixed, uniform grid solution obtained by using the same number of grid nodes. To achieve the same level of accuracy with the fixed uniform grid required significantly more computational resources than the adaptive grid solution. In this paper, we describe how the adaptive grid algorithm was implemented in an urban-to-regional scale AQM. After a brief discussion of model components, we report preliminary results from the first application of the adaptive grid AQM.

5.2 Methodology

An adaptive grid AQM simulation has two fundamental steps: a grid adaptation step, that is responsible for repositioning of grid nodes according to the grid resolution requirements, and a solution step, that simulates the physical and chemical processes that occur in the atmosphere. The solution (i.e., concentration fields) remains unchanged during the adaptation step, and the weight function clusters the grid nodes in regions where finer resolution grids are required. In preparation for the solution step, the fields of meteorological inputs and emissions must be mapped onto the new grid locations. This task is also considered part of the adaptation step and is undertaken by efficient search and intersection algorithms. During the solution step, the grid nodes remain fixed while the solution is advanced in time. Ideally, the adaptation step should be repeated after each solution step owing to the change in resolution requirements. However, since the mapping of meteorological and emissions data is computationally expensive, we have chosen to apply the adaptation step less frequently. Whereas, the solution is advanced in time by 1 hour in several time steps, the adaptation step is performed once every hour. In order to ensure numerical stability, we require that the Courant number be smaller than unity while determining the time step of the solution. The rest of this section consists of a more detailed description of the adaptation and solution steps.

5.2.1 Adaptation Step

The key to adaptation is a weight function that determines where grid nodes need to be clustered for a more accurate solution. Such a weight function, w, can be built from a linear combination of the errors in the concentrations of various chemical species:

$$w \propto \sum_n \alpha_n \nabla^2 c_n \tag{1}$$

where ∇^2, the Laplacian, represents the error in c_n, the computed value of the concentration of species *n*. The chemical mechanisms used in AQMs usually have a large number of species. Due to non-homogeneous distribution of emissions and disparate residence times, each species may have very different resolution requirements. Determining α_n such that pollutant concentrations (e.g., ozone) can be estimated most accurately is a current research topic. Here, all α_n are set to zero, except the one for nitric oxide (NO). Further, the grid adaptation is restricted to the horizontal plane, and the same grid structure, which is determined by the surface layer NO concentrations, is used for all vertical layers. This, combined with the requirement that the Courant number should be less than unity, may result in very small solution time steps because of high wind speeds aloft. Adaptation in the vertical direction is possible but more complicated.

The grid nodes are repositioned by using the weight function. The new position of the grid node *i*, $\vec{P}_i^{new}$, is calculated as:

$$\vec{P}_i^{new} = \sum_{k=1}^{4} w_k \vec{P}_k \Big/ \sum_{k=1}^{4} w_k \tag{2}$$

where $\vec{P}_k$, $k = 1,\ldots,4$, are the original positions of the centroids of the four cells that share the grid node *i*, and w_k is the weight function value associated with each centroid.

Once the grid nodes are repositioned, cell-averaged species concentrations must be recomputed for the adapted grid cells. Holding the concentration field fixed and moving the grid is numerically equivalent to simulating the advection process on a fixed grid. Therefore, we use a high-order accurate and monotonic advection scheme known as the piecewise parabolic method (Collela and Woodward, 1984) to interpolate concentrations from the old to the new grid locations.

The calculation of the weight function, the movement of the grid nodes, and the interpolation of species concentration from the old to the new grid locations are three distinct tasks of an iterative process. The process continues until the maximum grid node movement is less than a preset tolerance. A very small tolerance may lead to a large number of iterations. On the other hand, a large tolerance may not ensure adequate resolution of the solution field. Currently, we stop iterating when, for any grid node, the movement is less than 5% of the minimum distance between the node in question and the four nodes to which it is connected.

After the grid nodes are repositioned, emissions and meteorological data must be processed to generate the necessary inputs for the solution step. Note that, unlike the practice with fixed grid AQMs, this processing could not be performed prior to the simulation because there is no *a priori* knowledge of where the nodes would be located at any given time. In case of meteorological data, an ideal solution would be to run a meteorological model (MM), which can operate on the same adaptive grid, in parallel with the AQM. This

would ensure dynamic consistency of meteorological inputs, but such a MM is currently nonexistent. Therefore, hourly meteorological data are obtained from a high-resolution, fixed-grid MM simulation and interpolated onto the adaptive grid. For mass conservation, as a minimum requirement, the vertical wind components are readjusted later during the solution step as described in Odman and Russell (2000).

The processing of emission data is computationally expensive, requiring identification of various emission sources in the adapted grid cells. Here, we treat all emission sources in two categories: point and area sources. For simplicity, the mobile sources have been included in the area-source category, but treating them as line sources would yield better resolution. For the point sources, the grid cell containing the location of each stack must be identified. The search may be quite expensive if there are thousands of stacks in the modeling domain. However, assuming that the cell containing the stack before adaptation would still be in close proximity of the stack after adaptation, the search can be localized. The localization of the search provides significant savings over more general, global searches. As for the area sources, they are first mapped onto a uniform high-resolution *emissions grid* using geographic information systems. This is done in order to avoid higher computational costs associated with processing of emissions from highly irregular geometric shapes presented by highways and counties. Around each adaptive grid cell there is a box of emissions grid cells $E_i, i = 1,\ldots,n$, as illustrated in Figure 5-1. Once each E_i is identified, then their polygonal intersections with the adaptive grid cell are determined. Finally, the areas of these polygons, S_i, are multiplied by the emission fluxes of E_i and summed over n to yield the total mass emitted into the adaptive grid cell. This process is performed for all adaptive grid cells.

The final step in preparation for the solution step is reestablishing a uniform grid for easy computation of the solution. This requires computation of a transformation from the (x, y) space where the grid is non-uniform to the (ξ, η) space where the grid would be uniform. The calculation of the Jacobian of the transformation and other necessary metrics (i.e., $\partial\xi/\partial x, \partial\xi/\partial y, \partial\eta/\partial x, \partial\eta/\partial y$) concludes the adaptation step.

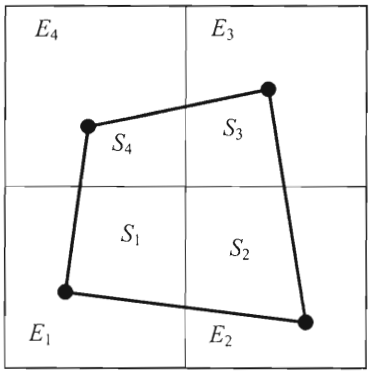

Figure 5-1 Intersection of an adapting grid cell with the area-source emissions grid.

5.2.2 Solution Step

The atmospheric diffusion equation in the (ξ,η,σ) space can be written as

$$\frac{\partial(Jc_n)}{\partial t}+\frac{\partial(Jv^{\xi}c_n)}{\partial \xi}+\frac{\partial(Jv^{\eta}c_n)}{\partial \eta}+\frac{\partial(Jv^{\sigma}c_n)}{\partial \sigma}+\frac{\partial}{\partial \xi}\left(JK^{\xi\xi}\frac{\partial c_n}{\partial \xi}\right) + \frac{\partial}{\partial \eta}\left(JK^{\eta\eta}\frac{\partial c_n}{\partial \eta}\right)+\frac{\partial}{\partial \sigma}\left(JK^{\sigma\sigma}\frac{\partial c_n}{\partial \sigma}\right)=JR_n+JS_n \tag{3}$$

where c_n, R_n, and S_n are the concentration, chemical reaction, and emission terms of species n, respectively, and σ is a terrain-following vertical coordinate. J is the Jacobian of the coordinate transformation:

$$J=\frac{1}{m^2}\frac{\partial z}{\partial \sigma}\left(\frac{\partial x}{\partial \xi}\frac{\partial y}{\partial \eta}-\frac{\partial y}{\partial \xi}\frac{\partial x}{\partial \eta}\right) \tag{4}$$

where m is the scale factor of a conformal map projection in the horizontal. The components of the wind vector in ξ and η directions are v^{ξ} and v^{η}:

$$\begin{aligned} v^{\xi} &= m\frac{\partial \xi}{\partial x}U+m\frac{\partial \xi}{\partial y}V \\ v^{\eta} &= m\frac{\partial \eta}{\partial x}U+m\frac{\partial \eta}{\partial y}V \end{aligned} \tag{5}$$

where U and V are real horizontal wind velocities rotated in the map's coordinate directions. The turbulent diffusivity tensor is assumed to be diagonal, and its elements are $K^{\xi\xi}$, $K^{\eta\eta}$, and $K^{\sigma\sigma}$. $K^{\sigma\sigma}$ can be expressed in terms of the vertical diffusivity K^{zz} as:

$$K^{\sigma\sigma}=\left(\frac{\partial \sigma}{\partial z}\right)^2 K^{zz}. \tag{6}$$

The expressions for v^{σ} (the wind component in the σ direction), $K^{\xi\xi}$, and $K^{\eta\eta}$ are omitted here due to space limitations. Since the grid is uniform in the (ξ,η) space, solution algorithms can be taken directly from existing AQMs. We use those described by Odman and Ingram (1996).

5.3 Model Verification

The adaptive grid AQM is being verified by simulating ozone air quality in the Tennessee Valley region for the July 7-17, 1995, period. Meteorological data from a 4×4 km resolution simulation with the Regional Atmospheric Modeling System (RAMS) are being used. The emissions inputs for the region were developed from the Southern Appalachian Mountains Initiative (SAMI) inventory. There are over 9000 point sources in this domain including some of the largest power plants in the U.S.A. The area sources were mapped onto a 4×4 km emissions grid. The AQM grid consists of 112 by 64 cells, initially at 8×8 km

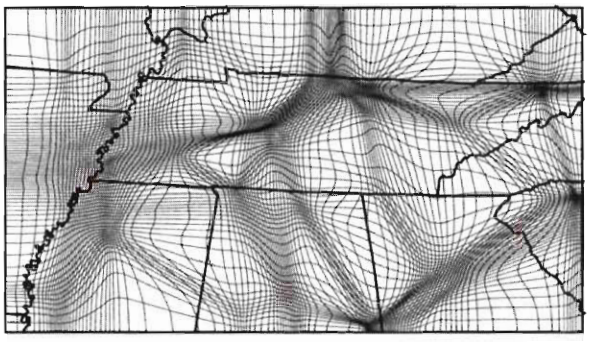

Figure 5-2 The grid used from 7:00 to 8:00 EST during the simulation of July 7, 1995.

resolution. In the vertical, there are 20 unequally spaced layers extending from the surface to 5340 m. Starting with 32 m, the thickness of each layer increases with altitude.

Figure 5-2 shows the grid at 7:00 EST on July 7. Since the adaptation step is performed once an hour, the grid shown will not change until 8:00 EST. Note that the grid size is reduced to few hundred meters around large point sources. With wind speeds larger than 10 m/s aloft, the solution time step can drop below 1 minute to keep the Courant number less than unity. Because of this, the simulation is progressing at the speed of about 2 hours of CPU time per simulation hour on a SUN Blade workstation (Model 1000) with a 750 MHz Ultra SPARC III processor.

The surface layer NO concentrations at 7:00 EST that were used in generating the grid in Figure 5-2 are shown in Figure 5-3 (top frame). Also shown are the NO concentrations at the same hour from a 4×4 km resolution fixed grid AQM simulation (bottom frame). The adaptive grid captures the NO gradients near source areas with a level of detail that is far superior to the fixed grid even though the latter used 4 times more grid nodes. Note that some large power plant stacks, such as Cumberland, are emitting above the stable boundary layer at this hour. Since their plumes do not affect the surface layer NO concentrations, no grid clustering is observed in Figure 5-2 around such stacks. During daytime hours, as such plumes mix down and start affecting the surface layer NO concentrations, grid nodes are clustered around them, along with other sources.

Figure 5-4 shows the ozone (O_3) concentrations obtained from the adaptive grid AQM simulation at 17:00 EST on July 7, 1995. Since this is only the first day of the simulation, the O_3 concentrations are probably still sensitive to the uniform initial conditions (35 ppb everywhere). However, the observed level of variability in the field and the captured detail in the gradients are encouraging. Once this simulation is finished, O_3fields will be compared to those obtained from fixed grid AQM simulation at 4×4 and 8×8 km resolutions using the same inputs and solution algorithms. To complete the verification, all simulated O_3 fields will be compared to observations from routine monitoring network as well as intensive field studies conducted in the region during this episode.

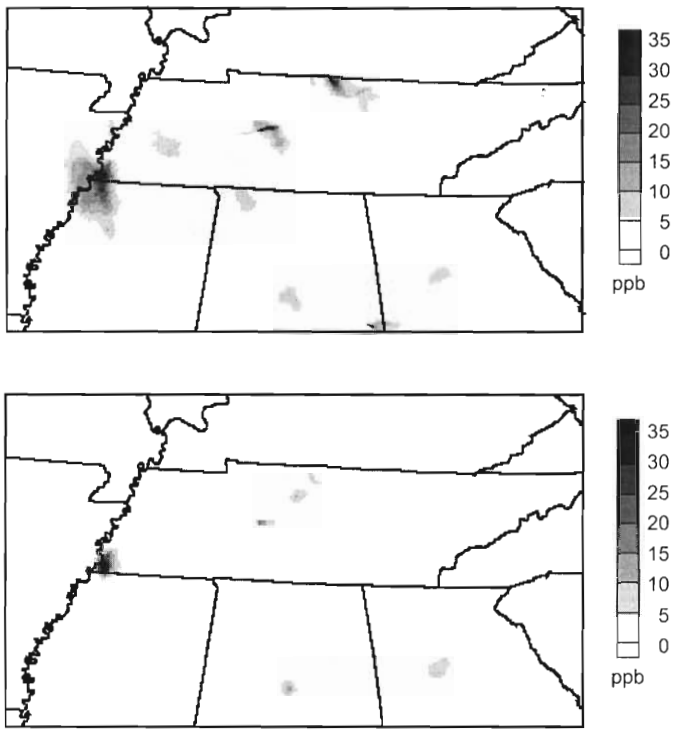

Figure 5-3 NO concentrations at 7:00 EST on July 7, 1995, from adaptive grid (top) and 4x4 km fixed grid (bottom) AQM simulations.

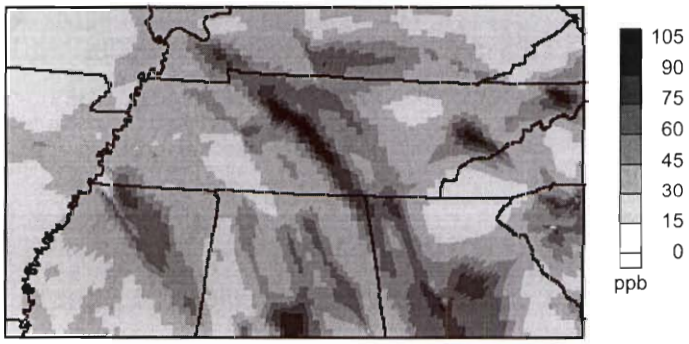

Figure 5-4 Ozone concentrations at 17:00 EST on July 7, 1995, from the adaptive grid AQM simulation.

5.4 Conclusion

An adaptive grid, urban-to-regional scale AQM has been developed. A simulation with this model evolves as a sequence of adaptation and solution steps. During the adaptation step, the solution (i.e., concentration fields) is frozen in time. A weight function that can

detect the error in the solution is used to move the nodes of a structured grid. Iterative movement of the grid nodes continues until the solution error is reduced sufficiently. During the solution step, the grid is held fixed and the solution is advanced in time. However, before this can be done, the meteorological and emissions inputs must be mapped onto the adapted grid. For meteorological inputs, data are interpolated from a very-high-resolution mesoscale model simulation. For emissions, efficient search and intersection algorithms were developed to ensure proper allocation of point and area sources to the cells of the adapted grid. Using coordinate transformations, the non-uniform grid can be mapped into a space where it becomes uniform. The atmospheric diffusion equation in this new space has been derived. Since the form of the equation is very similar to forms in existing AQMs and the grid is uniform, numerical algorithms developed for fixed uniform grid AQMs can be used to advance the solution.

To verify the model, the July 7-17, 1995, ozone episode in the Tennessee Valley is being simulated. So far, the grid is adapting to dynamic changes in the NO fields as expected. Nodes are clustered around major emission sources with grid resolutions around 200 m. The NO and O_3 fields show gradients with a level of detail that is likely unprecedented for a regional simulation of this scale. However, the simulation is progressing slowly due to very short solution time steps. This will probably necessitate changes in solution algorithms such as using an implicit advection scheme that is not subject to the Courant stability limit. Adaptation criteria are also being developed that would consider the errors not only in NO but in other species as well, especially those involved in important O_3 formation reactions.

Acknowledgements

This research is supported by U.S. Environmental Protection Agency Grant No. R 827028-01-0. We thank Steve Mueller of the Tennessee Valley Authority for providing the meteorological data.

References

Benson, R. A., and McRae, D. S., 1991, A Solution adaptive mesh algorithm for dynamic/static refinement of two and three-dimensional grids, in: *Proceedings of the Third International Conference on Numerical Grid Generation in Computational Field Simulations*, Barcelona, Spain, p. 185.

Collela, P., and Woodward, P. R., 1984, The piecewise parabolic method (PPM) for gas-dynamical simulations, *J. Comput. Phys.* **54**:174.

Odman, M. T., and Russell, A.G., 1991, A multiscale finite element pollutant transport scheme for urban and regional modeling, *Atmos. Environ.* **25A**: 2385.

Odman, M. T., and Ingram, C., 1996, *Multiscale Air Quality Simulation Platform (MAQSIP): Source Code Documentation and Validation*, MCNC Technical Report ENV-96TR002, Research Triangle Park, North Carolina, pp.11-32.

Odman, M. T., Mathur, R., Alapaty, K., Srivastava, R. K., McRae, D. S., and Yamartino, R. J., 1997, Nested and adaptive grids for multiscale air quality modeling, in: *Next*

Generation Environmental Models and Computational Methods, G. Delic, and M. F. Wheeler, eds., SIAM, Philadelphia, pp. 59-68.

Odman, M. T., Russell, A. G., 2000. Mass conservative coupling of non-hydrostatic meteorological models with air quality models, in: *Air Pollution Modeling and its Application XIII*, S.-E.Gryning, and E. Batchvarova, eds., Kluwer Academic/Plenum Publishers, New York, pp. 651-660.

Srivastava, R. K., McRae, D. S., and Odman, M. T., 2000, An adaptive grid algorithm for air quality modeling; *J. Comput. Phys.* **165**: 437.

Srivastava, R. K., McRae, D. S., and Odman, M. T., 2001(a), Simulation of a reacting pollutant puff using an adaptive grid algorithm, *J. Geophys. Res.*, in press.

Srivastava, R. K., McRae, D. S., and Odman, M. T., 2001(b), Simulation of dispersion of a power plant plume using an adaptive grid algorithm, *Atmos. Environ.,* in press.

6 Modeling Plumes with Adaptive Grid Air Quality Model

Abstract

A three-dimensional adaptive grid air quality model has been developed that clusters the grid nodes in regions with potentially large errors. Higher grid resolution in such regions enables the model to better track the dynamics of plumes that originate from various emission sources and source regions and improves the overall accuracy of air quality modeling predictions. The model was applied to a geographic domain that includes some of the fastest growing urban areas and transportation coordinates in the southeastern United States. This paper compares the adaptive grid air quality modeling simulation results with observations as well as with predictions from a conventional static grid air quality model. The results indicate that by dynamically adjusting the shape and the size of the grid cells, the adaptive grid air quality model is able to capture the structure and dynamics of plumes better than its static grid counterpart.

Various grid adaption criteria for more accurate ozone modeling were evaluated in this research work. The results show that, although the use of upper layer NO concentrations and ozone production rates to cluster the grid nodes increases the ability of the adaptive grid model to capture plumes that originate from elevated sources, the normalized error in ozone prediction at monitoring station is higher as compared to an adaptive grid simulation that utilizes the surface NO concentration field.

6.1 Introduction

Air quality models have seen an increasing use in air quality management over the last two decades. They provide a scientific basis of linking emissions and future changes in emissions to future air quality (Russell, 1997) and are thus reliable tools for developing and evaluating emission control strategies. However, air quality model results have an uncertainty associated with them from various sources. The lack of understanding of the physical and chemical processes that occur in the atmosphere, the absence of quality input data, limitations of the numerical techniques that are used to solve the governing equations that describe the atmospheric processes, computational limitations (e.g. grid resolution) and the procedures adopted to process the input data are only some of the factors responsible for this uncertainty.

Inaccuracies resulting from inadequate grid resolution become acute in case of regional scale modeling, where computational limitations necessitate the use of a grid resolution that is insufficient to capture the non-linear dynamics of pollutant species. To address this issue modeling techniques have been developed that use finer grids in regions of interest (e.g. cities) and coarse grid elsewhere (Odman et al. 1997; Alapaty et al. 1998). Techniques using multiple grid sizes are called nested or multi-scale modeling techniques. Another approach that can be used to achieve appropriate grid resolution involves dynamic adaptive grids (Srivastava, 2000; 2001a; 2001b). In preliminary applications involving dispersion and chemistry of puffs and plumes, the adaptive grid modeling technique proved to be more accurate and efficient than the conventional fixed grid approach. It is expected

that by clustering the grid nodes in regions with higher grid resolution requirements, the accuracy of air quality modeling predictions can be improved at significantly lower computational costs. The technique has been recently incorporated (Odman et al. 2002) into an ozone AQM developed by Odman and Ingram (1996). Several modifications were necessary. First, the governing equations were modified to accommodate the coordinate transformation that maps the non-uniform adapted grid onto a uniform grid in computational space. An emissions processor was developed that maps point, area and mobile sources onto the non-uniform grid cells after every grid adaption. For efficiency, this processor uses customized intersection algorithms instead of more general algorithms available through geographic information systems. A meteorological processor was also developed that can map the output of a uniform grid mesoscale meteorological model onto the adapted grid. This paper discusses in detail the performance of this model when it is applied to simulate an air pollution episode over Tennessee Valley and surrounding areas.

6.2 Description of Model Application

A simulation with an adaptive grid AQM can be viewed as a sequence of adaptation and solution steps. During the adaptation step, the solution (i.e., concentration fields) is frozen in time. A weight function that can detect the error in solution is used to move the grid nodes. Iterative movement of the grid nodes continues until the error is reduced sufficiently. During the solution step, the grid is held fixed and the solution is advanced in time. However, before this can be done, the meteorological and emissions data has to be mapped onto the adapted grid. Finally, using coordinate transformation, the non-uniform adapted grid is mapped onto a uniform grid in the computational space. Once, this is done, all the numerical solution algorithms developed for static grid AQMs become available for time advancement of the solution. The model requires more extensive source specific emissions data efficient algorithms to map the emissions on an adapting grid. A fine resolution meteorological modeling run is used to map the meteorological data on the adapting grid. Whereas, the computational efficiency of the adaptive grid model is largely dependent on the emissions and meteorological data processing algorithms, the accuracy of the modeling results is largely dependent on how accurately the weight function is able to determine the grid resolution requirements. Detailed description of the model has been provided in Odman et al. (2002).

6.2.1 Modeling Domain

The adaptive grid air quality model was applied to a geographic region that extends from the Appalachian Mountains to Arkansas in the east-west direction and from southern Kentucky to South Georgia in the north-south direction (Figure 6-1). Located within the domain are some of the fastest growing urban areas and transportation corridors in the southeastern United States. Also located within the domain are some of the biggest power plants in the United States. The region has experienced several severe air pollution episodes over the last decade and almost all major cities located within the modeling domain violate the current one-hour and the proposed eight-hour ozone standard. Whereas the anthropogenic emissions of Volatile Organic Compounds (VOC) and Nitrogen Oxides (NO_x) are concentrated around the urban centers and transportation corridors, the biogenic emissions, predominantly of isoprene, are more or less evenly distributed throughout the domain. The

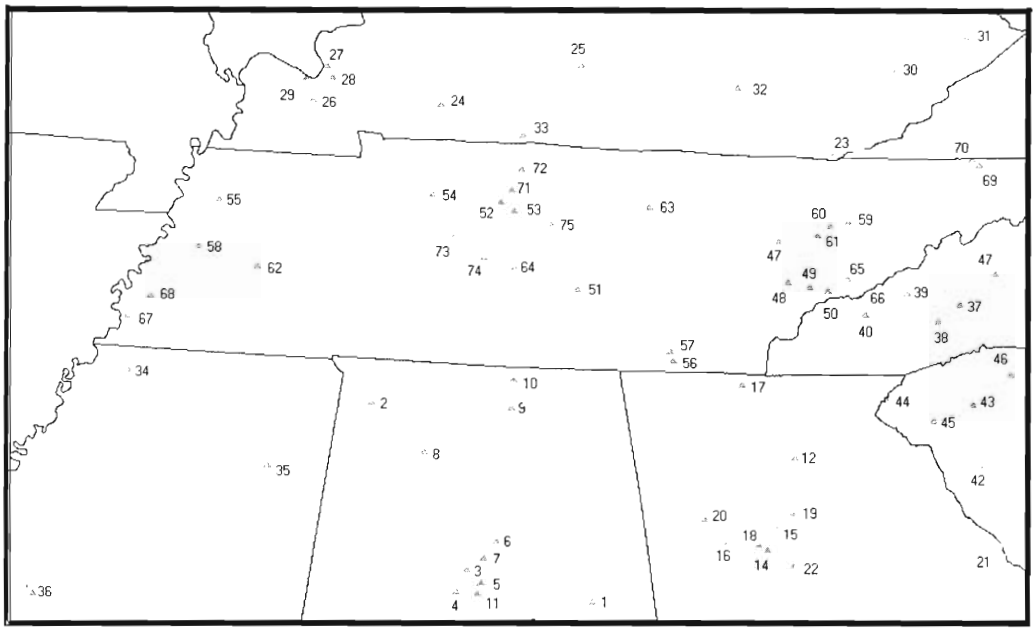

Figure 6-1 Modeling Domain and locations of monitoring stations

complex interaction of NO_x emissions from urbanized areas and point sources with highly reactive VOC emissions from biogenic sources makes the region an ideal candidate for the application and evaluation of a three-dimensional adaptive grid air quality model.

6.2.2 Modeled Episode

The July 7-17, 1995 air pollution episode was selected for this research work. The episode is known for a relatively short but intense heat wave. A high-pressure system advanced from the northwest resulting in high temperature and humidity that resulted in significant build up of ozone and aerosols in the eastern United States (Doty et al. 2001). Various monitoring stations located within the domain recorded multiple exceedances of the one-hour ozone standard. Public interest in this particular air pollution episode led to the development of an extensive meteorological and air quality database. This database has been extensively used in various air quality modeling studies (e.g., Odman et al. 2002) and has thus undergone various quality assurance checks. Following sections describe briefly the input data preparation steps required for conducting static grid simulations at 4 and 8-km grid resolution and an adaptive grid simulation in order to evaluate the performance of the adaptive grid air quality model.

6.2.3 Meteorological Data

Researchers at the Tennessee Valley Authority (TVA) conducted fine resolution meteorological modeling for this episode using the Regional Atmospheric Modeling System (RAMS) (Pielke et al. 1992). The meteorological modeling simulation was conducted on a 227x131x20-cell grid at 4-km horizontal and variable vertical grid resolution. The results

from this simulation were processed to generate the meteorological input files for static and adaptive grid simulations. Air density, deposition and friction velocities, surface heat fluxes, ground surface temperatures, etc., that were not provided by the RAMS simulation were computed using the Meteorology Chemistry Interface Processor (MCIP) (Byun and Ching, 1999).

6.2.4 Emissions Data

Pechan/Avanti Group developed the base emissions data for the region as part of the SAMI air quality modeling study (Odman et al. 2002). The Emissions Modeling System (EMS-95) (Wilkinson et al. 1994) was used to process this database and generate the emissions for the modeling domain. EMS-95 generates speciated day-specific, hour-by-hour gridded emission inputs for static grid air quality modeling simulations. For the adaptive grid air quality model, minor modifications to EMS-95 and additional processing were required to generate the source specific data. In case of point sources: source specific plume rise was computed using source coordinates, stack parameters and meteorological variables available in the emissions and meteorological databases. Emissions from area, mobile and biogenic sources have been mapped onto a uniform 8-km resolution grid that serves as an area source emission grid for all three simulations.

6.2.5 Initial and Boundary Conditions

Initial conditions are species concentrations specified at all grid cells at a date and time that corresponds to the starting date and time of the modeling simulation. Boundary conditions consist of time and space variant species concentrations at the boundary grid cells of the modeling grid. For this research work, initial and boundary conditions of CO, SO_2, NO and O_3 were developed from observations recorded at monitoring stations during this air pollution episode. The observed concentrations were interpolated from the observational network onto the modeling grid (including the boundary grid cells) using special interpolation functions. The interpolation was performed once over the entire domain for initial conditions and along the boundaries during the entire simulation for boundary conditions. Detailed description of these interpolation functions has been provided in Odman et al. (2002).

6.3 Model Evaluation

A detailed model performance was undertaken in order to validate the adaptive grid air quality modeling results. For this purpose, air quality modeling simulations were conducted using a conventional static grid air quality model at 4 and 8 km grid resolutions. These simulations are referred from hereafter as the "fine" and "coarse" grid simulations respectively. For all three simulations, the predicted O_3 concentrations and observations recorded at the monitoring stations were used to compute normalized station error, NSE_i, defined as:

$$NSE_i = \frac{1}{N_i^{obs}} \sum_{ihour=1}^{nhour} \frac{\left| O_3^{observed} - O_3^{predicted} \right|}{O_3^{observed}}$$

where, $O_3^{predicted}$ and $O_3^{observed}$ are model-predicted and observed concentrations at station i and N_i^{obs} are the number of valid prediction-observation pairs drawn from the monitoring station data during the simulation. Since the normalized quantities can become large when observations are small, a cut-off value of 40 ppb is used in conjugation with the above equation. Whenever the observation is smaller than the cut-off value, that prediction-observation pair is excluded from the calculations.

The normalized error for the fine, coarse and adaptive grid simulations, for all 69 stations located within the modeling domain (Figure 6-1), is 43.9, 42.1 and 40.7 percent respectively. The cumulative distribution of the difference in the normalized error predicted

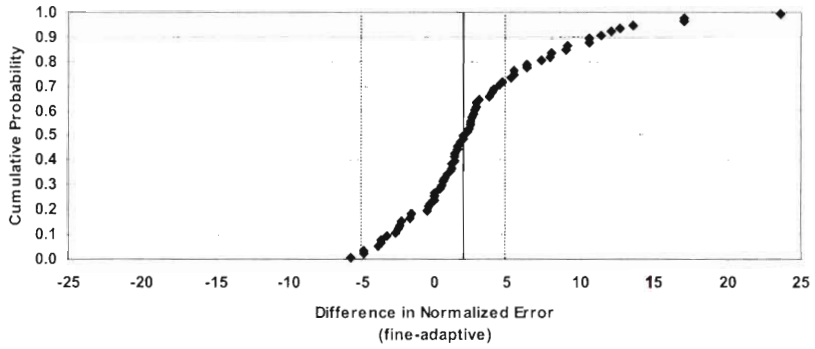

(a)

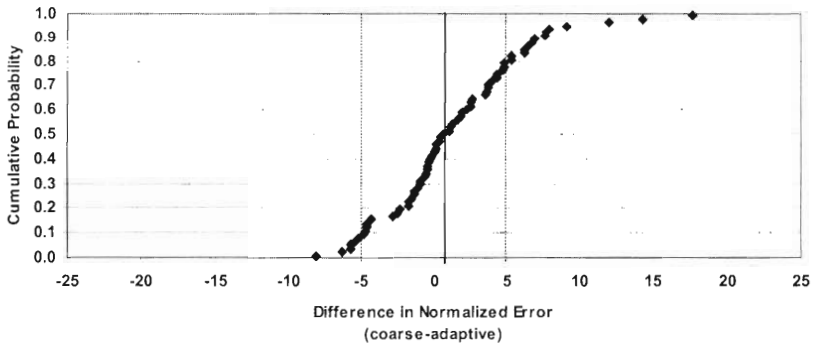

(b)

Figure 6-2 Cumulative probability distribution of the difference in the average normalized error between the fine and adaptive grid simulations (a) and coarse and adaptive grid simulations (b).

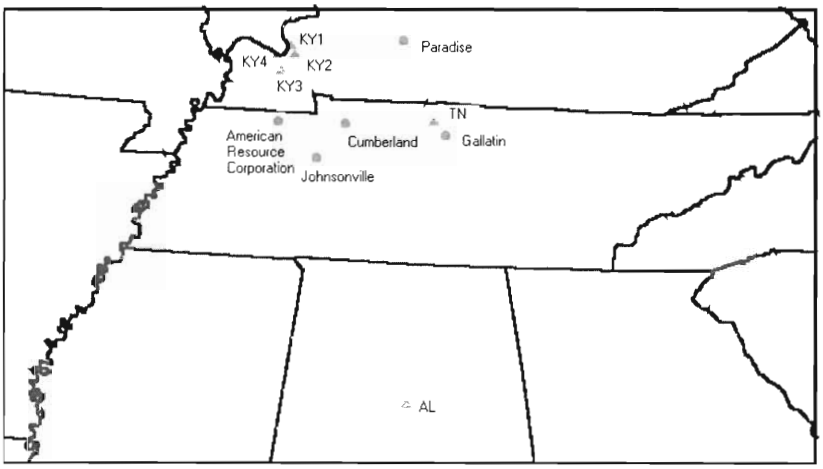

Figure 6-3 Location of industrial sources (circles) and monitoring stations (triangles)

by the adaptive and static grids is shown in Figure 6-2. Figure 6-2a shows that the adaptive grid predicted a lower normalized error at almost 80 percent of the stations when compared with the fine grid simulation. The decrease in error for the adaptive grid at these 50 stations ranges from 0.4 to 23.6 percent with an average of 5.4 percent. On 16 stations at which the adaptive grid showed an increase in error, the minimum, maximum and average increase in normalized error is 0.4, 5.8 and 2.8 percent respectively. Three stations showed no difference in the normalized error. Figure 6-2b shows that the adaptive grid showed a lower normalized error at more than 50 percent of the stations when compared with the coarse grid. The decrease in normalized error at these 39 stations ranges from 0.1 to 17.6 with an average of 4.7 percent. On the 22 stations that showed higher normalized error for the adaptive grid, the increase in normalized error ranges from 0.1 to 8.1 with an average of 3.5 percent. Eight stations showed no difference in normalized error.

In order to further investigate the performance of the adaptive grid air quality model, the simulation results at five monitoring stations were studied in greater detail. The location of these monitoring stations is shown in Figure 6-3. Also shown in Figure 6-3 are the American Resource Corporation industrial facility, and power plants Cumberland, Johnsonville, Gallatin and Paradise.

Although the magnitude of the difference in normalized error predicted by the fine and coarse grid simulations at most stations is small, the fact that a finer grid simulation resulted in a higher normalized error at a number of stations required investigation. One such station was Tarrant City, Jefferson County, Alabama (labeled AL in Figure 6-3). The averaged normalized error for the fine, coarse and adaptive grid simulations on July 14th was 73, 22 and 34 percent respectively. Time series at one such station located in is shown in Figure 6-4.

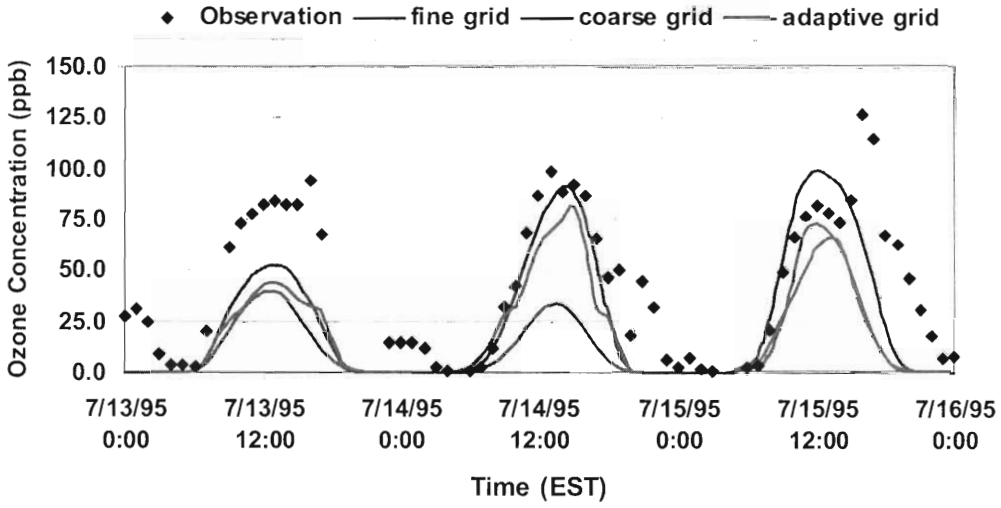

Figure 6-4 Observations, fine, coarse and adaptive grid simulation results at Tarrant City, Jefferson County, Alabama on July 14th, 1995.

Shown in Figure 6-5 is the location of this monitoring station; location of the fine, coarse and adaptive grid cells that contain the monitoring station at 1400 EST on July 14th, as well as the location of the point sources in the coarse grid cell. Since the prevailing wind direction was northwesterly during the mid-afternoon hours of July 14th, the monitor is not directly affected by point sources that are located northeast of it. However, since in Eulerian models, emissions from sources are allocated to the grid cells that contain those sources, emissions from all point sources that are located in the coarse grid cell shown in Figure 6-5 have been allocated to that cell. The allocation of emissions to a grid cell causes artificial dilution of these emissions and an instantaneous increase in the concentration of the primary emitted species (i.e., nitrogen oxides) in the grid cell. The NO mass emission rates in the fine and the coarse grid cells on 1400 EST on July 14th are 48.0 and 132.0 grams/seconds respectively which translate to an instantaneous concentration increase of 0.27 and 0.18 ppm. Compared to the coarse grid cell, the significant instantaneous increase in concentration of NO in the fine grid cell causes loss of ozone due to NO titration. In comparison, the adaptive grid cell only encloses point sources that are located northwest of the monitor. Only July 14th, 1400 EST the adaptive grid cell has a lower NO mass emission rate of 22.0 grams/seconds in a 14 km^2 grid cell resulting in an instantaneous concentration increase of 0.14 ppm which leads to less NO titration in the adaptive grid cell.

Time series of the predictions (Figure 6-6) from the static grid simulations and observed concentrations at the four monitoring stations located along the Missouri-Kentucky-Arkansas border shows that the fine and coarse grids over-predict the ozone concentration at these stations by as much as 190 ppb on July 12th, 1995. The adaptive grid performs much better and over-predicts by 25 ppb.

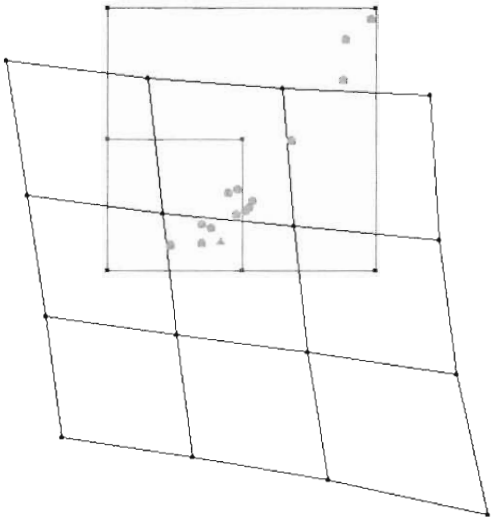

Figure 6-5 Location of monitoring station (orange triangle), Point sources (orange circle), coarse grid cell (red), fine grid cell (blue) and adaptive grid cell (black).

In case of the fine grid simulation, hourly surface concentration plots (Figure 6-7) show a well defined O_3 plume south-southeast of the monitoring stations around 1200 EST on July 12th. The plume is transported towards the monitoring station by southeasterly winds during the afternoon hours. Surface NO concentration plots (Figure 6-7) show that early morning NO emissions from the American Resource Corporation facility located in Henry County, Tennessee and the TVA Cumberland Steam Plant located in Stewart County, Tennessee contribute to the formation of this O_3 plume. Of special interest are the NO emissions from Cumberland Steam Plant. In the fine grid simulation (Figure 6-8), calm northeasterly winds during the mid-afternoon hours of July 11th, keep the concentrated NO plume in the vicinity of the source and facilitate ozone production. The core of the ozone plume is approximately 25 km southwest of the plant. As the winds change direction from northeasterly to southeasterly and pick up speed, the NO plume disconnects from the source and moves in the direction of the monitor as a puff. By 0900 EST on July 12th, the puff is 55 km from the plant. During the morning hours, injection of fresh VOC and NO emissions result in rapid production of ozone and its subsequent transport to the monitoring locations. The adaptive grid model simulates a completely different trajectory of the Cumberland puff and does not show that fresh morning emissions from the Cumberland Plant and American Resource Corporation facility and/or un-reacted upper layer NO concentration cause significant production of ozone in the vicinity of the monitors on July 12th (Figure 6-9). In the adaptive grid simulation, the puff gets disconnected from the source during the mid-afternoon hours of July 11th. By 2000 EST, the puff is at a distance of approximately 50 km to the southwest of

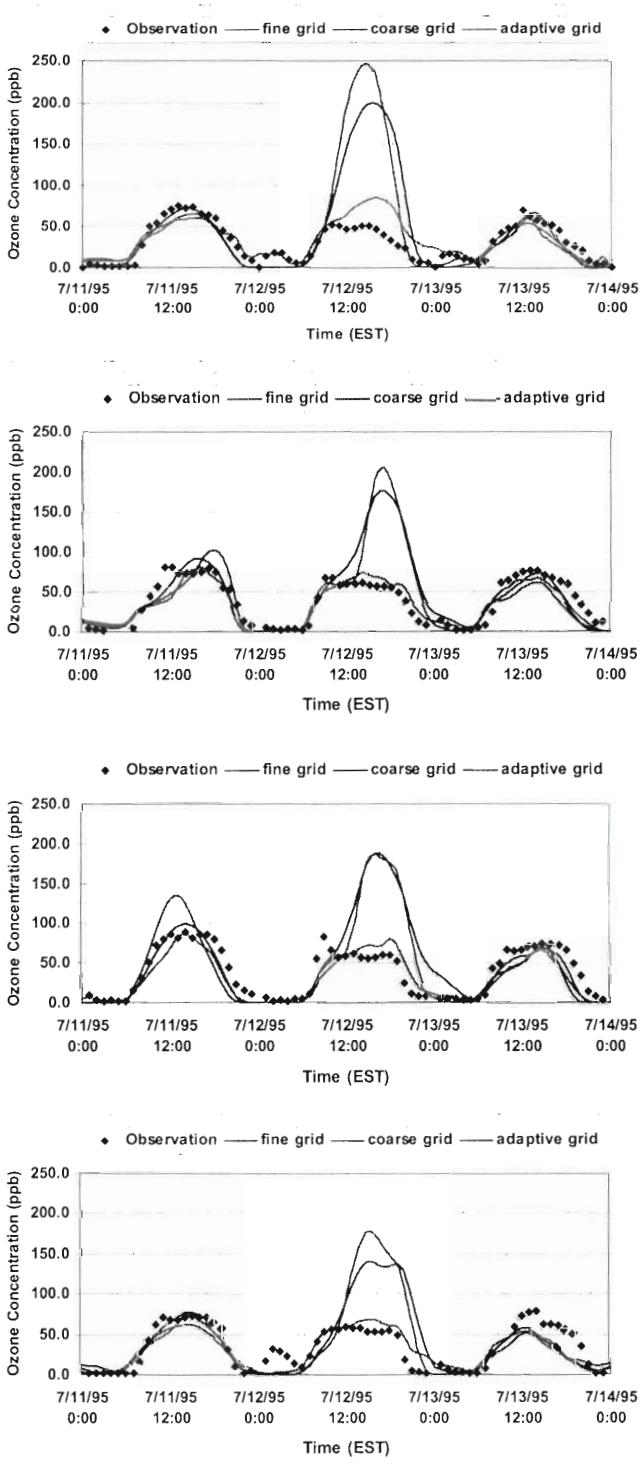

Figure 6-6 Time Series Analysis: Observations, fine, coarse and adaptive grid simulation results on July 11th, 12th and 13th at four observation stations in Kentucky (From top: referenced as KY1, KY2, KY3 and KY4 in Figure 6-3).

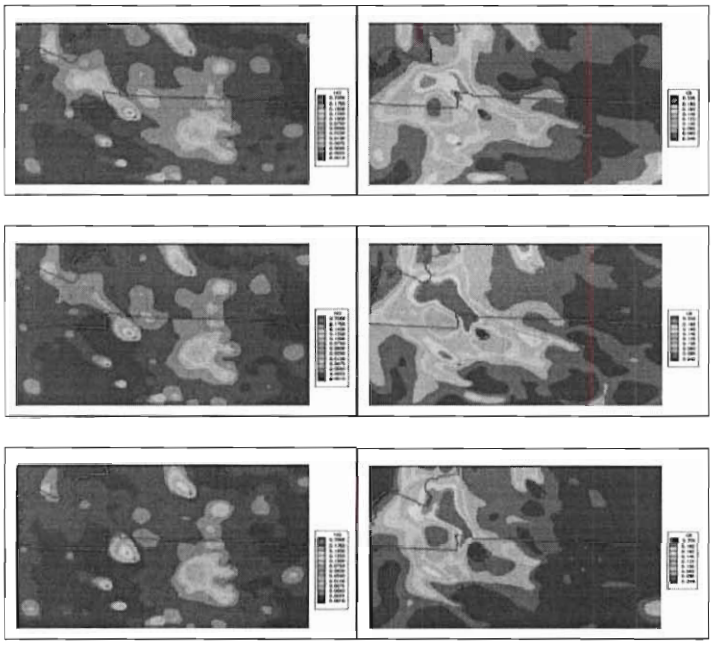

Figure 6-7 Spatial plots: Surface NO (left) and O_3 (right) concentration predicted by the fine grid on July 12th, 1995 at 1200 EST (1st row), 1500 EST (2nd row) and 1800 EST (3rd row)

the source before changing wind direction begins to transport the puff in a westerly direction. The maximum ozone produced by the NO puff during this journey is approximately 35 km from the source. As the adaptive grid model clusters the grid nodes over the Cumberland puff, grid cells become larger over the Cumberland plant and the American Resource Corporation facility. Dumping of the same mass of NO emissions in a larger grid cell results in a lower NO concentrations and reduced production of ozone downwind of the source. The difference in the trajectory of the puff (the fine grid places the puff at a distance of 55 km northwest, the adaptive grid places it 50 km southwest of the source at 2300 EST on July 11th) as simulated by the adaptive and static grid can be explained by analyzing the wind field at 250 meters on July 11th at 1700 EST (Figure 6-10). The position of the puff at this hour as simulated by the adaptive and static grid models is also shown in Figure 6-10. Note that the trajectory of the Cumberland puff may be substantially different even for a small change in its location. Therefore, while it takes northwesterly course in the fine grid simulation, its trajectory is westerly in the adaptive grid simulation. It is this difference in the trajectory of the puff and the coarsening of the grid over the Cumberland plant and the American Resource Corporation facility as explained above, that leads to the difference in ozone at the monitors.

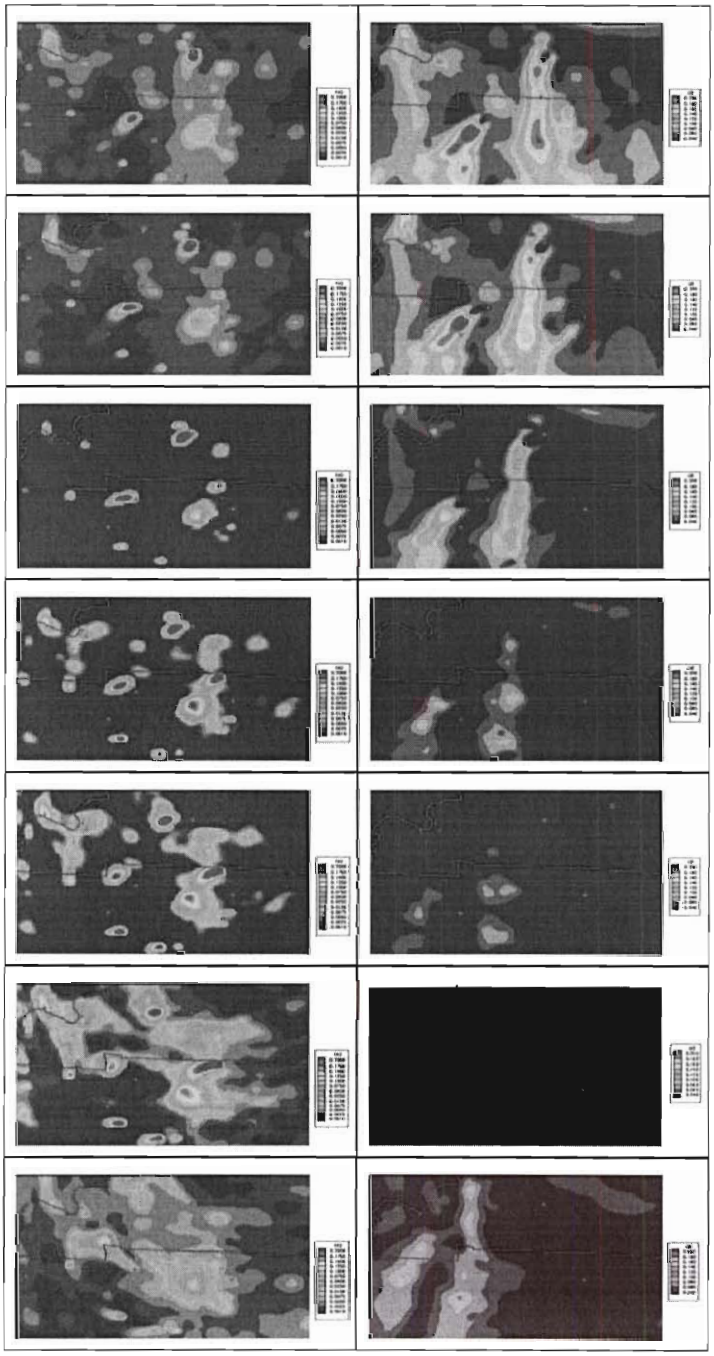

Figure 6-8 Spatial plots: Surface NO concentration (left) and O_3 concentration (right) predicted by the adaptive grid simulation on July 11th and 12th 1995. Starting from top: 1500, 1800, 2100 EST on July 11th and midnight, 0300, 0600, 0900 EST on July 12th

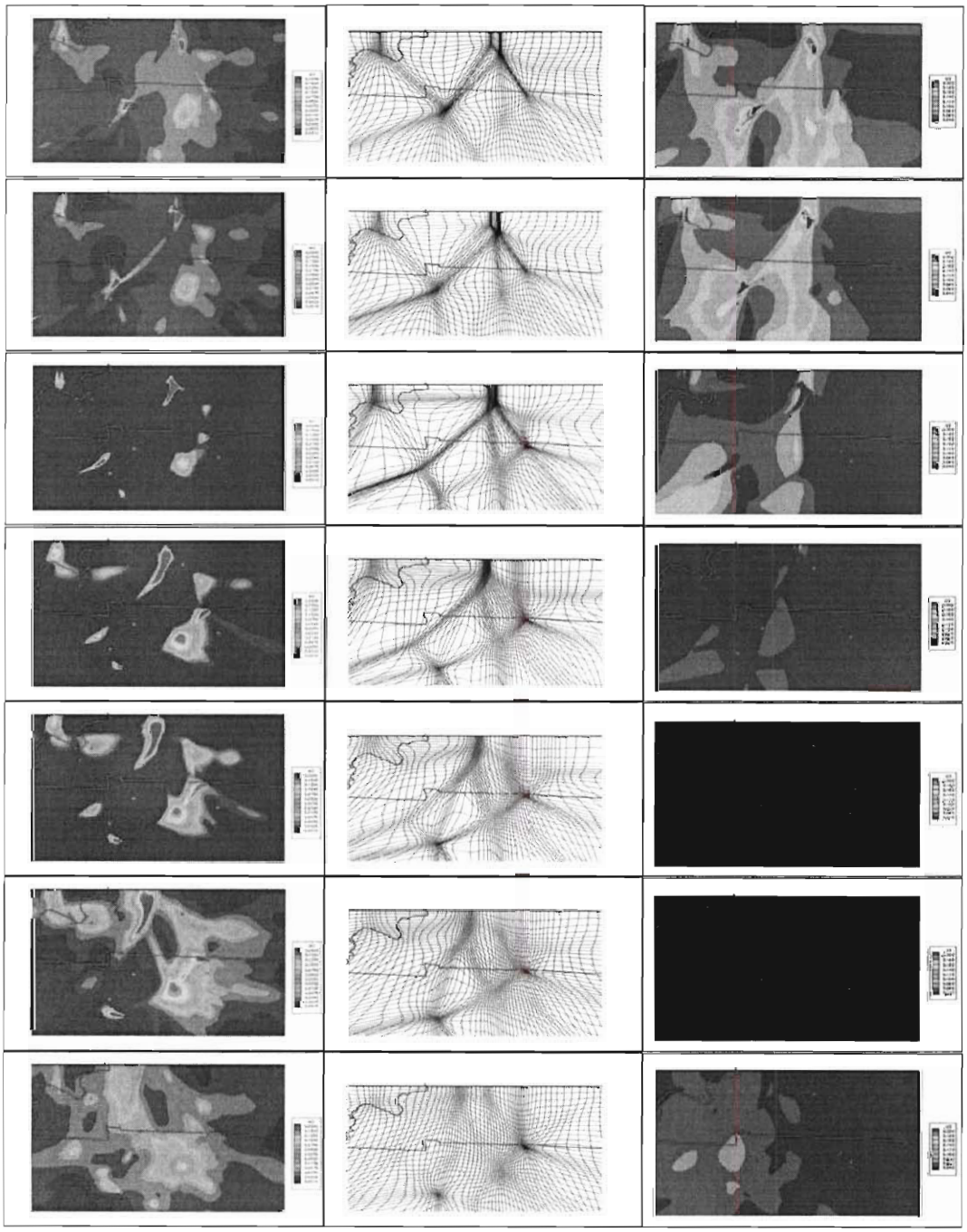

Figure 6-9 Spatial plots: Surface NO concentration (left), adapted grid (center) and surface O_3 concentration (right) predicted by the adaptive grid simulation on July 11th and 12th 1995. Starting from top: 1500, 1800, 2100 EST on July 11th and midnight, 0300, 0600, 0900 EST on July 12th.

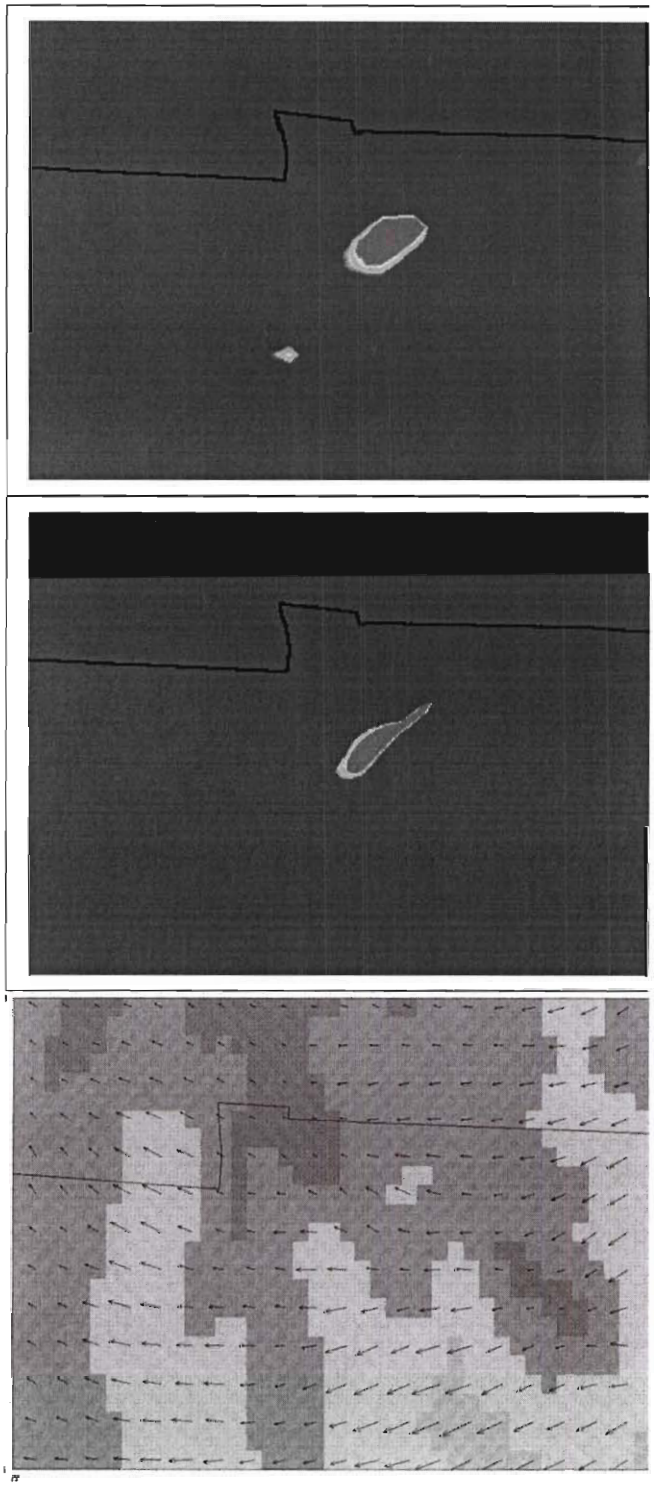

Figure 6-10 Cumberland Power Plant Plume as simulated by the fine (top) and adaptive grids (middle) and the wind field at 250 meter at 8-km resolution on July 11th, 1700 EST

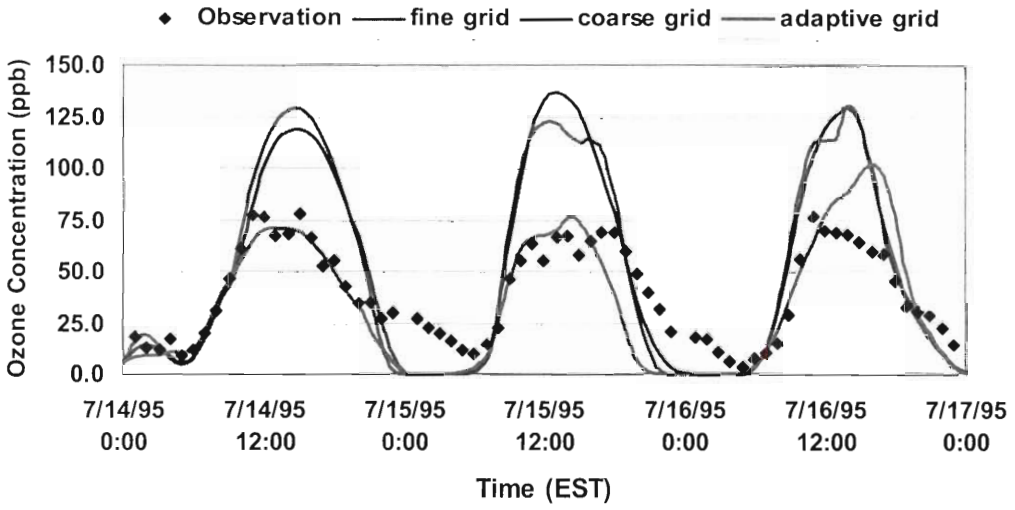

Figure 6-11 Time Series Analysis: Observations, fine, coarse and adaptive grid simulation results at the Observation station (referenced as TN in Figure 6-3) in Tennessee from 0000 EST July 14th to 0000 EST July 17th, 1995.

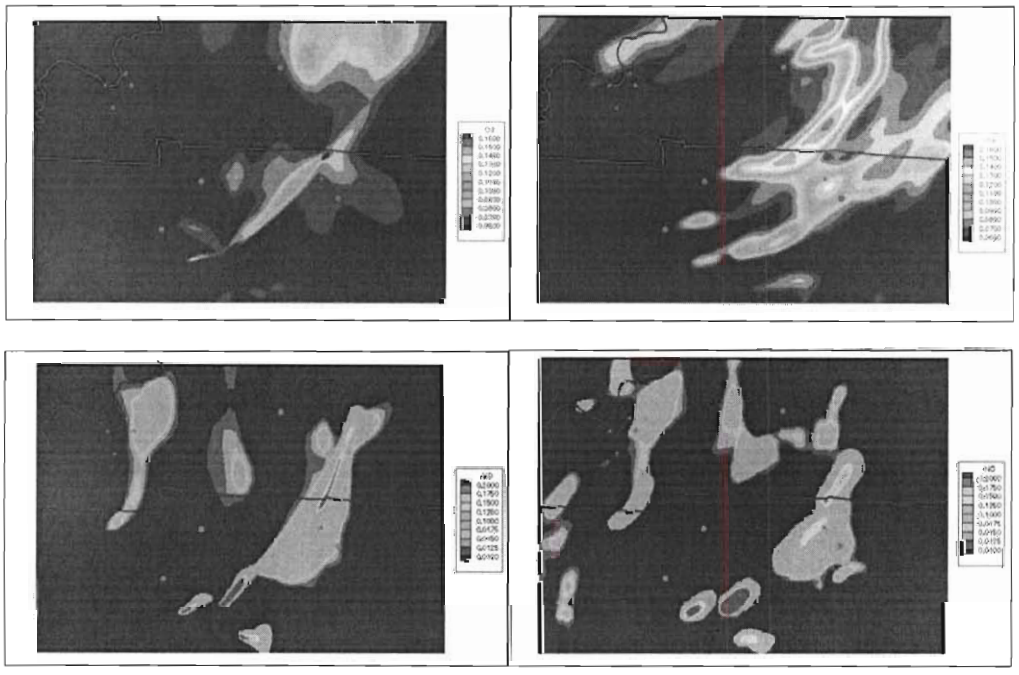

Figure 6-12 Spatial plots: 1st row: Surface O_3 concentration predicted by adaptive grid (left) and fine grid (right) at 1200 EST on July 15th. 2nd row: Surface NO concentration predicted by adaptive (left) and static (right) at 0600 EST on July 15th.

The fifth monitoring station that was selected for an in-depth analysis is located in Summer County, Tennessee, 20 km northeast of Nashville. Time series (Figure 6-11) revealed an over prediction by the static grids by as much as 55 ppb on July 15th. Analysis of the surface NO concentration field predicted by the fine grid (Figure 6-12) shows that the southwesterly winds during the early morning hours on July 15th 1995 transport a large NO plume from Nashville towards the monitor. Low wind speeds provide sufficient time for the plume to produce large amounts of ozone. The adaptive grid (Figure 6-12) on the other hand simulates a narrower NO plume from Nashville travels west of the monitor. Clearly, the adaptive grid results are more consistent with observations at the monitoring station.

6.4 Adaptation Criteria for Ozone Modeling

Although relatively well understood, the formation, destruction and transport of tropospheric ozone is a complex process. A weight function can be built as a linear combination of the error in the species concentration and/or of variables (i.e., reaction rates, mixing heights, etc) that are responsible for the production and/or destruction of ozone. However, owing to the heterogeneous distribution of emissions over the modeling region and the non-linear physical and chemical processes that affect ozone formation, the contribution of these variables to the error in ozone prediction in one region of the domain might be significantly different from those in another region. Thus, a quantitative assessment of the contribution of these variables towards the error in ozone prediction is non-trivial.

Here, we discuss the development and evaluation of a grid node repositioning criteria (also referred to as the weight function) for more accurate ozone modeling. A description of the weight function variables that have been evaluated is followed by a discussion of the modeling results when the adaptive grid model is used to simulate an air pollution episode over Tennessee Valley and surrounding areas.

Table 6-1 Description of the weight function for the Adaptive grid simulations

Simulation name	**Weight function description**	**Mathematical formulation**
Simulation # 1	Surface NO concentration	$[NO]_{(i,j,1)}$
Simulation # 2	Maximum Column NO concentration	$[NO]_{(i,j,\max k)}$
Simulation # 3	Sum of normalized column maximum NO concentration and O_3 production rate	$\frac{[NO]_{(i,j,\max k)}}{[NO]_{\max(i,j,k)}} + \frac{[PO_3]_{(i,j,\max k)}}{[PO_3]_{\max(i,j,k)}}$

6.4.1 Weight Functions Used

The adaptive grid modeling simulation above used the surface NO concentration field (simulation # 1) to build the weight function for grid node repositioning. Although significant grid node clustering was observed during night time hours over NO plumes that originated from ground level emission sources, limited grid node clustering occurred in the vicinity of elevated sources. Two additional adaptive grid simulations were conducted to further improve the ability of the model to capture ozone plume dynamics. In the first simulation (simulation # 2), the three dimensional NO concentration field was used to build the weight function for grid adaption. This is intended to cluster the grid nodes over NO plumes that originate from elevated sources. The second simulation (simulation # 3) uses a linear combination of the three dimensional NO concentration field and ozone production rate P (O_3) (Table 6-1) to cluster the grid nodes. The ozone production rate is derived from the radical budget equation applicable to low and high NO_x conditions. Adapted from Kleinmen et al. (1997), the following is a brief description of derivation for the analytical expression for the ozone production rate.

The only significant net chemical source of NO_2 in the troposphere is from the reaction of peroxy radicals with NO.

$$HO_2 + NO \xrightarrow{k_1} NO_2 + OH \qquad (R_1)$$

$$RO_2 + NO \xrightarrow{k_2} (1-\delta)NO_2 + (\delta)organic\ nitrates \qquad (R_2)$$

where k_1 and k_2 are the rate constants for two reactions. This is followed by the photolysis of NO_2 resulting in production of the O atom and the subsequent production of ozone.

$$NO_2 + h\nu \longrightarrow NO + O^1(D) \qquad (R_3)$$

$$O^1(D) + O_2 \rightarrow O_3 \qquad (R_4)$$

The ozone production rate can be defined as a function of per-oxy radical and nitrogen oxide concentrations.

$$P(O_3) = k_t([HO_2] + [RO_2])[NO]$$

where k_t is the weighted average rate constant for reactions R_1 and R_2 and is defined as,

$$k_t = \frac{[HO_2]}{[HO_2]+[RO_2]}k_1 + \frac{[RO_2]}{[HO_2]+[RO_2]}(1-\delta)k_2$$

The variables discussed above can result in a highly non-uniform field resulting in the formation of concave or highly skewed grid cells. To avoid this, the Laplacian operator (∇^2)

followed by a diffusive filter (Srivastava, 2001a; 2001b) is applied to the weight function variable.

$$w_{i,j} = \sum_{n} \nabla^2 wf + w_{\min}$$

In the above equation, the Laplacian operator represents the error in the computed value of the weight function variable with respect to value obtained from interpolation from the neighboring cells. The variable $w_{\min}$ is the minimum allowable weight function and is computed as:

$$w_{\min} = 0.05 MAX\left(wf_{i,j}\right) + w_t .$$

where, w_t, is set to 0.001 in order to ensure a non-zero weight function. The final weight function is obtained by applying an area weighting to the filtered weight function.

$$w_{i,j} = A_{i,j}^{1+e}\left(w_{i,j}^{\text{filtered}}\right)$$

The parameter e controls the weighting with respect to the cell area A. A positive value gives more weight to larger cells and promotes gradual transition from larger to smaller cells. For this research work, the parameter e is set to -0.5.

6.4.2 Adaptive Grid Modeling Results

Adaptive grid simulations were conducted using the weight functions discussed above. A major objective of this research work was to study the effects of different grid adaption criteria on adaptive grid model predictions. To understand this effect, an assessment of the grid adaption criteria is useful.

Shown in Figure 6-13 are the adapted grids at 0300, 0900, 1500 and 2100 EST on July 13, 1995 for Simulations # 1 (left), # 2 (center) and # 3 (right) respectively. All three simulations show grid node clustering in the vicinity of major urban areas and NO_x sources. Compared to Simulations # 2 and # 3, simulation # 1 has more intense grid node clustering in the early morning and evening hours, resulting in a grid that has a significant number of voids (very large grid cells adjacent to very small grid cells). At 0900 and 1500 EST, simulation # 1 has an adapted grid with considerably lighter adaption than what is observed at 0300 and 2100 EST. This is also true for the other two simulations, but of a far lesser degree. In a qualitative sense, the degree of grid adaption in simulation # 3 is somewhere between Simulations # 1 and # 2.

The degree of grid adaption and the quality of adapted grid is consistent with expectations. In simulation # 1, stronger grid adaption is observed at night and in the early morning hours due to the presence of concentrated NO plumes (larger curvature of the surface NO concentration field). Injection of fresh emissions during the daylight hours; increased daytime mixing and photochemistry results in a more uniform surface NO concentration field (smaller curvature) which leads to relatively lighter grid adaption. A

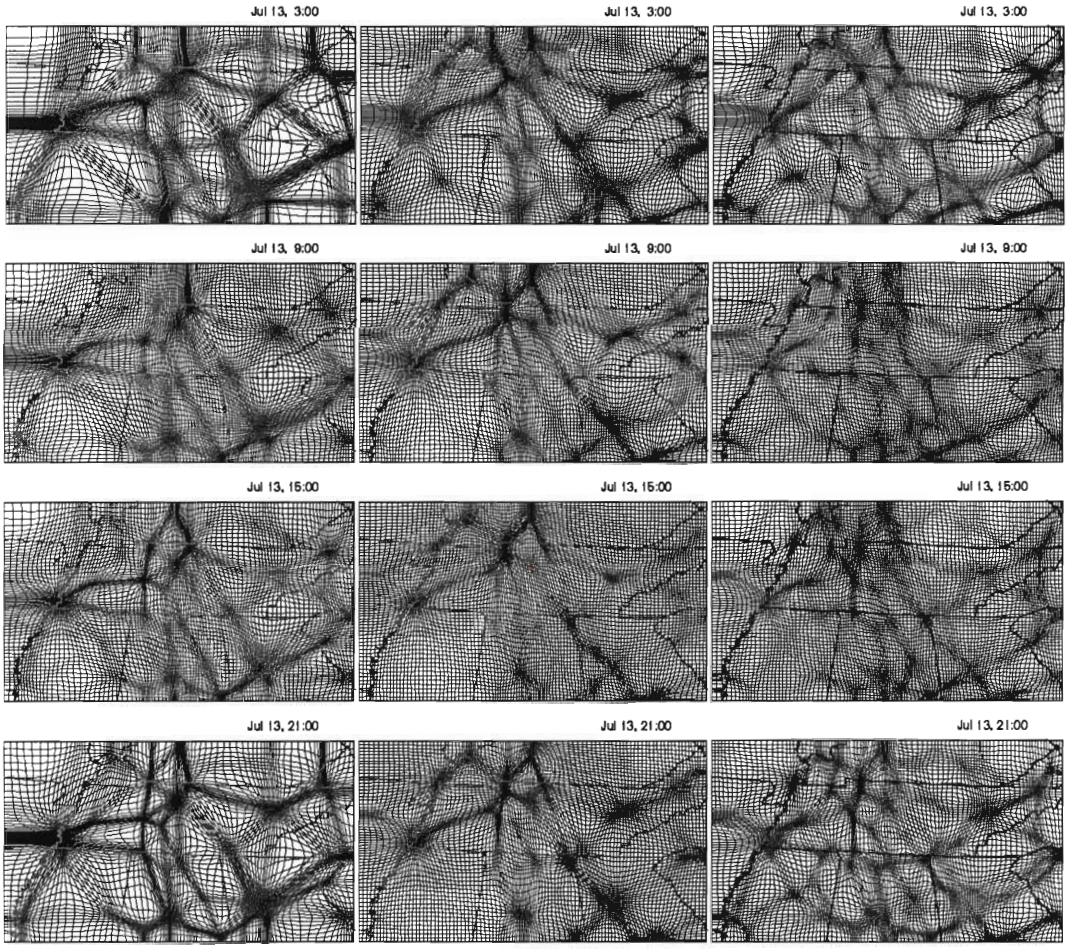

Figure 6-13 Adapted grids for Simulation # 1 (left), Simulation # 2 (middle) and Simulation # 3 on July 13th, 1995

similar effect (i.e., lighter grid adaption) is obtained when upper layer NO concentrations are used to build the weight function, as is the case in Simulation # 2. As observed in Simulation # 1, the weight function built on the surface NO concentration would not cluster the grid nodes over NO plumes that originate from sources that are emitting above the stable nighttime planetary boundary layer (PBL). An exception to this are NO plumes that originate from elevated sources and are located in close proximity to ground-level sources and traveling in the same direction. The weight function in Simulation # 3 clusters the grid nodes in regions with concentrated NO plumes and high ozone production rates. Compared to Simulations # 1 and # 2, Simulation # 3 has a larger number of regions with higher grid resolution.

Surface concentration plots and the adapted grid at 1400 EST on July 10th (Figure 6-14) reveal differences in the simulated concentrations. The most significant of which is observed 34 km south-southeast of the Cumberland Plant where simulation # 1, # 2 and # 3 predict a ozone concentrations of 155, 45 and 99 ppb, respectively. Also important to note is

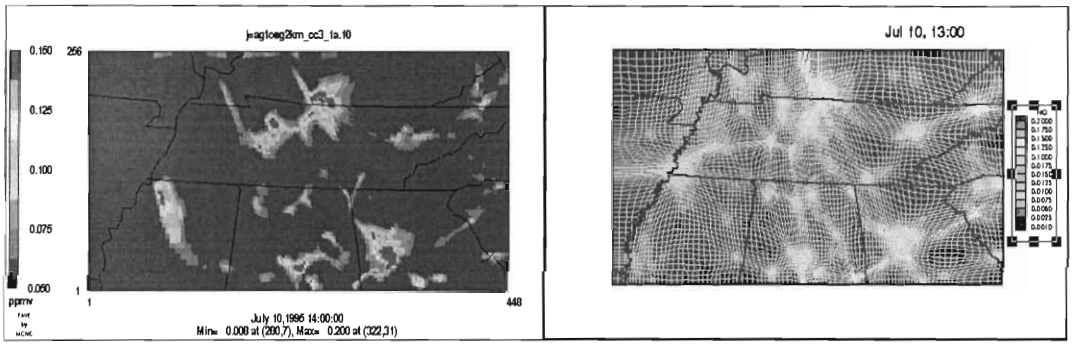

(a)

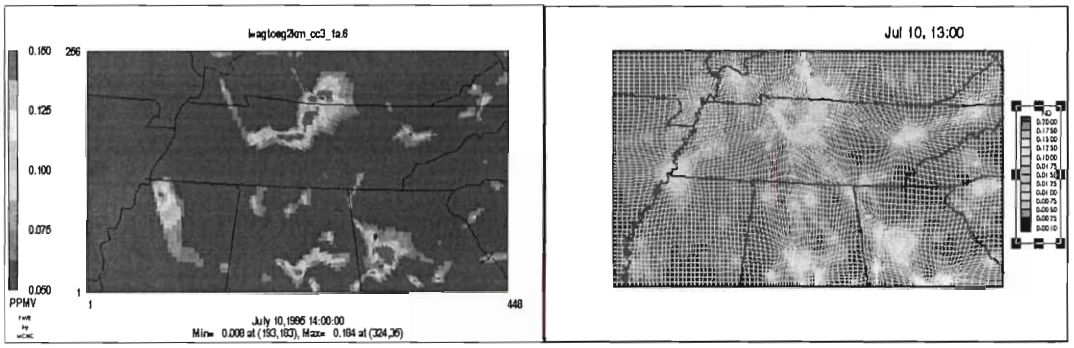

(b)

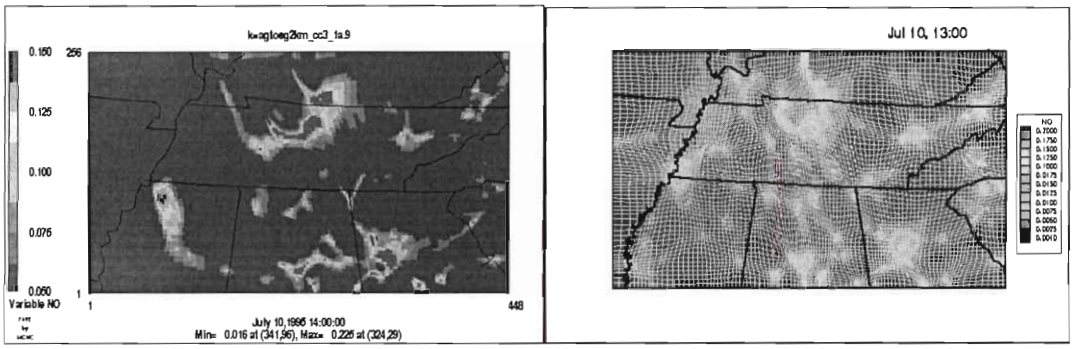

(c)

Figure 6-14 Surface O_3 and NO concentrations predicted by simulations # 1 (a), # 2 (b) and # 3 (c) and the resulting adapted grid on July 10th 1995 at 1400 EST

the lack of correlation between regions with strong grid node clustering and high surface NO concentration in simulations # 2 and # 3 as shown in Figure 6-14b and Figure 6-14c. Much better correlation is seen in simulation # 1 (Figure 6-14a).

Following is a theoretical explanation of the differences in ozone concentrations and the lack of correlation between the surface NO concentration and the adapted grid observed in simulations # 2 and # 3. Compared to the surface layer, higher wind speeds in the upper

layers transport the emissions longer distances. This is especially true at night time hours when a stable atmosphere prevents any significant downward mixing. The grid nodes in simulation # 1 cluster in regions where the curvature in the surface NO concentration field is high. Since each layer has different grid resolution requirements and since the grid adaption is the same for all layers, adaption to surface concentrations can lead to coarser grid resolution in regions that require finer grid resolution to capture elevated plumes. Lack of appropriate grid resolution results in an inaccurate representation of NO plumes from elevated sources. Conversely, grid adaption to upper layer NO concentrations can result in unresolved surface NO plumes as indicated by the lack of correlation between high surface NO concentration and the adapted grid.

Similar differences in the predicted ozone concentrations can be noted at 1600 EST on July 16th (Figure 6-15). Whereas Simulation # 1 predicts a plume with a maximum ozone concentration of 100 ppb 70 km east of Cumberland Plant in Tennessee, simulations # 2 and # 3 predict it at a distance of 78 and 64 km northeast of the plant with a maximum plume concentration of 130 and 140 ppb respectively. Clustering of grid nodes to upper layer concentrations in simulations # 2 and # 3 resulted in these differences. Although simulations # 2 and # 3 predict the Cumberland plume to be approximately at the same location, it is better resolved in simulation 3. The use of three dimensional ozone production rates in the development of the weight function enhances the ability of the adaptive grid to resolve the plume features.

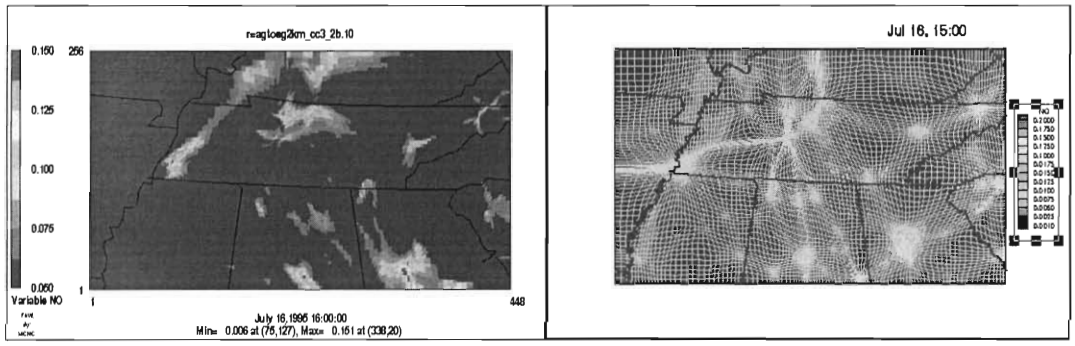

(a)

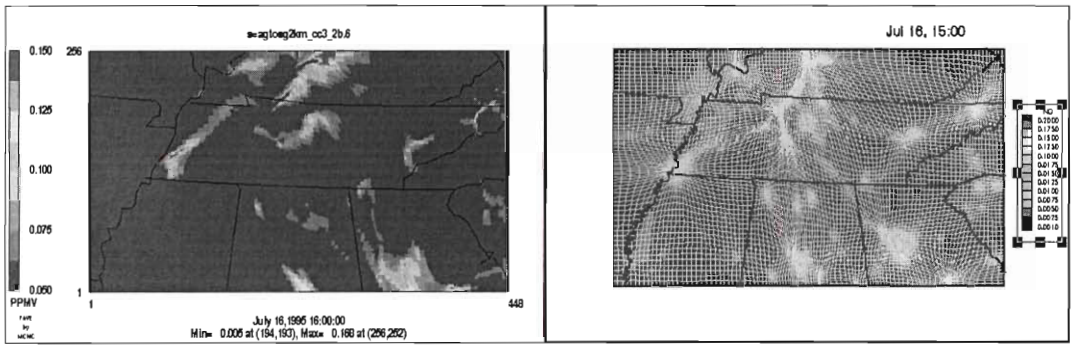

(b)

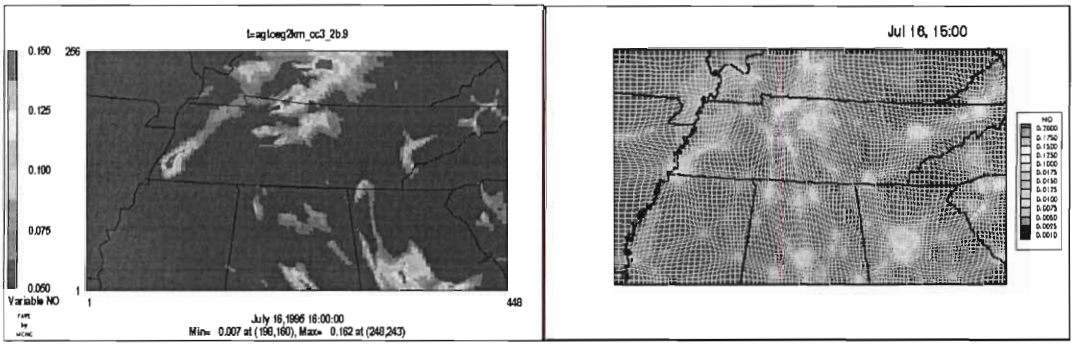

(c)

Figure 6-15 Surface O_3 and NO concentrations predicted by simulations # 1 (a), # 2 (b) and # 3 (c) and the resulting adapted grid on July 16th 1995 at 1600 EST

Another case where significant differences in the simulated concentrations from the three adaptive grid simulations were observed was at 1500 EST on July 17th (Figure 6-16). Simulation # 1 predicts an ozone plume 56 km south-southeast of the Cumberland Plant with a maximum surface ozone concentration of 120 ppb that extends all the way west of Chattanooga. At the same location, Simulations # 2 and # 3 predict an ozone concentration of 40 and 60 ppb respectively. Simulations # 2 and # 3 predict the maximum ozone in the plume

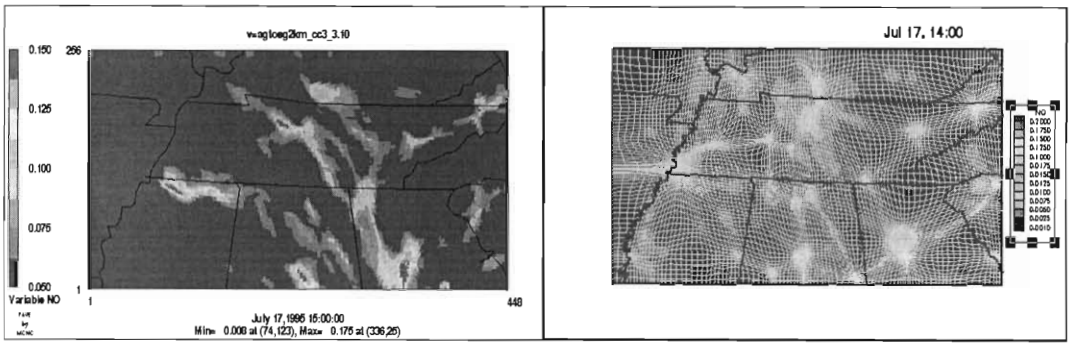

(a)

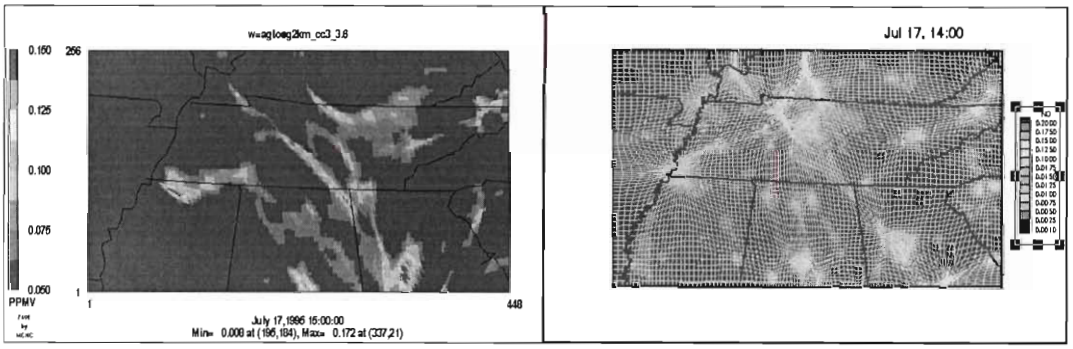

(b)

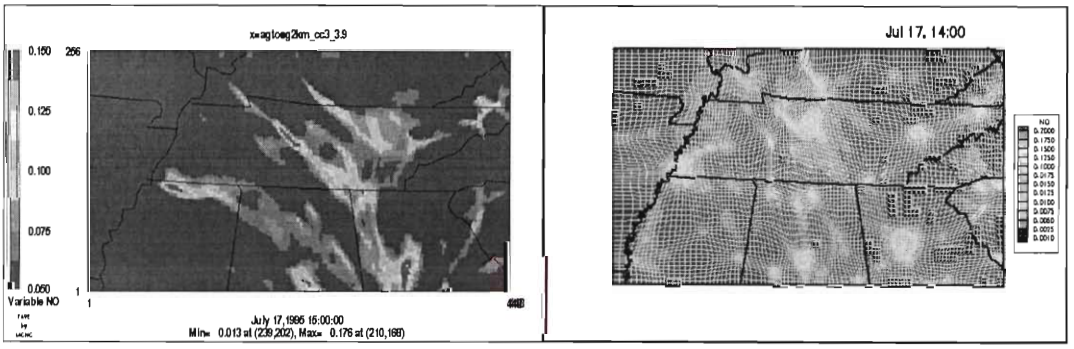

(c)

Figure 6-16 Surface O_3 and NO concentrations predicted by simulations # 1 (a), # 2 (b) and # 3 (c) and the resulting adapted grid on July 17th 1995 at 1500 EST

at a distance of 90 and 60 km south-southwest of the Cumberland Plant with a maximum ozone plume concentration of 132 and 152 ppb. Again, Simulation # 3 resolves the plume features more closely than Simulations # 1 and # 2.

6.5 Conclusion

An historical air pollution episode experienced by Tennessee Valley and surrounding areas was simulated using adaptive and static grid air quality models. Compared to the static grid simulation, the adaptive grid simulation is able to provide noticeable improvement in results at the monitoring stations. It is also able to more accurately simulate the long-range transport of a significant number of plumes from individual sources and source regions. Since the adaptive grid utilizes the curvature of surface NO concentration field to repositioning the grid nodes, and since a large number of monitoring stations are located in urban areas with high NO concentrations but low NO curvature, grid node clustering did not occur over a large number of stations. In addition, grid node repositioning driven by surface NO concentration field results in coarser grids over elevated sources unless they are in close vicinity of ground level sources.

Adaptive grid simulations were conducted using a weight function built from surface and three dimensional concentration fields aimed at improving the accuracy of ozone modeling results. Although, the modeling simulations did not result in significant differences at observation stations, analysis of concentration and adapted grid plots revealed significant differences. The use of upper layer concentrations in Simulation # 2 resulted in a more uniform adapted grid and a higher normalized error at 75 percent of the stations when compared with Simulation # 1 and at 70 percent of the stations when compared with Simulation # 3. Although the degree of grid adaption was strongest for Simulation # 1, NO plumes that originated from elevated sources are likely to have remained unresolved since larger grid cells might have resulted in diffusion of plume in the upper layers. Plume features were better resolved when the ozone production rate derived from the radical budget equation was incorporated into the weight function.

References

Alapaty, K., Mathur, R., and Odman, M. T., 1998, Intercomparison of spatial interpolation schemes for use in nested grid models. *Monthly Weather Review*, 126, 243-249

Boylan, J., Development of comprehensive, multiscale "One Atmosphere" modeling system: Application to Southern Appalachian Mountains, Submitted to *Atmospheric Environmen.t*

Doty, K. G., Tesche, T. W., and Timin, B., 2001, Meteorological Modeling for the Southern Appalachian Mountain Initiative, Final Report, *Southern Appalachian Mountain Initiative*, Ashville, NC.

Khan, M., Development of emission processing algorithms for an Adaptive Grid Air Quality model, *A Thesis* (To be presented) to the School of Civil and Environmental Engineering, Georgia Institute of Technology, Atlanta, Georgia, USA.

Odman, M. T., and Ingram, C., 1996, *Multiscale Air Quality Simulation Platform (MAQSIP): Source Code Documentation and Validation*, MCNC Technical Report ENV-96TR002, Research Triangle Park, North Carolina, pp.11-32.

Odman, M. T., Mathur, R., Alapaty, K., Srivastava, R. K., McRae, D. S., and Yamartino, R. J., 1997, Nested and adaptive grids for multiscale air quality modeling, in: *Next Generation Environmental Models and Computational Methods*, G. Delic, and M. F. Wheeler, eds., SIAM, Philadelphia, pp. 59-68.

Odman, M. T., Boylan, J. W., Wilkinson, J. G., Russell, A. G., Muller, S. F., Imhoff, R. E., Doty, K. G., Norris, W. B., and McNider, R. T., 2002, SAMI Air Quality Modeling Final Report, *Southern Appalachian Mountain Imitative*, Ashville, NC.

Pielke, R. A., Cotton, W. R., Walko, R. L., Tremback, C. J., Lyons, W. A., Grasso, L. D., Nicholls, M. E., Moran, M. D., Wesley, D. A., Lee, T. J., and Copeland, J. H., 1992, A comprehensive meteorological modeling system – RAMS, Meteorology and Atmospheric Physics, 49, 69.

Russell, A. G., 1997, Regional photochemical air quality modeling: Model formulations, history, and State of science, Annual Review Energy & Environment, 22, 537-588.

Srivastava, R. K., McRae, D. S., and Odman, M. T., 2000, An adaptive grid algorithm for air quality modeling; *J. Comput. Phys.* 165: 437.

Srivastava, R. K., McRae, D. S., and Odman, M. T., 2001(a), Simulation of a reacting pollutant puff using an adaptive grid algorithm, *J. Geophys. Res.*, in press

Srivastava, R. K., McRae, D. S., and Odman, M. T., 2001(b), Simulation of dispersion of a power plant plume using an adaptive grid algorithm, *Atmos. Environ.,* in press.

Wilkinson, J.G., Loomis, C.F., McNally, D.E., Emigh, R.A. and Tesche, T.W., 1994. *Technical Formulation Document: SARMAP/LMOS Emissions Modeling System (EMS-95)*. AG-90/TS26 & AG-90/TS27. Alpine Geophysics, Pittsburgh, PA.

Acknowledgements

This research is supported by U.S. Environmental Protection Agency Grant No. R 827028-01-0. We thank Dr. Steve Mueller of the Tennessee Valley Authority for providing the meteorological data.

7 Conclusions

The inconsistency of data from non-hydrostatic meteorological models (MMs) may lead to instabilities in air quality models (AQMs). Meteorological data can be made consistent without sacrificing the mass conservation characteristics of the AQM. Adjusting the vertical wind component proved to be an effective technique. We implemented and compared three methods for obtaining the vertical wind component from the discrete continuity equation. The methods differ in their vertical advection schemes. We found that the methods produced very similar vertical wind fields but these fields differed from those supplied by the MM. The adjustments reduced the vertical wind speed by an average of about 30% near the surface. The reduction was more pronounced at night when the winds have a weaker downward component. Also, the reduction decreased with altitude in the PBL but started increasing again in the free troposphere where the winds are practically horizontal. Thus, the adjustments may be large relative to the vertical winds but this is generally the case when the wind speeds are small. This implies that overall tracer transport would not be significantly affected by the adjustments. The tracer experiment simulation provided partial support for this hypothesis. Along a limited number of trajectories the original and adjusted wind fields yielded similar results. Unfortunately, the uncertainties in the tracer data and other parameters of the AQM are too large for more definite conclusions. We were unable to determine which one of the three methods best characterizes tracer transport. In an air quality simulation there were small differences in ozone levels predicted by the three methods. These are due to the use of vertical advection schemes of different accuracies. Methods with higher-order schemes seem to perform better but a more complete evaluation is needed at this point. In the absence of a clear winner among the three methods, the simplest method (inverse donor-cell) was adopted for use in our AQMs.

Sub-grid scale reactive plume models are used as a means of improving the accuracy with which point emission sources can be included in regional air quality model simulations. However, in the past, these models have not improved the predictive skill of AQMs, at least on a regional scale. An analysis of mesh resolution and mesh related errors related to this issue was performed. Based on this analysis and the fundamental properties of numerical simulation, it was determined that the sub-grid models were being handed over to the regional model before the plume was developed sufficiently for resolution by the much coarser regional grid. The result was loss of information due to cell averaging of the detailed plume concentrations.

New hand-over criteria have been developed that will automatically assess the development and maturity of the plume relative to the resolution provided by the regional grid. Once these criteria are satisfied, then the plume can be injected into the regional grid with minimal loss of information. The procedure uses the fact that a curve or surface in space can be constructed by determining proper coefficients to a sufficient number of terms in a Fourier series. However, a computational grid will only resolve a range of frequencies determined by the grid spacing, essentially acting as a band pass filter. The smallest spacing in the computational grid will then absolutely determine the resolution available to represent any function on that grid.

The criteria are implemented by selecting the feature that is to be assessed against the resolution ability of the regional grid (e.g., concentrations of certain species). A line or surface is defined that is perpendicular to the principle direction of advection, again assuming a plume feature. The concentration information is interpolated to an evenly spaced grid on the line or surface. A Fourier transform is performed to extract the frequencies present in the sub-grid solution, the range of which will be a function of the solution and the mesh. This transform is filtered to remove frequencies not resolved by the regional mesh and an inverse transform is performed to physical space. Comparison of the original and filtered distributions will then provide an indication of information loss due to the transfer without having to perform it. An energy method assessment of the two distributions has been shown to provide an initial criterion for automatically assessing the loss of information. Testing of the procedure on model problems and simulated 2-D and 3-D plumes demonstrated that this procedure provides a reliable indication of when a plume can be injected without significant degradation. The procedure can be included in sub-grid simulation codes as an automated check.

During the investigation of hand-over criteria above, it was found that plume-in-grid models would be most useful when regional scale AQMs have relatively fine grid resolution. Grid resolution in AQMs can be increased most efficiently by the use of an adaptive grid modeling technique. Next, the grid node repositioning and the point-source-grid-cell intersection algorithms were evaluated, both for efficiency and accuracy, using terrain elevation data. The algorithms were found efficient enough that the overhead of grid adaptations or re-gridding of emissions should not be restrictive in AQM simulations. The adaptive grid improved the accuracy considerably over a uniform grid with the same number of nodes. The maximum error decreased by 25% due to grid adaptations in an application to the terrain of the United States-Mexico border area. The adaptive grid algorithm performs better when regions with large curvature in surface elevation are located away from the boundaries of the domain. This is evident from the analysis of error at nodes that are located more than 100 km from the domain boundaries. The decrease in maximum error at such nodes is 35%. Finally, in a second application to a region surrounding the island of Hawaii where the changes in terrain slope are far away from the boundaries, the maximum error decreased by 60% and the cumulative error decreased by 25%. Similar improvement of accuracy can be expected in AQM results where pollutant fields resemble terrain fields in terms of complexity. The boundaries of the domain must be far away from emission sources that may create large changes in the gradients of pollutant concentrations.

An adaptive grid, urban-to-regional scale AQM has been developed. A simulation with this model evolves as a sequence of adaptation and solution steps. During the adaptation step, the solution (i.e., concentration fields) is frozen in time. A weight function that can detect the error in the solution is used to move the nodes of a structured grid. Iterative movement of the grid nodes continues until the solution error is reduced sufficiently. During the solution step, the grid is held fixed and the solution is advanced in time. However, before this can be done, the meteorological and emissions inputs must be mapped onto the adapted grid. For meteorological inputs, data are interpolated from a very-high-resolution mesoscale model simulation. For emissions, efficient search and intersection algorithms were developed to ensure proper allocation of point and area sources to the cells of the adapted grid. Using coordinate transformations, the non-uniform grid can be mapped into a space where it

becomes uniform. The atmospheric diffusion equation in this new space has been derived. Since the form of the equation is very similar to forms in existing AQMs and the grid is uniform, numerical algorithms developed for fixed uniform grid AQMs can be used to advance the solution.

To verify the model, a historic ozone episode in the Tennessee Valley was simulated. The grid adapted to dynamic changes in the NO fields as expected. Nodes were clustered around major emission sources with grid resolutions around 200 m. The NO and O_3 fields show gradients with a level of detail that is likely unprecedented for a regional simulation of this scale. However, the simulations progressed slowly due to very short solution time steps. This necessitates changing the solution algorithms such as using an implicit advection scheme that is not subject to the Courant stability limit or designing a variable time-step algorithm that can integrate the governing equations with the characteristic time step of each grid cell. Adaptation criteria were developed that would consider the errors not only in NO but in other species as well, especially those involved in important O_3 formation reactions.

Surface observations at AIRS stations in the Tennessee Valley during the July 7-17, 1995 period were used to evaluate the model results (both adaptive and static grid AQM results). Compared to the static grid simulation, the adaptive grid simulation provided noticeable improvement in ozone estimates at the monitoring stations. The adaptive grid AQM predicted a lower normalized error at almost 80 percent of the stations when compared with a static grid simulation using four times more grid cells (and about two times more computational resources). The decrease in error for the adaptive grid at these stations ranges from 0.4 to 23.6 percent with an average of 5.4 percent. At the remaining stations where the adaptive grid showed an increase in error, the minimum, maximum and average increase in normalized error was 0.4, 5.8 and 2.8 percent respectively. Since the adaptive grid utilized the curvature of the surface NO concentration field to repositioning the grid nodes, and since some monitoring stations were located in urban areas with high NO concentrations but low NO curvature, grid node clustering did not occur over those stations. In addition, grid node repositioning driven by surface NO concentration field sometimes resulted in coarser grids over elevated sources unless they were in close vicinity of ground level sources. The adaptive grid AQM was able to simulate with more detail the long-range transport of a number of plumes from individual sources to distant receptors. Unfortunately, these source-receptor relationships could not be established from the scarce observations.

Adaptive grid simulations were conducted using different weight function built from three dimensional concentration fields aimed at improving the accuracy of ozone modeling results. Surface NO, vertical column NO, and O_3 production rate were tried and they all produced very different grid adaptations. The use of column NO captured the plumes above the stable nighttime boundary layer that the surface NO weight function missed but also resulted in a more uniform grid during the day. Column NO_x resulted in higher normalized error at 75 percent of the stations when compared with surface NO Simulation # 1 and at 70 percent of the stations when the ozone production rate derived from the radical budget equation was incorporated into the weight function. A linear combination of the O_3 production rate and column NO_x seemed to produce the most desirable grid resolution characteristics but the differences in O_3 between the different simulations were too small to determine which weight function produces the best results.

Aircraft observations are made along a flight path with constantly varying altitude and surface position coordinates, so a routine was developed to interpolate the simulation data to the aircraft position so that a direct exact comparison can be made between them. A linear plot of these data can provide a comprehensive assessment of the simulation over large portions of the domain, as opposed to relying on point assessment. These results revealed a fundamental problem in how initial and boundary conditions are determined in AQM simulations and also revealed some issues in the collection and presentation of the aircraft data. Although a widely accepted routine was used to initialize the simulation from surface observations, average concentration levels proved to be in error by as much as a factor of two when compared with aircraft observations. This problem can be mitigated if the ideas developed in this research are used to create a new paradigm for simulation initiation. It was concluded that aircraft/Lidar should be used to make observations along the boundary of the simulation domain, which would then be used in a new routine based on the techniques developed herein to initialize the domain and boundaries. This would serve to provide much more accurate background data along the boundaries and should lead to much more useful verification data for simulation.

In summary, this research contributed to regional-scale air quality modeling by introducing new methods and improving existing methods for the treatment of emission sources. The transport, transformation and fate of the plumes from emission sources were simulated with unprecedented accuracy and the model estimates of pollutant levels downwind were significantly improved. This should result in more accurate predictions of future air quality and lead to the design of more effective emission control strategies. The major benefit would be more economical solutions to air pollution problems and, consequently, less risk to human health. The methods developed can individually be used in existing regulatory models, or the framework developed here can be adopted as a prototype for the next generation of air quality models.